

โพรเพนไฮโดรจิโนลิซิสบนตัวเร่งปฏิกิริยาโลหะคู่ที่มีแพลทินัมบน
ซีโอไลต์บีตาซึ่งสังเคราะห์ด้วยซิลิกาจากแกลบ

นายสิทธิชัย กุลวงศ์

วิทยานิพนธ์นี้เป็นส่วนหนึ่งของการศึกษาตามหลักสูตรปริญญาวิทยาศาสตรมหาบัณฑิต
สาขาวิชาเคมี
มหาวิทยาลัยเทคโนโลยีสุรนารี
ปีการศึกษา 2550

**PROPANE HYDROGENOLYSIS ON BIMETALLIC
CATALYSTS CONTAINING PLATINUM ON ZEOLITE
BETA SYNTHESIZED WITH RICE HUSK SILICA**

Sittichai Kulawong

**A Thesis Submitted in Partial Fulfillment of the Requirements for the
Degree of Master of Science in Chemistry
Suranaree University of Technology
Academic Year 2007**

**PROPANE HYDROGENOLYSIS ON BIMETALLIC
CATALYSTS CONTAINING PLATINUM ON ZEOLITE
BETA SYNTHESIZED WITH RICE HUSK SILICA**

Suranaree University of Technology has approved this thesis submitted in partial fulfillment of the requirements for the Master's Degree.

Thesis Examining Committee

M. Tangsathitkulchai
(Assoc. Prof. Dr. Malee Tangsathitkulchai)

Chairperson

Jatuporn Wittayakun
(Assoc. Prof. Dr. Jatuporn Wittayakun)

Member (Thesis Advisor)

Kunwadee Rangriwatananon
(Asst. Prof. Dr. Kunwadee Rangriwatananon)

Member

Sanchai Prayoonpokarach
(Dr. Sanchai Prayoonpokarach)

Member

P. Sattayatham
(Prof. Dr. Pairote Sattayatham)

Vice Rector for Academic Affairs

P. Manyun
(Assoc. Prof. Dr. Prapan Manyun)

Dean of Institute of Science

สิทธิชัย กุลวงศ์ : โพรเพนไฮโดรจิโนลิซิสบนตัวเร่งปฏิกิริยาโลหะคู่ที่มีแพลทินัมบน
ซีโอไลต์บีตาซึ่งสังเคราะห์ด้วยซิลิกาจากแกลบ (PROPANE HYDROGENOLYSIS ON
BIMETALLIC CATALYSTS CONTAINING PLATINUM ON ZEOLITE BETA
SYNTHESIZED WITH RICE HUSK SILICA) อาจารย์ที่ปรึกษา : รองศาสตราจารย์ ดร.
จตุพร วิทยาคุณ, 104 หน้า.

ซิลิกาจากแกลบเป็นสารตั้งต้นตัวหนึ่งในการสังเคราะห์ซีโอไลต์บีตาด้วยวิธีไฮโดรเทอร์มัล ซึ่งงานวิจัยนี้นำซีโอไลต์บีตาในรูปของโปรตอน (HBEA) มาเป็นตัวรองรับสำหรับตัวเร่งปฏิกิริยาโลหะเดี่ยวและโลหะผสมที่ประกอบด้วย Pt และ Co โดยทั้งตัวรองรับ HBEA ตัวเร่งปฏิกิริยาที่เตรียมมีปริมาณ Pt เท่ากับ 1% โดยน้ำหนัก ส่วน Co มีปริมาณเท่ากับ 5, 10 และ 15% โดยน้ำหนัก และตัวเร่งปฏิกิริยาบนตัวรองรับได้ผ่านการวิเคราะห์ลักษณะด้วยเทคนิคการเลี้ยวเบนรังสีเอกซ์ (XRD) ฟลูออโรสเปกโตรสโกปีอินฟราเรดสเปกโทรเมตรี (FTIR) การดูดซับแก๊สไนโตรเจนกล็องจุลทรรศน์อิเล็กตรอนแบบส่องผ่าน และเทคนิคการดูดกลืนรังสีเอกซ์ จากเทคนิค XRD และ FTIR พบว่าโครงสร้างของ HBEA ไม่มีการเปลี่ยนแปลงหลังจากเติมโลหะลงไป อย่างไรก็ตามเมื่อเพิ่มปริมาณโลหะลงไปพบว่าความเป็นผลึก พื้นที่ผิว และขนาดรูพรุนของ HBEA มีค่าลดลง นอกจากนี้ผลึกขนาดนาโนของ Pt (ความกว้างประมาณ 20 นาโนเมตร) สังเกตได้ในตัวเร่งปฏิกิริยา 1Pt/HBEA และในตัวเร่งปฏิกิริยาโลหะคู่บางตัว ส่วนอนุภาค Co มีรูปร่างที่ไม่แน่นอนน่าจะเป็นออสติเนียน และก่อนการใช้งานโคบอลต์บนตัวรองรับอยู่ในรูป Co^{2+} และล้อมรอบด้วยออกซิเจน

ตัวเร่งปฏิกิริยาบนตัวรองรับถูกนำไปทดสอบการเร่งปฏิกิริยาโพรเพนไฮโดรจิโนลิซิสสำหรับตัวเร่งปฏิกิริยาโลหะเดี่ยว 1Pt/HBEA ให้ค่าการแปลงผันของโพรเพนต่ำที่ 200 และ 250 องศาเซลเซียส (เท่ากับ 6.97 และ 21.14% ตามลำดับ) และอุณหภูมิที่ให้ค่าการแปลงผันสูงสุด คือ 300, 350 และ 400 องศาเซลเซียส (98 - 99%) โดยสารผลิตภัณฑ์หลักที่ 200 - 300 องศาเซลเซียสคือ มีเทนและอีเทน ขณะที่ 350 และ 400 องศาเซลเซียส ผลิตภัณฑ์หลักคือ มีเทนอย่างเดียว ในกรณีของตัวเร่งปฏิกิริยาโลหะเดี่ยว Co/HBEA ที่อุณหภูมิ 200 และ 250 องศาเซลเซียส ไม่เกิดการเร่งปฏิกิริยาและเมื่อเพิ่มอุณหภูมิพบว่ามีการแปลงผันสูงสุดที่ 400 องศาเซลเซียส เกิดผลิตภัณฑ์หลักบนตัวเร่งปฏิกิริยาโคบอลต์ทุกตัวคือมีเทน อย่างไรก็ตามพบว่าที่ปริมาณโลหะเท่ากับ 10 และ 15% โดยน้ำหนักทำให้เกิดการเสื่อมสภาพของตัวเร่งปฏิกิริยาเร็วกว่าตัวเร่งปฏิกิริยาที่มีปริมาณโลหะ 5%

เพื่อยืนยันว่าการเตรียมตัวเร่งปฏิกิริยาโลหะคู่ทำให้ประสิทธิภาพการเร่งปฏิกิริยาดีขึ้น ได้ทำการทดลองเพื่อเปรียบเทียบ ตัวเร่งปฏิกิริยาโลหะคู่ 5Co-1Pt/HBEA กับ ตัวเร่งปฏิกิริยาที่เป็น การนำตัวเร่งปฏิกิริยาโลหะเดี่ยว 1Pt/HBEA และ 5Co/HBEA มาผสมกัน ผลที่ได้เป็นที่น่าพอใจ

โดยตัวเร่งปฏิกิริยาโลหะคู่ให้ค่าการแปลงผันที่สูงกว่าและมีความทนทานต่อการเสื่อมสภาพได้ดีกว่า การเร่งปฏิกิริยาของตัวเร่งโลหะคู่ให้ค่าการแปลงผันของโพรเพนเพิ่มขึ้นเมื่อเพิ่มอุณหภูมิและให้ค่าสูงสุดที่อุณหภูมิ 300 และ 325 องศาเซลเซียส ซึ่งเป็นอุณหภูมิที่ต่ำกว่า ที่ให้ค่าการแปลงผันสูงสุดของตัวเร่งปฏิกิริยาโลหะเดี่ยวโคบอลต์ สมรรถนะการเลือกเกิดสารผลิตภัณฑ์บนตัวเร่งปฏิกิริยาโลหะคู่ไม่ขึ้นกับปริมาณของโคบอลต์ อย่างไรก็ตาม การเสื่อมสภาพจะขึ้นกับปริมาณของโคบอลต์ โดยสาเหตุหลักของการเสื่อมสภาพของตัวเร่งปฏิกิริยาคือการเกิดโค้ก ซึ่งกำจัดได้โดยการเผาไหม้ในบรรยากาศออกซิเจน ตัวเร่งปฏิกิริยาที่เหมาะสมที่สุดจากงานวิจัยนี้คือ 5Co-1Pt/HBEA

SITTICHAJ KULAWONG : PROPANE HYDROGENOLYSIS ON
BIMETALLIC CATALYSTS CONTAINING PLATINUM ON ZEOLITE
BETA SYNTHESIZED WITH RICE HUSK SILICA. THESIS ADVISOR :
ASSOC. PROF. JATUPORN WITTAYAKUN, Ph.D. 104 PP.

ZEOLITE BETA/HYDROGENOLYSIS/PROPANE/MONOMETALLIC/
BIMETALLIC

Silica from rice husk was used for the synthesis of zeolite beta (BEA) by hydrothermal method. The BEA in proton form (HBEA) was employed as a support for mono- and bimetallic catalysts containing Pt and Co. The Pt metal loading was fixed at 1 wt% and that of Co was 5, 10 and 15 wt%. The HBEA and HBEA-supported catalysts were characterized by X-ray diffraction (XRD), Fourier-transformed infrared spectroscopy (FTIR), nitrogen adsorption, transmission electron microscopy (TEM), and X-ray absorption. Results from XRD and FTIR indicated that the structure of HBEA did not change after impregnated with metal. However, with the increase of metal loading the HBEA crystallinity, surface area and pore volume decreased. Platinum nanocrystals (about 20 nm width) were observed in 1Pt/HBEA and in some bimetallic catalysts while cobalt seemed to form amorphous particles. The cobalt in the catalysts was in the form of Co^{2+} and it was surrounded by oxygen.

The HBEA-supported catalysts were tested for propane hydrogenolysis. The Pt/HBEA gave low propane conversion at 200 and 250°C (6.97 and 21.14%, respectively) and nearly complete conversion at 300, 350 and 400°C (98 - 99%). The

products from the reaction at 200 - 300°C were both methane and ethane while at 350 and 400°C was mainly methane. The propane conversion in Co/HBEA was not observed at 200 and 250°C and then increased with temperature. The maximum conversion at 400°C in all catalysts and the product was mainly methane. However, faster deactivation was observed with higher Co loading.

To confirm the improvement of bimetallic catalyst preparation, the performance of bimetallic 5Co-1Pt/HBEA catalyst was compared with a physically mixed catalyst 1Pt/HBEA and 5Co/HBEA. It was satisfactory that the previous catalyst had higher propane conversion and higher tolerance to deactivation. Further investigation over bimetallic catalysts showed that the propane conversion increased with the temperature and the maximum conversion at 300 and 325°C, lower than that in the monometallic cobalt catalysts. The selectivity did not depend on the amount of cobalt. However, the deactivation at high temperature increased with the amount of cobalt. The major cause of catalyst deactivation was coking which could be removed by combustion with oxygen. The best catalyst in this research was 5Co-1Pt/HBEA.

School of Chemistry

Academic Year 2007

Student's Signature_____

Advisor's Signature_____

CONTENTS (Continued)

		Page
II	EXPERIMENTAL	19
	2.1 Chemicals and materials.....	19
	2.2 Instrumentation.....	20
	2.2.1 X-Ray Diffraction (XRD).....	20
	2.2.2 Fourier Transform Infrared Spectrometry (FTIR).....	20
	2.2.3 Nitrogen Adsorption Isotherms.....	20
	2.2.4 Transmission Electron Microscopy (TEM).....	20
	2.2.5 XANES.....	21
	2.3 Experimental methods.....	21
	2.3.1 Silica preparation by acid leaching of rice husk.....	21
	2.3.2 Synthesis of zeolite beta in sodium form (NaBEA).....	22
	2.3.3 Conversion of NaBEA to HBEA.....	22
	2.3.4 Catalysts preparation.....	22
	2.4 Catalytic testing for propane hydrogenolysis.....	24
	2.4.1 Catalytic activation and testing for propane hydrogenolysis.....	24
III	CATALYST CHARACTERIZATION	28
	3.1 Characterization by XRD.....	28
	3.2 Nitrogen Adsorption-desorption.....	32
	3.3 FTIR spectrum of HBEA and BEA-supported catalysts.....	34

CONTENTS (Continued)

	Page
3.4 X-ray absorption near edge structure (XANES).....	36
3.5 Transmission electron microscope (TEM).....	37
IV CATALYTIC TESTING FOR PROPANE HYDROGENOLYSIS	50
4.1 Propane hydrogenolysis on monometallic catalysts.....	43
4.1.1 Propane hydrogenolysis over Pt/HBEA.....	43
4.1.2 Propane hydrogenolysis over Co/HBEA.....	46
4.2 Propane hydrogenolysis over bimetallic CoPt/HBEA.....	51
4.2.1 Propane hydrogenolysis over a physically mixed catalyst 1Pt/HBEA and 5Co/HBEA.....	51
4.2.2 Propane hydrogenolysis over CoPt/HBEA prepared by co-impregnation.....	53
4.2.3 Comparison between performance of 5Co-1Pt/HBEA prepared by co-impregnation and a physically mixed catalyst 1Pt/HBEA and 5Co/HBEA.....	58
4.2.4 Stability of 5Co-1Pt/HBEA.....	61
4.3 Surface mechanism of propane hydrogenolysis.....	62
4.4 Causes of catalyst deactivation.....	64
V CONCLUSION.....	66
REFERENCES.....	68

CONTENTS (Continued)

	Page
APPENDICES.....	73
APPENDIX A ADSORPTION ISOTHERMS OF HBEA AND HBEA-SUPPORTED CATALYSTS.....	74
APPENDIX B DETAILS OF CATALYTIC TESTINGS.....	79
APPENDIX C THESIS OUTPUT.....	93
CURRICULUM VITAE.....	104

LIST OF FIGURES

Figure	Page
1.1 Structure of BEA showing 4-, 5, 6-, and 12-membered ring.....	3
1.2 Framework of BEA viewed along a) [100], b) [001].....	3
1.3 Brönsted and Lewis acid sites in zeolite framework.....	6
1.4 Diagram of a zeolite framework surface (a) In the as-synthesized form, M^+ is either an organic cation or an alkali metal cation. (b) Ammonium ion exchange produces the NH_4^+ exchanged form. (c) Thermal treatment is used to remove ammonia, producing the H^+ , acid form. (d) Equilibrium form showing a silanol group adjacent to a tricoordinate aluminium.....	7
1.5 Proposed mechanism of butane hydrogenolysis over nickel catalyst in which adsorbed propane was generated in the third step.....	10
1.6 XRD patterns of NaBEA.....	13
1.7 Infrared frequency of vibration in BEA framework; (a) Asymmetric stretch, (insensitive to structure change) (b) Template stretch (c) Symmetric stretch, (sensitive to structure change) (d) Symmetric stretch, (sensitive) (e) Double ring (D6R and D4R) (sensitive to structure change) (f) T-O bending mode (insensitive to structure change).....	15

LIST OF FIGURES (Continued)

Figure	Page
1.8 Absorption of X-ray as a function of photon energy $E = hv$ by atoms in a lattice (a) and the fine structure represents the EXAFS function and energy at near edge absorption representing XANES (b).....	18
2.1 Reactor for analyzed hydrogenolysis reaction.....	27
3.1 XRD patterns of HBEA.....	29
3.2 XRD patterns of HBEA-supported monometallic Pt and Co catalysts...	30
3.3 XRD of HBEA-supported bimetallic catalysts.....	31
3.4 Nitrogen adsorption- desorption isotherm of HBEA at 77 K.....	33
3.5 IR spectra of (a) NaBEA, (b) HBEA, (c) HBEA-1 (1Pt/HBEA), (d) HBEA-2 (5Co/HBEA) and (e) HBEA-1 (1 Pt-5Co/HBEA).....	35
3.6 Co K-edge XANES of (a) Co foil, (b) CoCl_2 , (c) $\text{Co}(\text{NO}_3)_2$, (d) 10Co/HBEA, (e) 15Co/HBEA (f) 15Co-1Pt/HBEA, and (g) 10Co-1Pt/HBEA, respectively.....	37
3.7 Transmission electron microscopy images of 1Pt/HBEA: (a) 6k, (b) 120k, (c) 200k and (d) 200k.....	38
3.8 Transmission electron microscopy images of 10Co/HBEA: (a) 6k , (b) 60k, (c) 120k and (d) 200k.....	40
3.9 Transmission electron microscopy images of 5Co-1Pt/HBEA: (a) 2k, (b) 50k, (c) 50k and (d) 50k.....	41
3.10 Transmission electron microscopy images of 10 Co-1Pt/HBEA: (a)50k, (b) 200k, (c) 120k and (d) 120k.....	42

LIST OF FIGURES (Continued)

Figure	Page
4.1 Conversion and selectivities of propane hydrogenolysis over 1Pt/HBEA.....	44
4.2 Conversion of propane hydrogenolysis over 1Pt/HBEA as the temperature increased (▲) and decreased (■).....	45
4.3 Conversion and selectivities of propane hydrogenolysis over 5Co/HBEA.....	46
4.4 Conversion of propane hydrogenolysis over 5Co/HBEA as the temperature increased (▲) and decreased (■).....	47
4.5 Conversion and selectivities of propane hydrogenolysis over 10Co/HBEA.....	48
4.6 Conversion of propane hydrogenolysis over 10Co/HBEA as the temperature increased (▲) and decreased (■).....	49
4.7 Conversion and selectivity of propane hydrogenolysis over 15Co/HBEA.....	49
4.8 Conversion of propane hydrogenolysis over 15Co/HBEA as the temperature increased (▲) and decreased (■).....	50
4.9 Conversion and selectivities of propane hydrogenolysis over a physically mixed catalyst 1Pt/HBEA and 5Co/HBEA.....	52
4.10 Conversion of propane hydrogenolysis over a physically mixed 1Pt/HBEA and 5Co/HBEA as the temperature increased (▲) and decreased (■).....	53

LIST OF FIGURES (Continued)

Figure	Page
4.11 Conversion and selectivities of propane hydrogenolysis over 5Co-1Pt/HBEA.....	54
4.12 Conversion of propane hydrogenolysis over 5Co-1Pt/HBEA as the temperature increased (▲) and decreased (■).....	54
4.13 Conversion and selectivities of propane hydrogenolysis over 10Co-1Pt/HBEA.....	55
4.14 Conversion of propane hydrogenolysis over 10Co-1Pt/HBEA as the temperature increased (▲) and decreased (■).....	56
4.15 Conversion and selectivities of propane hydrogenolysis over 15Co-1Pt/HBEA.....	57
4.16 Conversion of propane hydrogenolysis over 15Co-1Pt/HBEA as the temperature increased (▲) and decreased (■).....	57
4.17 Conversion of propane over 5, 10 and 15Co-1Pt/HBEA.....	58
4.18 Compare conversions of propane over between 5Co-1Pt/HBEA and mix 5Co/HBEA with 1Pt/HBEA.....	59
4.19 Compare product selectivities over between a) 5Co-1Pt/HBEA and b) mix 5Co /HBEA with 1Pt/HBEA.....	60
4.20 Propane conversion and product selectivities over 5Co-1Pt/HBEA at 300°C.....	61
4.21 (a) A proposed mechanism of propane adsorption and cracking on the surface (b) dissociative adsorption of hydrogen on the surface.....	62

LIST OF FIGURES (Continued)

Figure	Page
4.22 A proposed mechanism of (a) ethane and (b) methane formation on surface.....	64
4.23 Deactivation mechanisms: (a) Coke formation, (b) Sintering of the active metal particles, and (c) Sintering and solid-solid phase transitions of the washcoat and encapsulation of active metal particles..	65

LIST OF TABLES

Table	Page
2.1 List of prepared catalyst and metal contents.....	23
2.2 The oven-programmed setup for GC.....	25
3.1 Relative crystallinity of HBEA-supported monometallic catalysts.....	30
3.2 Relative crystallinity of HBEA supported CoPt.....	32
3.3 Surface area and pore volume of HBEA and HBEA-supported catalysts.....	33
3.4 Assignment of IR peaks (in cm^{-1}) of the NaBEA, HBEA and BEA-supported catalysts.....	34

CHAPTER I

BACKGROUND AND LITERATURE REVIEW

Rice husk from milling is a cheap material and can be considered as a solid waste. Researchers, especially in rice producing countries, have tried to investigate possibilities to increase rice husk value. One possibility among several available uses is to extract silica out for further application. Because the silica extraction process is simple and inexpensive, it is beneficial to use rice husk as a natural silica source, instead of commercial silica. The extraction is generally performed by a leaching rice husk with acid to remove inorganic impurity. As reported by Khemtong et al. (2006), rice husk could be refluxed with hydrochloric acid and calcined at 550°C to produce rice husk silica (RHS) with 98% purity. This work focused on utilization of the rice husk silica for the synthesis of zeolite beta (BEA).

This work involved the synthesis of BEA by using RHS as a low cost silica source and tetraethylammonium hydroxide (TEAOH) as an organic template. The method was similar to that reported by Loiha et al. (2007) who investigated the optimum Si/Al ratio for BEA synthesis with RHS. The Si/Al ratio of 13 was selected in this work because it gave the highest surface area and crystallinity compared to the other ratio. Zeolite Beta in proton form (HBEA) was used as a catalytic support for monometallic Pt and Co and bimetallic CoPt catalysts. Both the HBEA and HBEA-supported metal catalysts were characterized by X-ray Diffraction (XRD) to confirm the BEA structure, Fourier transform Infrared spectroscopy (FTIR) to confirm

functional groups in BEA, nitrogen adsorption to study physical characteristics and to determine surface area and pore size and X-ray absorption near edge structure (XANES) to determine oxidation state of the metal component. Finally, the HBEA-supported metal catalysts were tested for propane hydrogenolysis in a flow reactor. Parameters including bimetallic ratio and temperature that affect the catalytic performance were studied.

1.1 Zeolite Beta (BEA)

The BEA can be synthesized by hydrothermal method from a gel consisting of silica, alumina, alkaline earth metal and organic templating agent. The main reagents are a silica source and an organic template. Several commercially available silica sources such as aqueous silica sol (Mies et al., 2007), colloidal silica (Kim et al., 2004) and tetraethyl orthosilicate (Eapen et al., 1994) have been widely used. The organic templating agents, such as dibenzyl-1,4-diazabicyclo(2,2,2) octane chloride dibenzyl dimethylammonium ion (Calvert et al., 1987), TEA halide diethanolamine (Saxton and Zajacek, 1996), TEAOH-TEA halide triethanol amine, TEABr-NH₄OH and TEAOH-TEABr chelates (Chang et al., 1987) were previously explored for the BEA synthesis.

BEA was first synthesized by Wadlinger et al. (1967) and it was explored as a powerful catalyst in petrochemical applications and fine chemical synthesis. BEA is a large pore zeolite with the formula Na_n{Al_nSi_{64-n}O₁₂₈} with n < 8 (Vaudry et al., 1997). The Si/Al ratio may vary from 8 to more siliceous (dealuminated) forms and ending with an aluminium-free homologue. Figure 1.1 show 3D structure of BEA showing 4-, 5-, 6-, and 12-membered ring. The BEA is a kind of high silicon zeolite

with 12-ring orifice ($12.6 \times 12.6 \times 26.2 \text{ \AA}$) and 3D pore structure ($7.6 \times 6.4 \text{ \AA}$ straight channels intersect $5.5 \times 5.5 \text{ \AA}$) as shown in Figure 1.2 (Jansen et al., 1997).

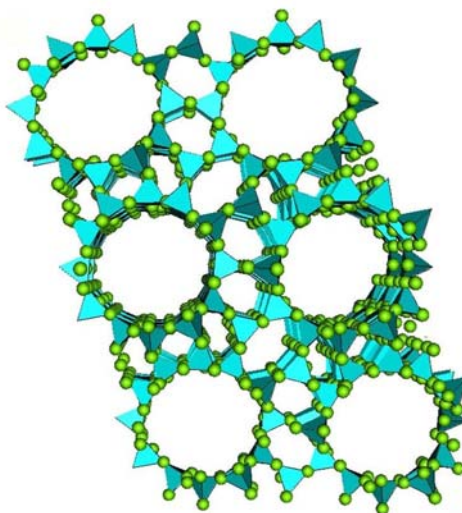


Figure 1.1 Structure of BEA showing 4-, 5, 6-, and 12-membered ring.

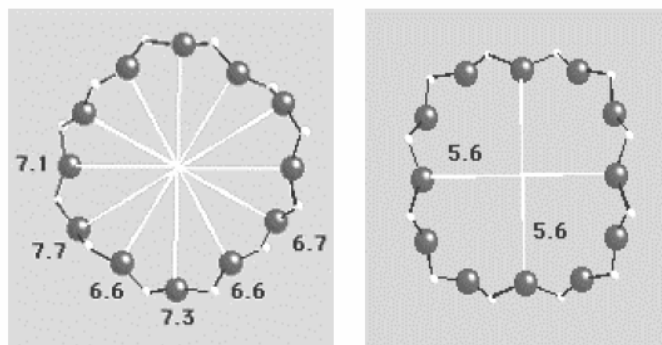


Figure 1.2 Framework of BEA viewed along a) [100] b) [001].

The RHS was used as a silica source for the synthesis of zeolite BEA with various Si/Al ratio including 8, 13, 15, 20, 50, 100, 150 and 200 under hydrothermal conditions (Loiha et al., 2007). Structure and morphology of the products were investigated by XRD and scanning electron microscopy (SEM). From XRD results, the samples with Si/Al ratio 8-20 contained a pure phase of BEA and the highest

crystallinity was obtained in the BEA with Si/Al ratio of 13. An addition information from nitrogen adsorption revealed that, this ratio gave the highest surface area. Thus, this work only the BEA with Si/Al ratio of 13 was used as a catalyst support.

The BEA is a stable zeolite upon thermal and acid treatment (Barrer, 1982). It is a good solid acid catalyst for many important industrial reactions, such as isobutene alkylation with n-butene (Degnan et al., 2001), diphenol production by phenol oxidation (Atoguchi et al., 2004), and Beckmann rearrangement (Dai et al., 1996). Moreover, successful applications of BEA included aromatic alkylation of biphenyl with propylene (Aguilar et al., 2000), aromatic acylation of 2-methoxynaphthalene (Casagrande et al., 2000), indole synthesis, aromatic nitration and aliphatic alkylation. It is effective in lowering the pour point of petroleum oil by isomerizing the normal alkanes to their branched isomers, rather than cracking them to lighter alkanes, as is done by other zeolites such as ZSM-5 and erionite (Absil and Hatzikos, 1998). The shape selective catalytic properties of BEA, especially in the cracking of alkanes and in the isomerization of m-xylene, were also reported (Corma et al., 1989).

Acidity is an important characteristic of zeolites which make them very useful in acid catalysis. A good understanding of the nature and number of acid sites in a zeolite is needed in developing improved and novel catalysts for applications in the chemical industries (Juttu, 2001). The reactivity and selectivity of zeolites as acid catalysts are determined by the surface acidity of active sites. It is clear that this activity is related to the acid strength of the intervening sites (Costa et al., 2000). The framework aluminium atoms are negatively charged and balanced by extra-framework cations, represent potential active acid site (Barrer, 1982). The acidic

properties of zeolites are mainly dependent on the Si/Al molar ratio as well as the temperature of activation. In zeolites, acid sites are classified to the classical Brønsted and Lewis acid (Figure 1.3). The Brønsted acidity corresponds to proton donor acidity, while the Lewis acidity corresponds to electron pair acceptor. The Brønsted acidity occurs when the cations used to balance the negatively charged framework are protons (H^+). A trigonally coordinated aluminium atom possessing a vacant orbital that can accept an electron pair, behaves like a Lewis acid site. To produce the zeolite acid catalysts, it is necessary to replace the cations present in the freshly synthesized material with protons. In zeolite, proton can be introduced by various methods. If an aluminium ion, which is trivalent, is substituted isomorphously for a silicon ion, which is quadrivalent, in a silica lattice comprising silica tetrahedral, the net negative charge must be stabilized by a nearby positive ion such as proton. This positive ion can be produced by the dissociation of water, forming a hydroxyl group on the aluminium atom. The resulting structure, in which the aluminium and the silicon are both tetrahedrally coordinated, side by side produces Brønsted acid. If this structure is heated, the occluded water in the zeolitic framework is driven off followed by condensation process and Brønsted acid sites are converted to Lewis acid sites. Some metal atoms are now three-coordinated and some four coordinated. The reverse can also occur. The addition of water and heating can convert Lewis acid sites back to Brønsted acid sites. The aluminium atom is electrophilic and can react with hydrocarbon to form an adsorbed carbenium ion (Charles, 1991).

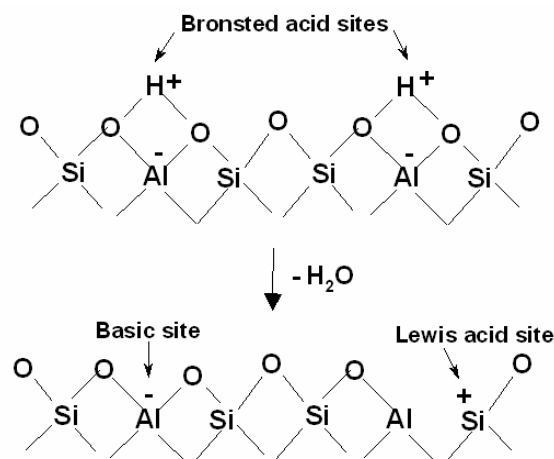


Figure 1.3 Brønsted and Lewis acid sites in zeolite framework.

In the majority of the as-synthesized commercial zeolites, the cation is sodium Na⁺ and the corresponding zeolite is referred to as the sodium form (Figure 1.4a). To obtain the acid form of zeolites, sodium ions are replaced by protons by ion-exchange with an ammonium salt (Figure 1.4b), followed by calcination at high temperature to decompose NH₄⁺ ions into H⁺ and NH₃ (Figure 1.4c). After the liberation of ammonia, protons are bonded with surface oxygens to give the bridging form -SiO(H)Al- of Brønsted acid sites. An equilibrium exists between this bridging form and the form in which silanol (-SiOH) group is adjacent to a tricoordinate aluminium that constitutes the Lewis acid site (Figure 1.4d). Furthermore increment in calcinations temperature (>500°C) of the zeolite results in the dehydroxylation process where Brønsted acid sites are converted to Lewis acid sites.

In general, a zeolite with a lower aluminium content or the higher the Si/Al ratio will have stronger Brønsted acidity. Several characterization techniques can estimate the acid sites qualitatively and quantitatively, and can reveal the relationship between catalytic behavior of zeolite and their acidity. The most widely used

techniques are FTIR spectroscopy and a catalytic testing in reaction (Bagnasco, 1996).

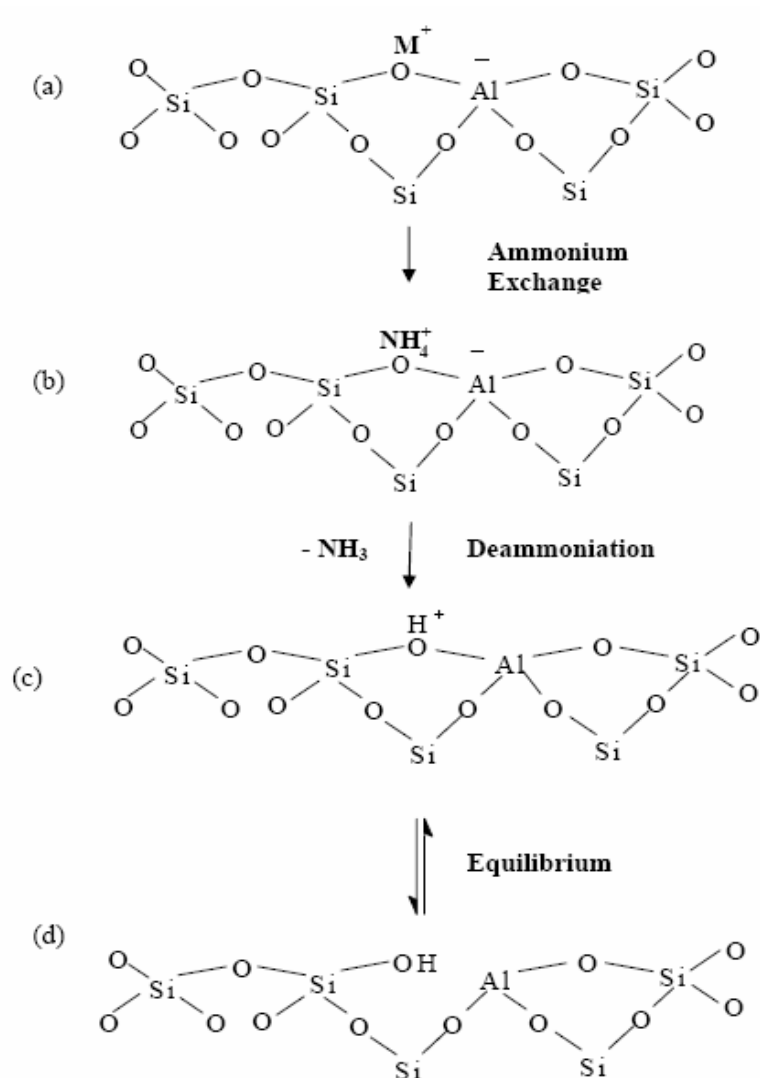


Figure 1.4 Diagram of a zeolite framework surface (a) In the as-synthesized form, M^+ is either an organic cation or an alkali metal cation. (b) Ammonium ion exchange produces the NH_4^+ exchanged form. (c) Thermal treatment is used to remove ammonia, producing the H^+ , acid form. (d) Equilibrium form showing a silanol group adjacent to a tricoordinate aluminium.

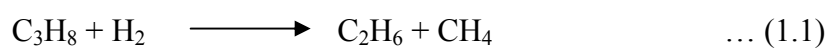
1.2 Application of supported metal over BEA catalysts

Alkane hydrogenolysis is a reaction between hydrocarbon compound and hydrogen resulting cleavages of C-C bonds accompanied by hydrogenation to form two hydrocarbon molecules. The hydrogenolysis of paraffins is important in petroleum processing in which it is sometimes a desired reaction, as in commercial hydrocracking, and sometimes not desired, as in catalytic reforming (Satterfield, 1980). The most active catalysts for this reaction are metals in group VIII (Sinfelt, 1980). The distribution of primary products from hydrogenolysis varies with the nature of the metal. In addition, the specific activity and selectivity of the catalysts have been found to be sensitive to the average metallic particle size.

The hydrogenolysis reactions usually require a relatively large ensemble or group of active sites on the surface of the catalyst. The alkane hydrogenolysis can be selectively suppressed by removing or poisoning a fraction of the active sites. This approach has been applied in the design of industrial reforming catalysts (Gellman et al., 1984). For example, the selectivity of Ni for dehydrogenation versus hydrogenolysis can be greatly increased by adding Cu which is an inactive metal to form an alloy. Metal-single crystals offer unique possibilities in the study of the effects of surface structure and composition upon the alkane hydrogenolysis. This work focused on bimetallic catalysts containing cobalt with a small amount of platinum. Besides the investigation on catalytic performance, catalyst characterization and deactivation were also studied.

The application of supported metal over BEA catalysts has been studied by several researchers. For example, Blomsma et al. (1997) studied the isomerization and hydrocracking of heptane over HBEA, loaded with platinum and palladium with

different amounts metal. Bifunctional catalysis with zeolites plays an important role in petroleum refining and is applied in processes such as hydrocracking, isomerization, and catalytic dewaxing. This work focused on propane hydrogenolysis, a reaction between propane and hydrogen to produce ethane and methane (Equations 1.1 and 1.2). This reaction is simple, structure sensitive, and can be use to determine the activity of catalysts of interest. The reaction pathway depends on the amount of hydrogen. With low amount of hydrogen, methane and ethane are the products. If there are excess hydrogen, ethane will further cracked to from methane. In addition, if ethane desorbs quickly from the catalyst before the further reaction with hydrogen, ethane will be present in the product stream.



Propane hydrogenolysis is a structure-sensitive reaction which has been utilized to study supported metal and bimetallic catalysts. Structure-sensitive reactions are useful in characterizing decoration of metal surfaces by catalyst modifiers such as reactions often require a relatively large ensemble of surface metal atoms for an active site. The larger the size of the reaction ensemble, the more structure sensitive the reaction.

For supported metal, the reaction on both Pt/SiO₂ (Sermon et al., 2000) and Ni/SiO₂ (Jackson et al., 1999) occurred through both pathways in equations 2.1 and 2.2. The performance of nickel depended on the type of support. The hydrogenolysis activities at low temperature were ranged as followed: Ni/SiO₂ > Ni/Al₂O₃ > Ni/MoO₃ due to degree of metal dispersion and interaction between the nickel and the each supports. Ni/MoO₃ catalyst had lower activity than the others because the type of carbon molecules at the first contact between the catalysts and the hydrocarbon feed had weak interaction. The higher specific rate of hydrogenolysis observed over the Ni/SiO₂ catalyst was likely to be an effect not only of the small particle size of the nickel but also the manner in which carbonaceous matter builds up on these particles. However, during hydrogenolysis, propane could be transformed to aromatics by oligomerization and cyclization.

In addition to monometallic catalyst, there were some reports on propane hydrogenolysis on bimetallic catalysts that had capability to improve selectivities and yields towards more useful products. This behavior can be explained by existence of metal-metal and metal-support interactions on surfaces which modify the catalytic performance of the metal alone. For example, Richard et al. (2004) studied the effect of Al₂O₃-supported Pt-Sn, Pt-Ir, and Ir-Sn catalysts for propane hydrogenolysis. Relative to platinum, iridium was more active because it has stronger metal-support interaction resulting in well-dispersed metal particles.

However, there are no reports of propane hydrogenolysis over supported cobalt-based catalyst. However, there was a report by Lomot et al. (2002) that studied the kinetics of ethane hydrogenolysis over cobalt catalysts supported on silica. Because the Co/SiO₂ was active for ethane hydrogenolysis, it is likely that Co

is also active for the propane hydrogenolysis. Thus, this work investigated catalytic activities of bimetallic catalysts containing platinum and cobalt for propane hydrogenolysis.

1.4 Characterization Techniques for HBEA and catalysts

Knowledge of the structure, physical and chemical properties of catalysts is important to understand the chemistry occurring on catalysis. In this work, four techniques were used: X-ray powder diffraction (XRD), Fourier transform infrared spectroscopy (FTIR), nitrogen adsorption isotherms and X-ray absorption near edge structure (XANES). The overview of each technique is given below.

1.4.1 X-ray Diffraction

Because zeolites are crystalline solids, the X-ray diffraction pattern can be used to identify the structure and to determine their degree of crystallinity. The diffractions of X-rays from zeolite crystallites produce a scattering pattern which is specific of the periodic arrangement of regular arrays of atoms or ions located within the zeolite structure. Each zeolite has its own specific pattern that can be used as reference for the determination of crystal phase. Figure 1.6 displayed the XRD pattern of BEA. This technique can also indicate whether the solid sample is amorphous or crystalline phase. The phase purity of the solid crystal will be measured by comparing the X-ray pattern of the sample with the pattern of the standard material.

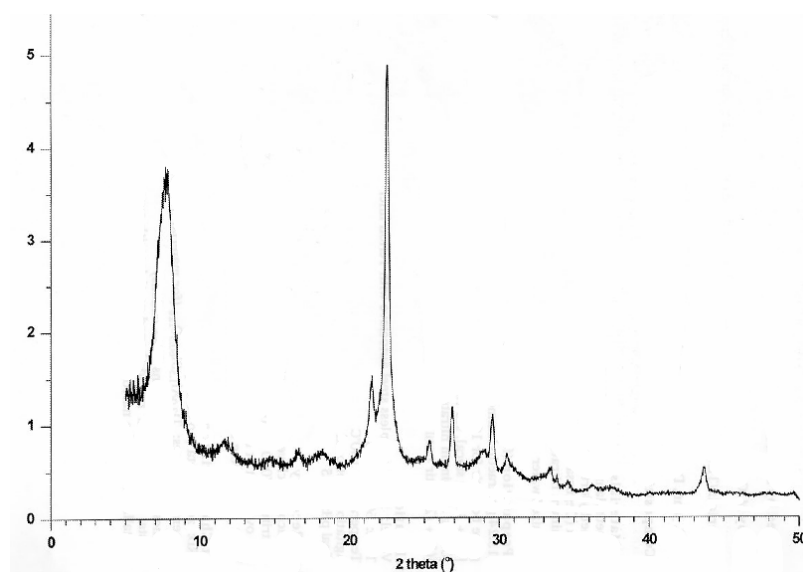


Figure 1.6 XRD patterns of NaBEA (Cambior, M. A. 1991).

The characteristic peaks of BEA are at 7.8, 22.5, 27.0, 29.5 and 43.2°. The degree of crystallinity can be determined from the summation of area of all the characteristic BEA peaks relative to that of standard BEA.

$$\% \text{ Crystallinity} = \frac{\sum \text{Area of BEA peaks of sample}}{\sum \text{Area of BEA peaks of standard}} \quad (1.3)$$

1.4.2 Infrared Spectroscopy

FTIR spectroscopy has been applied extensively to study the nature and the amount of acid sites present in a zeolite. IR studies of BEA have revealed two hydroxyl stretching bands, one at 3605 cm^{-1} and another at 3740 cm^{-1} . The first band has been identified as the hydroxyl stretch associated with the bridging Al-O(H)-Si (Kiricsi et al., 1994; Bourgeat Lami et al., 1991; Kuehl and Timken, 2000).

The main areas of the application of FTIR spectroscopy in zeolite research are the investigation of the framework properties and to study the active sites such as Brønsted or Lewis acid sites. In addition, the amount of adsorbed molecules in zeolite such as ammonia could be used to determine the zeolite acidity (Fierro, 1990). Basically, infrared spectroscopy provides information on short range and long range bond order caused by lattice coupling, electrostatic and other effects. The technique is based on the possibility to separate the energy of a molecule into three additive components associated with the rotation of the molecule as a whole, the vibration of the constituent atoms and the motion of the electrons in the molecule (Nakamoto, 1962).

Frequencies range of certain framework vibrations of which tetrahedral SiO_4 or AlO_4 linkages are in the mid-infrared region of $400 - 1400 \text{ cm}^{-1}$. Figure 1.7 shows FTIR spectrum of BEA framework in such region which is divided into two groups of vibration, the internal and external vibration. The internal vibration of TO_4 tetrahedral (T being the atom at the centre of the tetrahedron, e.g. Si, Al) is insensitive to the structure changes and present in each zeolite framework and silica.

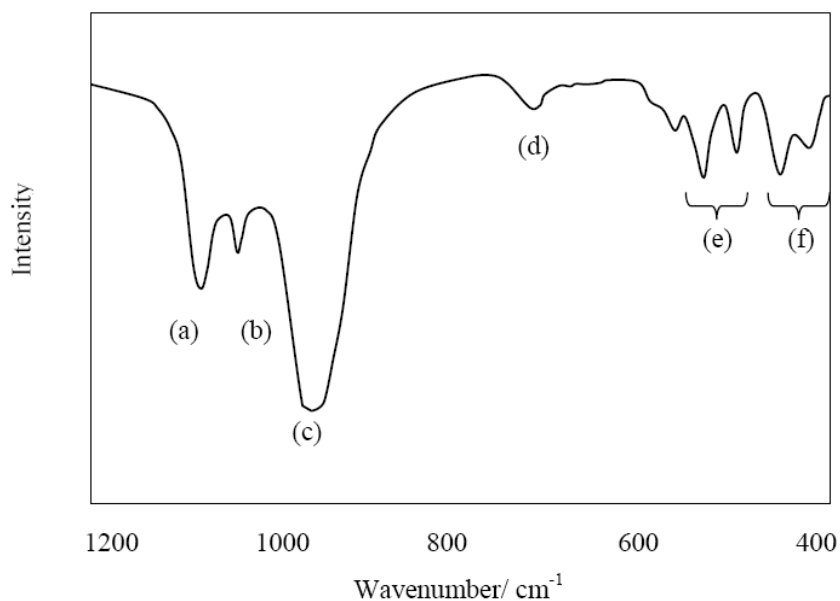


Figure 1.7 Infrared frequency of vibration in BEA framework; (a) Asymmetric stretch, (insensitive to structure change) (b) Template stretch (c) Symmetric stretch, (sensitive to structure change) (d) Symmetric stretch, (sensitive) (e) Double ring (D6R and D4R) (sensitive to structure change) (f) T-O bending mode (insensitive to structure change).

The internal vibration includes the T-O asymmetric stretch at 1250 - 950 cm⁻¹, T-O symmetric stretch at 720 - 650 cm⁻¹ and T-O bends at 500 - 420 cm⁻¹) (Flanigen., 1976). The T-O stretching is sensitive towards the composition of Al and Si in zeolite framework. The shifting of these stretching to higher wavenumber occurs when the aluminium contents in the framework decrease. The increase of wavenumber with the decreased in aluminium content is related to change of bond length and bond orders. The longer length of Al-O bond and the decrease in the electronegativity of Al results to the decrease of the forces constant and hence the wavenumber.

The external vibration occurs from the vibration of TO_4 tetrahedral linkages. This vibration is sensitive to the structure changes and tetrahedron linkages. It can be observed at $820 - 750 \text{ cm}^{-1}$ that assigned to symmetric stretching for T-O and at $1050-1150 \text{ cm}^{-1}$ for asymmetric stretching for T-O. The present of double rings (D4R and D6R) in the zeolites framework give a strong absorption band at $650 - 500 \text{ cm}^{-1}$. Besides, The T-O bending for tetrahedron that formed large pore opening was observed at $420 - 300 \text{ cm}^{-1}$.

1.4.3 Nitrogen adsorption isotherm

The total surface area of bulk catalysts is commonly measured by Brunauer-Emmet-Teller (BET) method. Determination of surface area of BEA is accomplished by using N_2 adsorption at liquid N_2 temperature in which adsorbed N_2 molecules adhere on surface site as monolayer. The reversible physical adsorptions of vapors onto high surface area adsorbents sometimes show a hysteresis near relative pressures of unity. One explanation of this hysteresis arises from the condensation of liquid in the capillaries.

Loiha studied the adsorption-desorption isotherm of BEA with Si/Al of 13 (2007). All sample with Si/Al ratio of 8 - 20 gave a type I isotherm which was a characteristic of microporous material such as zeolite. The adsorbed amount increased quickly after an exposure to nitrogen due to quick adsorption in micropores and external surface; and concave to nearly constant volume due to monolayer adsorption. The BET surface area of the BEA with Si/Al ratio of 13 was $669 \text{ m}^2/\text{g}$.

1.4.4 X-ray absorption spectroscopy

Even though IR spectroscopy provides information about the nature of adsorption of the precursor and sometimes can indicate whether bimetallic particles are formed or not, such information is not quantitative. Techniques that can provide additional insightful information are X-ray absorption spectroscopy technique such as X-ray absorption near edge structure (XANES) spectroscopy and extended X-ray absorption fine structure (EXAFS).

1.4.4.1 X-ray Absorption Near Edge Structure (XANES)

XANES is another technique of X-ray absorption spectroscopy. When an atom is bombarded with high-energy photon beam at increasing energies until the energy of this incident beam nears the ionization energy of target atom, the absorption occurs and one electron is emitted. The energy of the absorption edge and the presence of “pre-edge features” from XANES provide information about the oxidation state and coordination geometry of the absorbing atom. (Chotisuwan, 2004)

For example, the structure of Co/MCM-41 determined by XANES was predominant in the form of Co oxides in their as-prepared state. Two of the model compounds, CoO and Co(OH)₂, both consist of Co(II) ions in an octahedral environment, and thus have similar XANES profiles. (Vrålstad et al., 2005)

1.4.4.2 EXAFS spectroscopy

EXAFS refers to oscillatory structures which appear in the high energy side of characteristics X-ray absorption edges of elements. It appears only when the absorbing atoms are in a condensed phase, and reflects the local

structure around the atoms. Each element has its characteristic absorption energy in the X-ray region. When an atom absorbs an X-ray photon, a photoelectron emanates from the atom as an outgoing wave. If the atom is in a condensed phase, the photoelectron will be backscattered by surrounding atoms and interfere with the original wave (Figure 1.8a). Constructive interference increases the wave amplitudes while destructive interference causes the amplitude to disappear as in Figure 1.8b.

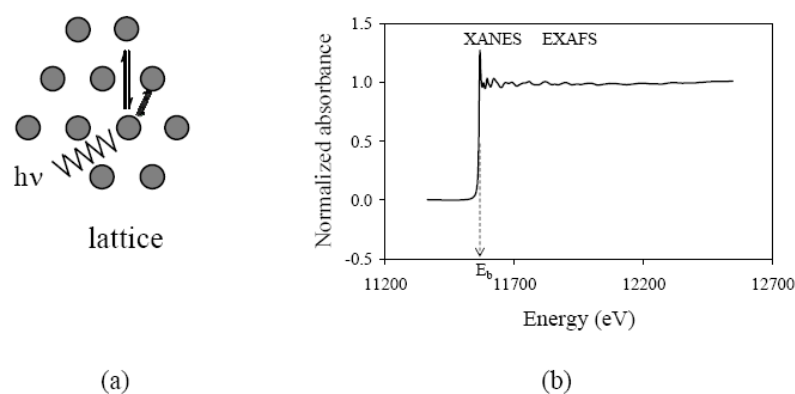


Figure 1.8 Absorption of X-ray as a function of photon energy $E = h\nu$ by atoms in a lattice (a) and the fine structure represents the EXAFS function and energy at near edge absorption representing XANES (b).

EXAFS as a tool for structural determination of various physical state including gases, liquids, solutions, amorphous solids, and crystalline solids has been used to determine the local structure of supported metal catalysts indicating whether metal-metal interactions occur or not after precursor is supported on a support. The data obtained from EXAFS are distance between absorbing atom and its surrounding coordination sphere, coordination number, identities of the absorber and its neighbors, and the dynamic and static disorder in the internuclear distances.

CHAPTER II

EXPERIMENTAL

2.1 Chemicals and materials

2.1.1 Chemical for silica extraction by acid leaching was concentrate hydrochloric acid (37% HCl, Carlo Erba).

2.1.2 Chemicals for HBEA synthesis and conversion included tetraethylammonium hydroxide solution 40% in water (40% in water TEAOH, Fluka), sodium chloride (99.9% NaCl, Carlo Erba), potassium chloride (99.8% KCl, Carlo Erba), sodium hydroxide (97% NaOH, Carlo Erba), sodium aluminate (Na 50 - 56% and Al 40 - 45%; NaAlO₂, Riedel-de Haen), rice husk silica and ammonium nitrate (NH₄NO₃, Univar (Ajax)) and rice husk silica from acid leaching.

2.1.3 Metal precursors for the catalyst preparation included dihydrogen hexachloroplatinate (IV) hexahydrate, ACS, Pt 99% (99% H₂PtCl₆·6H₂O, Alfa ESAR), cobalt (II) chloride (CoCl₂, Univar (Asia)).

2.1.4 Gases for catalytic testing included hydrogen (99.99% H₂, Linde), helium (99.99% He, UHP), propane (> 95% purity, TSG).

2.2 Instrumentation

2.2.1 X-Ray Diffraction (XRD)

Powder XRD patterns were obtained using Cu K_{α} radiation on a Bruker axs D5005 diffractometer. The X-ray was generated with 40 mA of current and 40 kV of potential. The XRD patterns were recorded at room temperature between the 2θ values from 3° to 50° .

2.2.2 Fourier Transform Infrared Spectrometry (FTIR)

The study was carried out with a FTIR spectrometer Perkin-Elmer: spectrum GX. The sample and KBr was dried at 120°C for 1 hour to remove humidity. The mixture of 0.5 mg of sample and 30 mg of KBr was ground and the homogeneous powder was transferred into a sample barrel and pressed with 13 tons of force for 1 minute and put on a V-mount cell. The range of measurement was between 4000 cm^{-1} and 400 cm^{-1} .

2.2.3 Nitrogen Adsorption Isotherms

Physical characteristics of the samples were determined by N_2 adsorption-desorption isotherm at 77 K for relative pressure from 0.001 to 0.99 on a Micromeritics ASAP 2010 analyzer. Before measurement, each sample was degassed at 573 K for 3 hours. The pore size and the pore volumes were calculated from the desorption branches of the isotherm using Brunauer-Emmet-Teller (BET) method.

2.2.4 Transmission Electron Microscopy (TEM)

This technique was used to observe the location and morphology of Pt and Co over HBEA for the selected sample area and magnification that provide clear images. The morphology of HBEA-supported catalysts was investigated with a TEM Joel JSM 2010 microscope with an accelerating voltage of 200 keV. Each sample

was suspended in ethanol and mixed by sonicator for 10 minutes and dropped on a copper grid-supported carbon film and dried at room temperature.

2.2.5 XANES

XANES spectra of catalysts containing Co and reference compound (CoCl_2 and $\text{Co}(\text{NO}_3)_2$) was measured in the energy region of the K-edge in transmission mode at XAFS beamline (BL-8) of National Synchrotron Research Center (NSRC). The X-ray beam was emitted for energy 2s by a storage ring running at 1.2 GeV. X-rays was monochromatized using double crystal monochromator crystal type Ge (220) with energy resolution of 1.0×10^{-4} - 5.0×10^{-4} eV. The monochromator covers the energy of photon in a range of 3,440 to 13,000 eV. The samples and reference compound were prepared by packing in a sample holder. Finally, incident beam intensity was monitored by Bonn monochromator in an ionization chamber filled with nitrogen and argon gas.

2.3 Experimental methods

2.3.1 Silica preparation by acid leaching of rice husk

The procedure to produce rice husk silica was similar to that reported in literature (Khemthong, et al. 2007). Briefly, rice husk was washed with water, dried at 100°C overnight, refluxed with 3 N HCl at 100°C for 3 hours, filtered and washed repeatedly with water until the filtrate was neutral. Then the leached rice husk was dried at 100°C overnight, pyrolyzed in a furnace at 550°C for 6 hours to give white powder of rice husk silica.

2.3.2 Synthesis of zeolite beta in sodium form (NaBEA)

The synthesis of NaBEA with the Si/Al ratio of 13 was modified from literature in which the original synthesis gel has molar composition of $1.97\text{Na}_2\text{O}:1.00\text{K}_2\text{O}:12.50(\text{TEA})_2\text{O}:\text{Al}_2\text{O}_3:50\text{SiO}_2:750\text{H}_2\text{O}:2.9\text{HCl}$ (Robson and Lillerud, 2001). The gel was transferred to a stainless steel autoclave and heated at 135°C for 3 days under autogenously pressure. After hydrothermal crystallization, the autoclave was quenched in cool water to give mother liquor with pH of approximately 12. The zeolite beta in sodium form was separated by centrifugation at 6,000 rpm. It was washed by water until pH of the washed solution is approximately 9 and dried overnight at 77°C .

2.3.3 Conversion of NaBEA to HBEA

The BEA in proton form (HBEA) was prepared from NaBEA zeolite. First NaBEA was converted to ammonium form NH_4BEA by repeated ion exchange with 1 M NH_4NO_3 for 2 times at 80°C . Then, the NH_4BEA was converted to HBEA by calcination at 550°C for 5 hours.

2.3.4 Catalysts preparation

Both monometallic and bimetallic catalysts were prepared by incipient wetness impregnation of $\text{H}_2\text{PtCl}_6 \cdot 6\text{H}_2\text{O}$ and/or CoCl_2 solution HBEA. The Pt and Co contents in of these catalysts were calculated from precursors to produce 1%wt of Pt and vary amount of Co (5, 10 and 15%wt). All catalyst samples were dried overnight at 120°C and calcined at 300°C for 3 hours.

The name of catalysts and metal content are listed in Table 2.1. In addition, a physically mixed between 1Pt/HBEA and 5Co/HBEA was prepared to compare with a bimetallic catalyst containing 1Pt and 5Co.

Table 2.1 List of prepared catalyst and metal contents.

Catalyst name	wt%Pt	wt%Co
1Pt/HBEA	1	-
5Co/HBEA	-	5
10Co/HBEA	-	10
15Co/HBEA	-	15
5Co-1Pt/HBEA	1	5
10Co-1Pt/HBEA	1	10
15Co-1Pt/HBEA	1	15
1Pt/HBEA+5Co/HBEA	1	5

A physically mixture of 1Pt/HBEA and 5Co/HBEA was prepared by mixing the two catalysts together. The performance of the physically mixed catalyst would be compared with bimetallic 5Co-1Pt/HBEA to observe the catalytic enhancement by bimetallic catalyst.

2.4 Catalytic testing for propane hydrogenolysis

2.4.1 Catalytic activation and testing for propane hydrogenolysis

The hydrogenolysis reactions of propane was studied in flow reactor in a quartz tube, designed to produce a controlled flow of helium, hydrogen and hydrocarbon over a small charge (approximately 0.2 - 0.4 g) of catalyst. The reactor scheme is showed in Figure 2.1. The reactor was operated at atmospheric pressure. The catalyst was reduced by heating to 450°C in a flow of hydrogen at the rate of 50 ml min⁻¹. The samples were held in flowing hydrogen at 450°C for 6 hours to ensure the complete reduction. Then it was cooled in flowing hydrogen to a desired reaction temperature before introducing a gas mixture containing the He:H₂:C₃H₈ were with approximately 4 : 4 : 1 ratio. In order to reach steady state conditions in the reactor, the reactant gases was flowed through the catalyst for 15 min before analyzing the reaction products, after the analysis, He and H₂ mixture was flowed through the catalysts for 15 min; after this process the He:H₂:C₃H₈ mixture was again introduced into the hydrocarbon reactor in order to study the reaction at different temperatures. Using this process reproducibility of reaction rates was observed even after temperature cycling. The reaction products were analyzed by a gas chromatography (SRI GC 610C) equipped with a Polar packed column and a thermal conductivity detector. The distribution of products could lead to a clear understanding of reaction pathway. Helium gas was used as the GC carrier gas and the oven-programmed setup is shown in Table 2.2. The catalytic for propane hydrogenolysis was tested in the temperature range of 200 - 400°C. The performance of each catalyst was reported in term of percent conversion and selectivity. The percent conversion and selectivity for propane are defined as follows:

$$\% \text{ Conversion} = \left(\frac{\text{Mole C}_3\text{H}_8 \text{ input} - \text{Mole C}_3\text{H}_8 \text{ output}}{\text{Mole C}_3\text{H}_8 \text{ input}} \times 100 \right) \dots(2.1)$$

$$\% \text{ Selectivity} = \frac{\text{Pr oduct of desired reaction}}{\text{Pr oduct from all reactions}} \times 100 \quad \dots(2.2)$$

$$\% \text{ CH}_4 \text{ selectivity} = \frac{\text{Mole CH}_4}{\text{Mole CH}_4 + \text{Mole C}_2\text{H}_6} \times 100 \quad \dots(2.3)$$

Table 2.2 The oven-programmed setup for GC.

Action	Value	Unit
Initial temperature	90	°C
Hold	12	min
Ramp	10	°C/min
Final temperature	110	min
Run time	30	min

Results from catalytic testing were propane conversion and product selectivities. Testings at the temperature range of 200 - 400°C of monometallic Pt and Co were compared with that of bimetallic catalysts.

In the catalytic testing, the temperature was increased from 200 to 400°C and a sampling to GC was done three times at each temperature. The testing as the temperature increased was referred to as “run-up”. After 400°C, the reactor was cooled down under helium flow and the sampling for GC was done at each

temperature again. The testing as the temperature decreased was referred to as “run-up”. Comparison between the run-up and run-down could indicate the stability of the catalyst, namely, the catalyst was not deactivated if both runs superimposed.

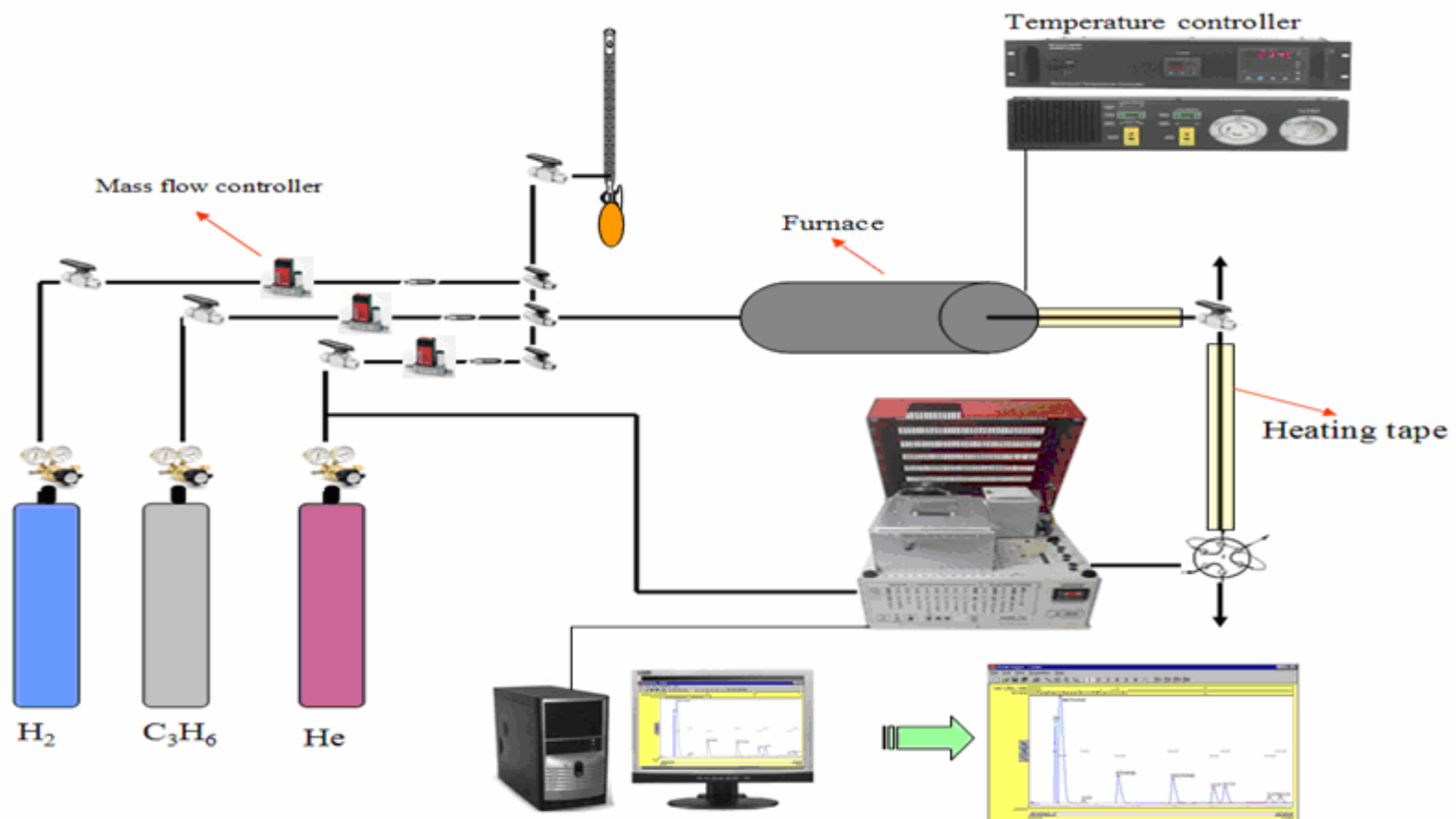


Figure 2.1 Reactor for analyzed hydrogenolysis reaction.

CHAPTER III

CATALYST CHARACTERIZATION

In this chapter the support HBEA was characterized by XRD and N₂ adsorption. The results were compared with the HBEA-supported catalysts. The changes of crystallinity with metal loading were studied by XRD. The changes of surface area and pore volume of the catalysts were studied by N₂ adsorption-desorption. In addition, the as-prepared catalysts were analyzed by TEM and XANES.

3.1 Characterization by XRD

NaBEA was synthesized with rice husk silica with Si/Al ratio of 13 and transformed to HBEA. The XRD patterns of HBEA displayed 2 θ peaks positions at 7.8, 22.5, 27.0, 29.5 and 43.2 degree (Figure 3.1). However, the peak with the highest intensity of HBEA was 22.5.

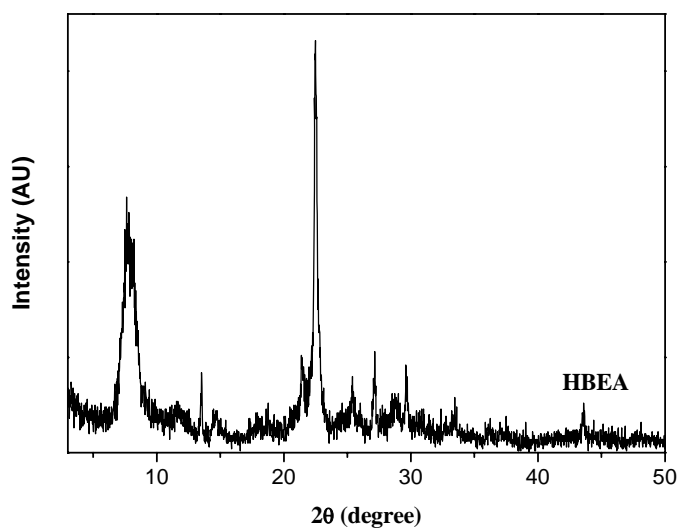


Figure 3.1 XRD patterns of HBEA.

HBEA was employed as a support for monometallic Co, Pt and bimetallic PtCo catalysts which were prepared by wet impregnation. The XRD patterns of all HBEA-supported monometallic catalysts are shown in Figure 3.2. The monometallic Pt (1wt%) and Co (5, 10 and 15wt%) catalysts gave similar XRD pattern to that of the parent HBEA indicating the BEA framework was retained after loaded with Pt and Co. The peaks of Pt or Co were not observed indicating that the metals were well dispersed in these catalysts. Only in the 15Co/HBEA that peaks of Co were observed at 16 degree indicating that Co particles in this sample were larger than those in the other samples.

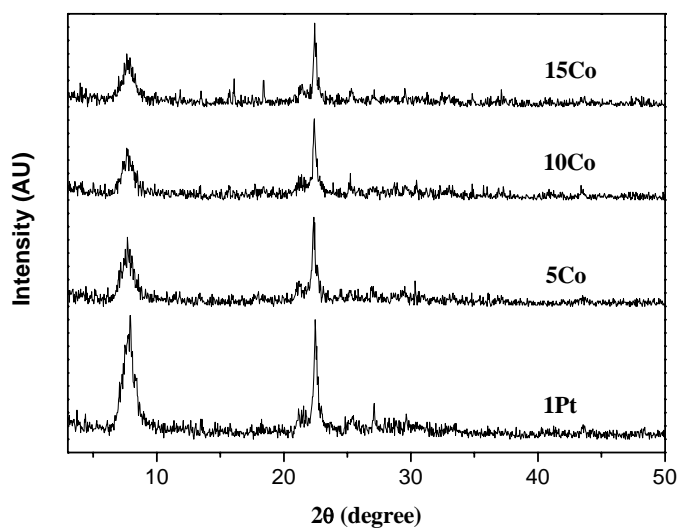


Figure 3.2 XRD patterns of HBEA-supported monometallic Pt and Co catalysts.

The crystallinity of BEA of monometallic catalysts were calculated relative to that of HBEA and the results are shown in Table 3.1. The addition of metal reduced the crystallinity of BEA and the crystallinity decreased as the amount of metal increased.

Table 3.1 Relative crystallinity of HBEA-supported monometallic catalysts.

Monometallic	
Samples	% Relative crystallinity
HBEA	100
1Pt/HBEA	62
5Co/HBEA	52
10Co/HBEA	30
15Co/HBEA	25

The XRD patterns of the bimetallic catalysts with 1Pt and 5, 10, or 15Co are displayed in Figure 3.3. The characteristic peaks on BEA were still observed indicating that the support structure did not change upon metal loading. The XRD peak of Co was observed in all catalysts at 16 degree and the area of this peak increased with Co loading. This observation indicated that the cobalt particle size increased with the amount of Co loading.

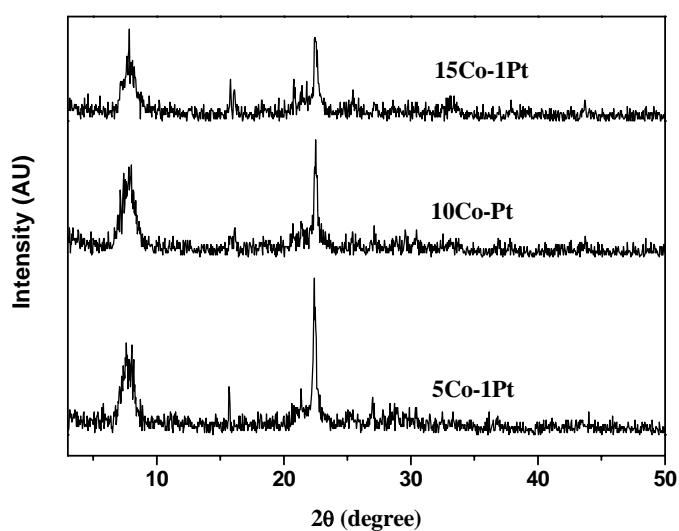


Figure 3.3 XRD of HBEA-supported bimetallic catalysts.

Similar to monometallic catalysts, the BEA crystallinity of bimetallic catalysts were determined relatively to that of the HBEA support. The results are shown in Table 3.2. As the amount of cobalt increased, the BEA crystallinity decreased.

Table 3.2 Relative crystallinity of HBEA supported CoPt.

Bimetallic	
Samples	% Relative crystallinity
5Co-1Pt/HBEA	36
10Co-1Pt/HBEA	26
15Co-1Pt/HBEA	22

3.2 Nitrogen Adsorption-desorption

Figure 3.4 exhibits nitrogen adsorption-desorption isotherm of the HBEA. The isotherm was type I which is a characteristic of microporous materials. In this type, a quick adsorption occurred at low relative pressure and became monolayer for the rest of the pressure. The isotherms of BEA-supported catalysts were similar to that of the HBEA support (see Appendix A). Their surface area and micropore volume are summarized in Table 3.3.

The BET surface area was highest in HBEA and decreased with the amount of metal added. Thus, the order of surface area was as follow: HBEA > 1Pt/HBEA > 5Co/HBEA > 5Co-1Pt/HBEA. The volume of micropores were also in the same order indicating that the metal might reside in the micropores. In addition, the surface area was related to the BEA crystallinity as it was shown previously that HBEA had the highest crystallinity (see Tables 3.1 and 3.2). The adsorption and desorption of all samples overlapped with each other indicating the absence of mesopores.

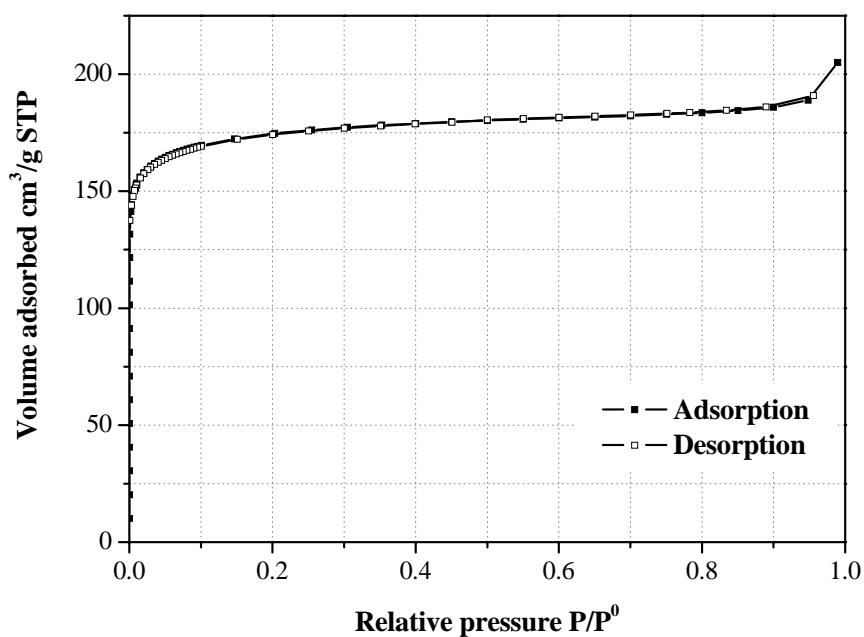


Figure 3.4 Nitrogen adsorption- desorption isotherm of HBEA at 77 K.

Table 3.3 Surface area and pore volume of HBEA and HBEA-supported catalysts.

Samples	BET surface area (m ² /g)	Micropore volume (cm ³ /g)	Maximumpore
			volume (cm ³ /g)
HBEA	625	0.2515	0.2969
1Pt/HBEA	579	0.2221	0.2753
5Co/HBEA	495	0.1883	0.2356
5Co-1Pt/HBEA	464	0.1772	0.2208

3.3 FTIR spectrum of HBEA and BEA-supported catalysts

The NaBEA, HBEA and BEA-supported catalysts were also characterized by FTIR in the wavenumber range of 1300 - 400 cm^{-1} and the obtained spectrum are shown in Figure 3.5. All spectrums were similar and confirmed functional groups in the BEA structure. The peak assignments are displayed in Table 3.4 including asymmetric and symmetric stretching of TO_4 centered at 1083 - 1088 cm^{-1} and 790 - 792 cm^{-1} , respectively. Moreover, when noble metal added were impregnated to the HBEA, no change was observed in the IR spectrum indicating the retention of the HBEA framework.

Table 3.4 Assignment of IR peaks (in cm^{-1}) of the NaBEA, HBEA and BEA-supported catalysts.

Sample	External vibration		Internal tetrahedral vibration		Double ring		T-O bend	
	Asymmetric stretch	Symmetric stretch	Asymmetric stretch	Symmetric stretch	D6R	D4R		
NaBEA	1083	789	1223	-	571	521	464	426
HBEA	1088	791	1226	-	573	524	464	428
HBEA-1	1088	792	1226	-	573	523	464	428
HBEA-2	1088	790	1227	-	570	523	463	424
HBEA-3	1088	791	1226	-	571	523	463	426

HBEA-1 : 1Pt/HBEA, HBEA-2 : 5Co/HBEA and HBEA-3 : 5Co-1Pt/HBEA.

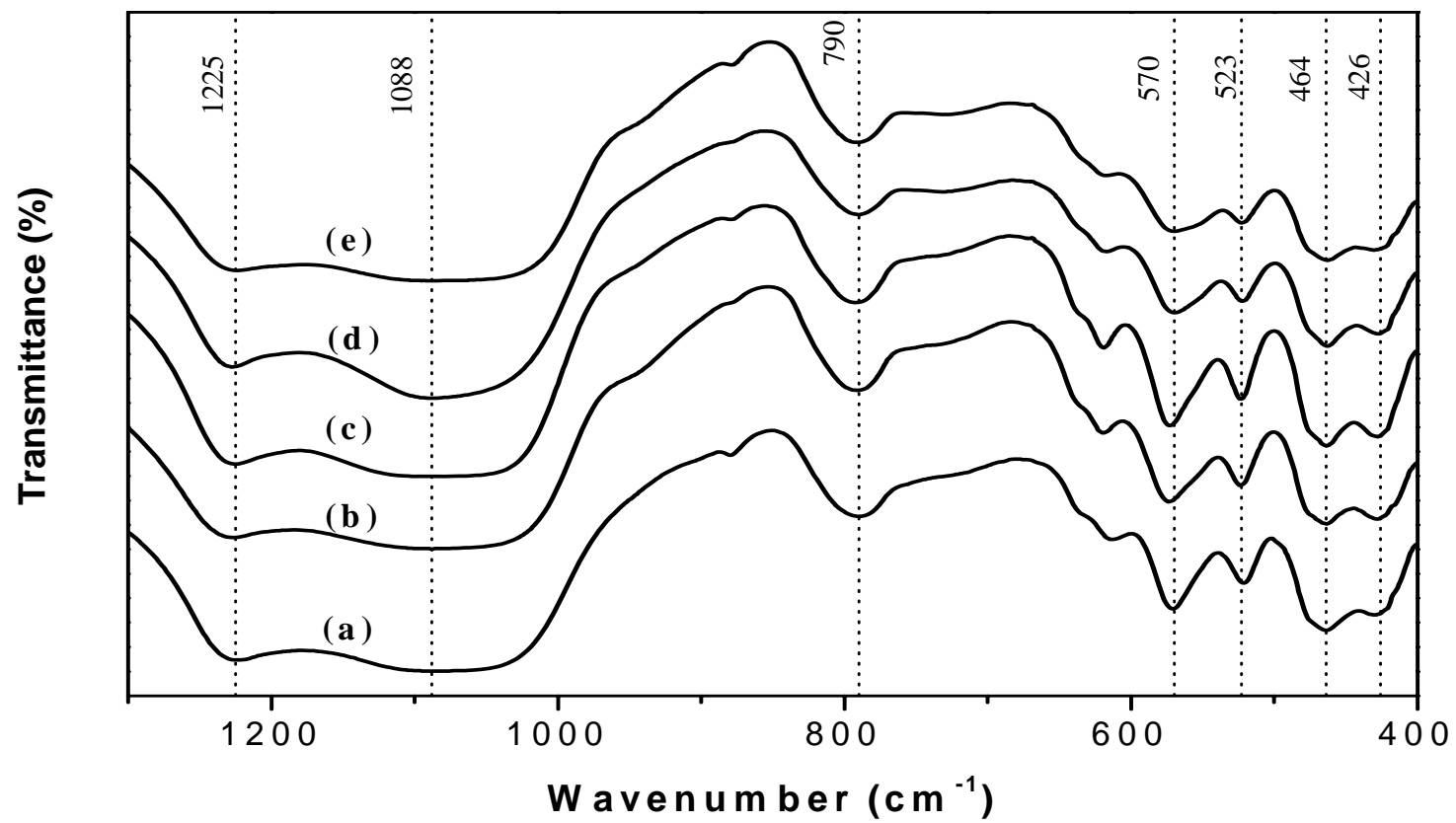


Figure 3.5 IR spectra of (a) NaBEA, (b) HBEA, (c) HBEA-1(1Pt/HBEA), (d) HBEA-2(5Co/HBEA) and (e) HBEA-1(1Pt5Co/HBEA).

There was a slight change in the IR spectra of BEA samples in which the asymmetric TO_4 band at 1083 cm^{-1} in NaBEA shifted to 1088 cm^{-1} in HBEA. This peak is a characteristic vibration of asymmetric T-O stretching which is sensitive to the content of the framework silicon and aluminum. It will be shifted toward higher frequency after converted to proton form due to Si/Al ratio was higher than sodium formed. (Thongkasam, 2006) The bands at $789 - 792\text{ cm}^{-1}$ were assigned to the asymmetric stretching and internal symmetric stretching of T-O tetrahedral vibration, which are not sensitive to zeolite structure. The bands at $570 - 573$ and $521 - 524\text{ cm}^{-1}$ were assigned to double 6-ring (D6R) and double 4-ring (D4R) which are sensitive to zeolite structure (Flanigen, 1976; Bhat and Kumar, 1990). The band at $463 - 464\text{ cm}^{-1}$ was assigned to T-O bending mode, which is not sensitive to zeolite structure, while the band at $424 - 428\text{ cm}^{-1}$ was attributed to T-O bending mode having pores structure in BEA (Eapen et al., 1994).

3.4 X-ray absorption near edge structure (XANES)

The X-ray absorption spectrum of Co in both mono- and bi-metallic catalysts were collected in transmission mode with photon energy range of $7669 - 7769\text{ eV}$ and scan rate of 0.25 eV/min . The spectrum were compared to that of the standards containing Co in different forms including Co metal foil (zero oxidation state), $\text{Co}(\text{NO}_3)_2$ and CoCl_2 (both with +2 oxidation state). The spectrum of all monometallic Co/HBEA catalysts were similar to that of CoCl_2 and $\text{Co}(\text{NO}_3)_2$ indicating that the Co in HBEA catalysts had oxidation state of +2. In the bimetallic catalysts, a slight shift to lower energy was observed in both 10Co-1Pt/HBEA and 15Co-1Pt/HBEA indicating that the oxidation state of Co might be slightly different

from that in the monometallic catalysts, probably due to the presence of Pt in these samples.

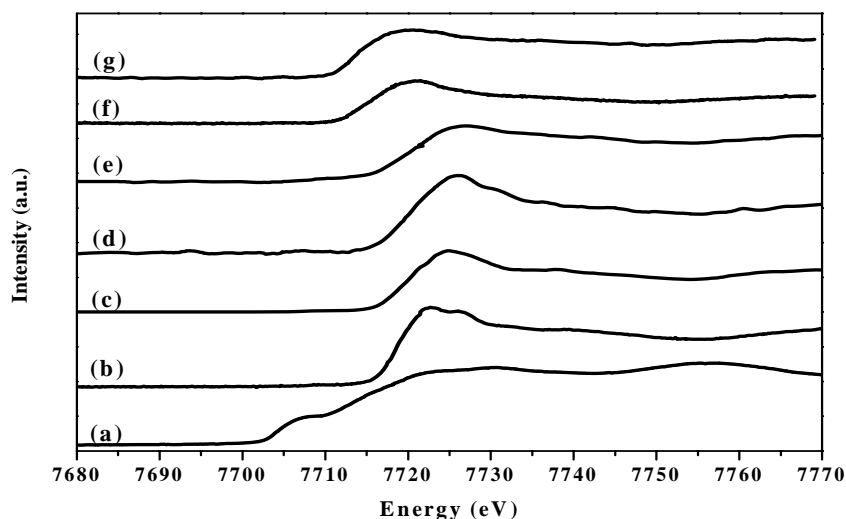


Figure 3.6 Co K-edge XANES of (a) Co foil, (b) CoCl_2 , (c) $\text{Co}(\text{NO}_3)_2$, (d) 10Co/HBEA, (e) 15Co/HBEA (f) 15Co-1Pt/HBEA, and (g) 10Co-1Pt/HBEA, respectively.

3.5 Transmission electron microscope (TEM)

HBEA-supported catalysts were also characterized by transmission electron microscopy to observe the morphology of Pt and Co particles over HBEA. The TEM micrographs of 1Pt/HBEA with magnification of 6k, 120k and 200k are shown in Figure 3.7a-d. Figure 3.7a shows shape of the catalysts with particle sizes varied from less than $1\mu\text{m}$ to $3\mu\text{m}$. Figure 3.7b show the texture of HBEA and a crystal of Pt with the size about 20 nm. Figure 3.7c and d also showed crystals of Pt on a different catalyst particle with the size about 20 nm as well. Because the Pt loading

was low, these crystals were difficult to locate and were not close to each other indicating that the chance of sintering was low. These micrographs confirmed that Pt particles were on the surface of HBEA. However, it could not rule out the idea that the Pt ions might be in the BEA structure as well because they could not be seen by TEM.

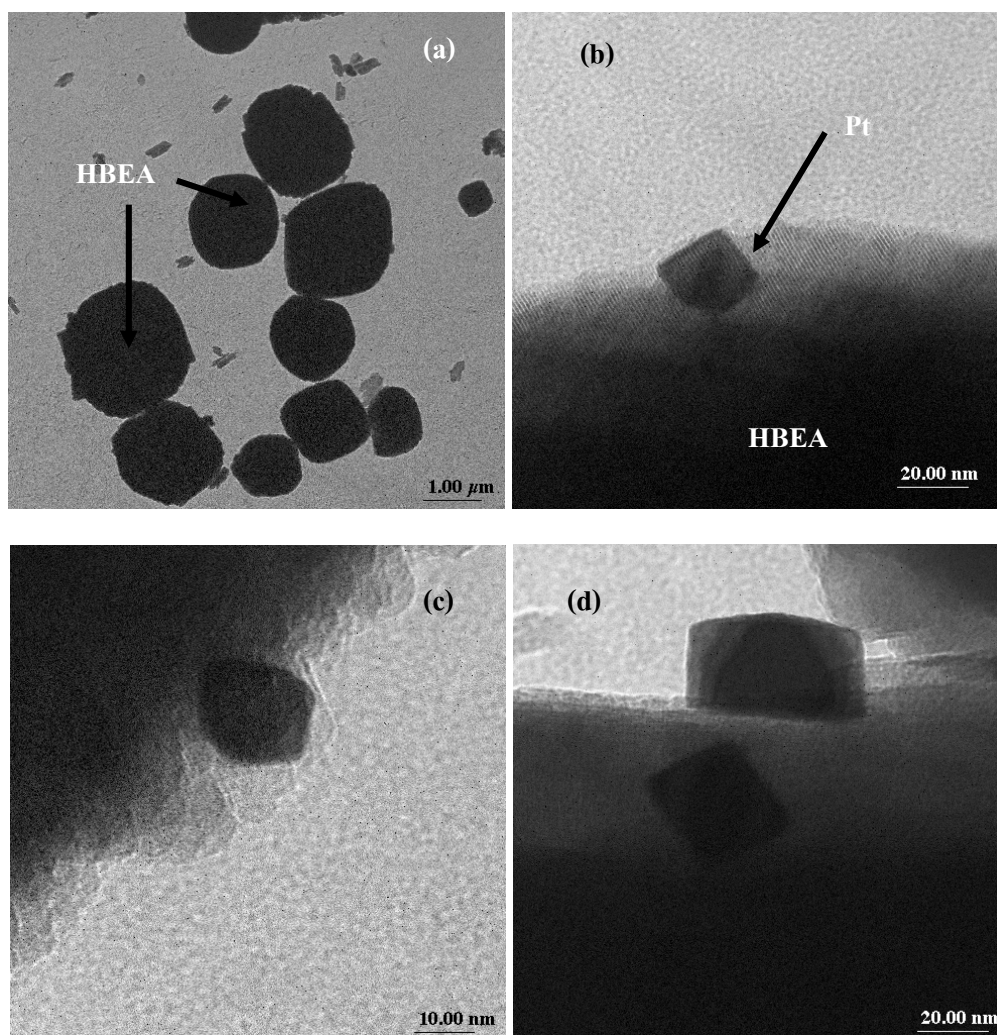


Figure 3.7 Transmission electron microscopy images of 1Pt/HBEA: (a) 6k, (b) 120k, (c) 200k and (d) 200k.

TEM micrographs of 10Co/HBEA with magnification of 6k, 60k, 120k and 200k are displayed in Figure 3.8a-d. There were some particles on HBEA as displayed in Figure b-d that might be the particle of Co. These particles did not show any crystalline characteristics such as clear edge or faces thus, Co particles might be present in an amorphous form in this catalyst. Because the atomic number of Co was much lower than that of Pt (namely, 27 versus 78), its ability to back-scatter electron was much less than Pt. Thus, the particle of Co was not as dark as Pt and was difficult to distinguish from the HBEA texture since HBEA composed of Si and Al (atomic numbers are 14 and 13, respectively).

The TEM micrographs of 5Co-1Pt/HBEA with magnification of 2k, 50k are shown in Figure 3.9a-c. Figure 3.9a shows shape of the catalysts with particle sizes varied from less than 1 μ m to 3 μ m. Figure 3.9b and c show crystals of Pt on the surface of HBEA with the size about 20 nm, similar to the particle observed in 1Pt/HBEA. These crystals were not easily found on the catalysts and were not close to each other indicating that the chance of Pt sintering was also low. Figure 3.9c and d show amorphous particles which were likely to be Co on HBEA. The shape and size of these particles were not uniform. Because the Co loading was higher than Pt, it was possible that Co might cover the Pt particles and make them difficult to locate.

Figure 3.10a-d show micrographs of 10Co-1Pt/HBEA with magnification of (a) 50k, (b) 200k and (c, d) 120k, respectively. Again, it was difficult to locate the Pt crystals because of the low loading and the higher possibility that Co might cover the Pt particles. Figure 3.10a shows dark area that might be the location of Co or Pt. Figure 3.10a shows dark area that might be the location of Co or Pt. Figure 3.10b shows some area of HBEA that still maintained high uniformity. Figure 3.10c and d show some non-uniform particles on the surface of HBEA.

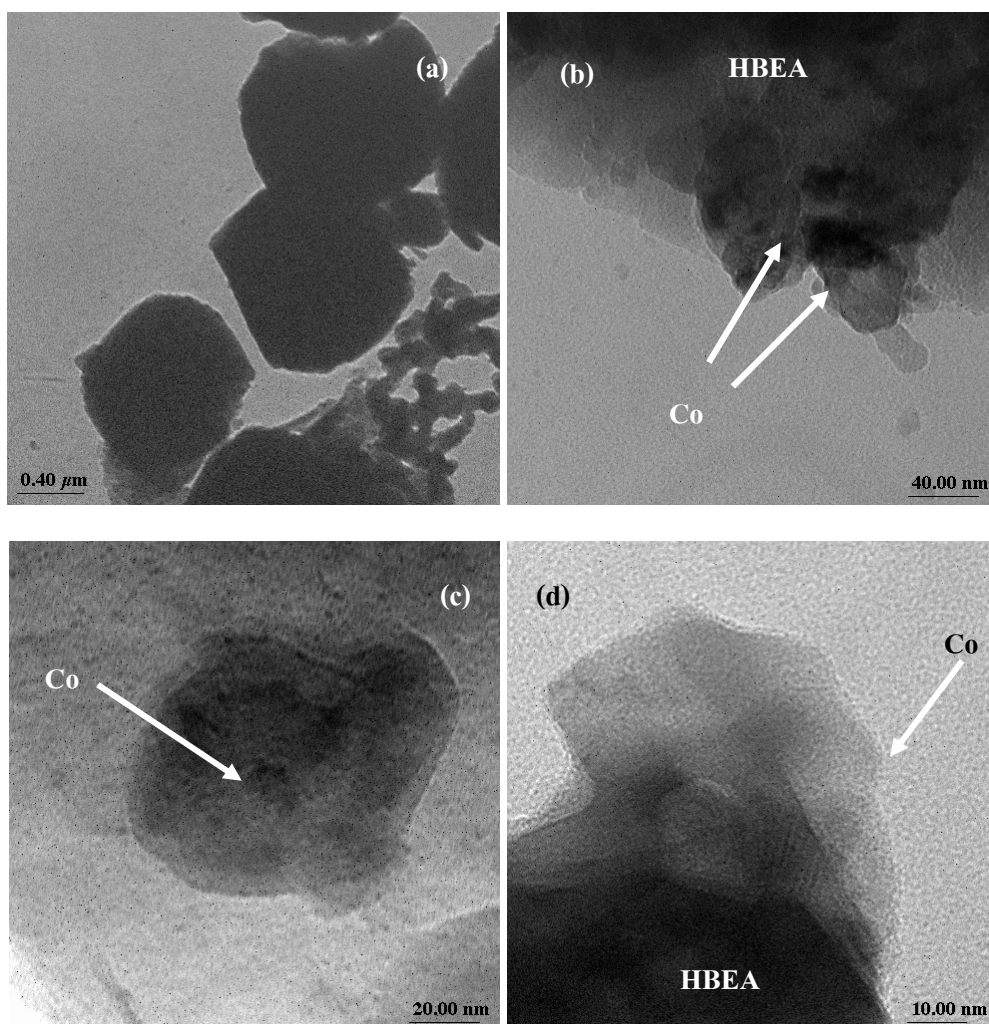


Figure 3.8 Transmission electron microscopy images of 10Co/HBEA: (a) 6k, (b) 60k, (c) 120k and (d) 200k.

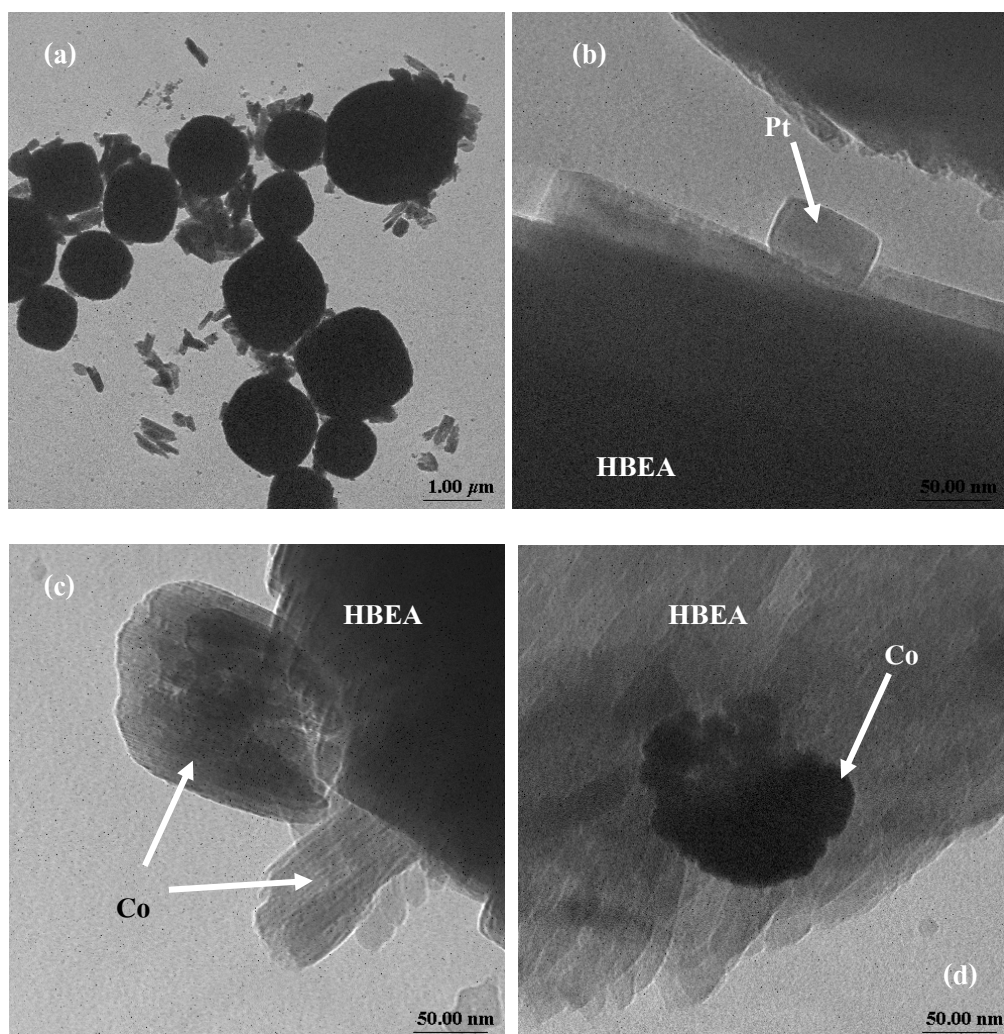


Figure 3.9 Transmission electron microscopy images of 5Co-1Pt/HBEA: (a) 2k, (b) 50k, (c) 50k and (d) 50k.

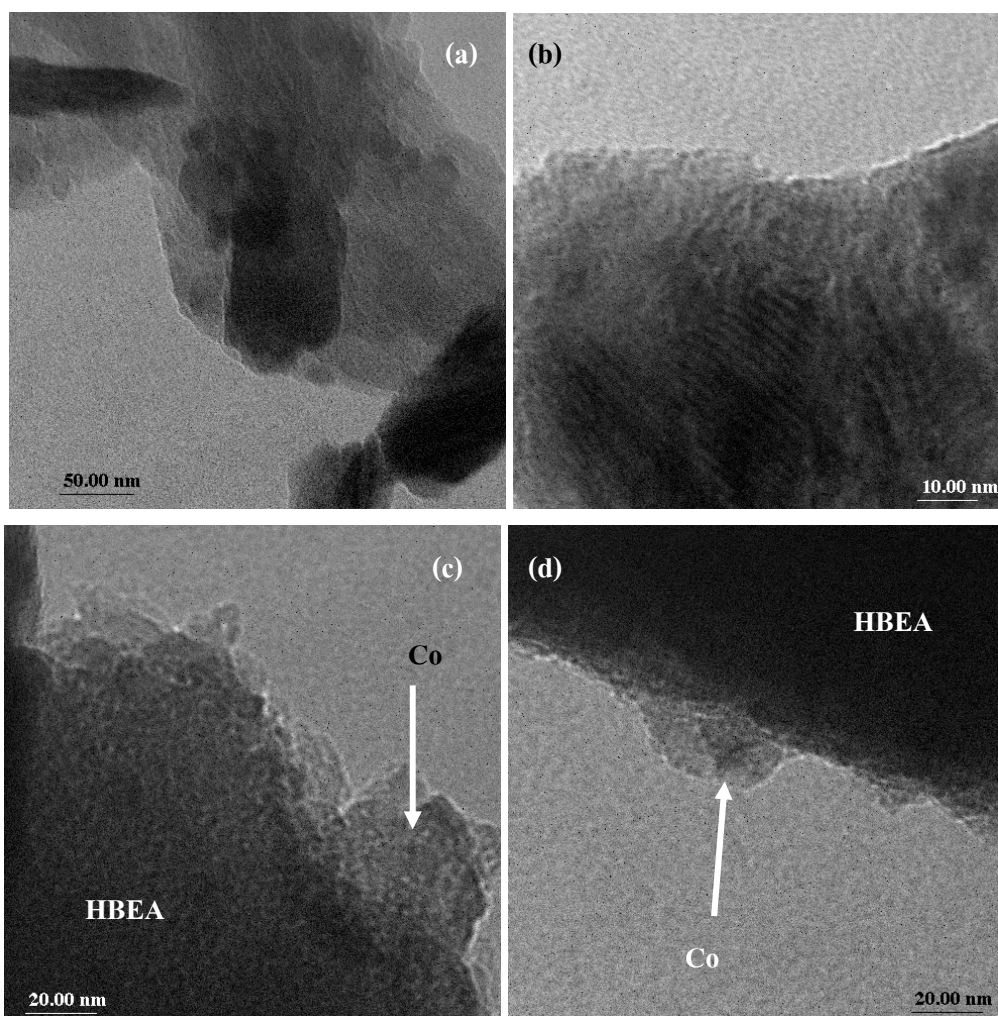


Figure 3.10 Transmission electron microscopy images of 10Co-1Pt/HBEA: (a) 50k, (b) 200k, (c) 120k and (d) 120k.

Finally, from TEM results can be concluding that Pt nanocrystals were observed in mono and bimetallic catalysts with the size about 20 nm. For Co particles both in mono and bimetallic catalysts are show characteristic of amorphous.

CHAPTER IV

CATALYTIC TESTING FOR PROPANE

HYDROGENOLYSIS

The catalytic performance of monometallic Pt and Co catalysts were studied at 200 - 400°C. The results were compare with bimetallic catalyst and physically mixture between monometallic Pt and Co.

4.1 Propane hydrogenolysis on monometallic catalysts

Because the main interest in this work was the performance of bimetallic catalysts for propane hydrogenolysis. The tests on monometallic catalysts were first performed for further comparison. These catalysts were 1Pt/HBEA, 5Co/HBEA, 10Co/HBEA and 15Co/HBEA. The results from the evaluation at 200 - 400°C including conversions and selectivities are displayed in Figure 4.1 through 4.20.

4.1.1 Propane hydrogenolysis over Pt/HBEA

The average conversion and product distribution of propane hydrogenolysis over 1Pt/HBEA evaluated at 200, 250, 300, 350 and 400°C are displayed in Figure 4.1. The full details of the evaluation and conditions can be found in appendix B. The conversion increased with temperature from 200 to 300°C. The conversion at 200 and 250°C were 6.97 and 21.14% respectively. Nearly complete conversion (98 - 99%) was obtained at 300, 350 and 400°C. This result indicated that

1Pt/HBEA was an effective catalyst for propane hydrogenolysis.

The products from propane hydrogenolysis are mainly methane and ethane. At 200°C the methane selectivity was about 90% and it increased when the temperature was increased to 250 and 300°C. At these temperatures propane and hydrogen adsorbed on the catalysts and reacted, causing a cleavage of C-C bond and produce both methane and ethane. Then ethane subsequently reacted with hydrogen to produce methane or desorbed from the catalyst. At these temperature, the sequential hydrogenolysis was slow and ethane desorption was observed in large amount. At 350 and 400°C, the methane selectivity was 98.7 and 99.8%, respectively. At these temperatures, the sequential hydrogenolysis was more feasible than the ethane desorption, resulting in the less amount of ethane and higher methane selectivity.

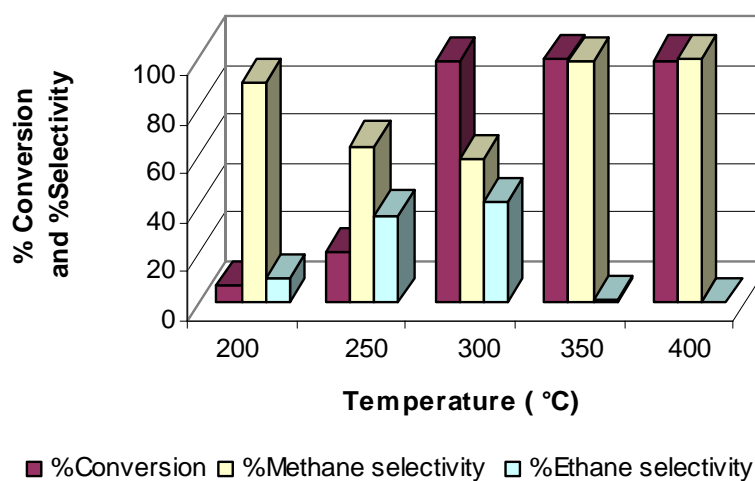


Figure 4.1 Conversion and selectivities of propane hydrogenolysis over 1Pt/HBEA.

The run-up and run-down conversions over 1Pt/HBEA displayed in Figure 4.2. The conversion with the increased temperature is referred to as “run-up” and the conversion with the decreased temperature is referred to as “run-down”. After testing at 400°C, the catalysts were cooled down and the catalytic performance was repeated with similar conditions. At 350°C the conversion remained the same but at 300, 250 and 200°C, the conversion decreased indicating that deactivation occurred. The cause of deactivation was likely coking, a carbonaceous deposition that covered the catalytic active sites. This was confirmed by the appearance of the catalyst. The catalyst color after the reaction was darker than at the beginning of the test. The other cause of deactivation was metal sintering in which small metal particles aggregated to form larger particles. However, the chance for sintering was for this catalyst because the metal loading was low.

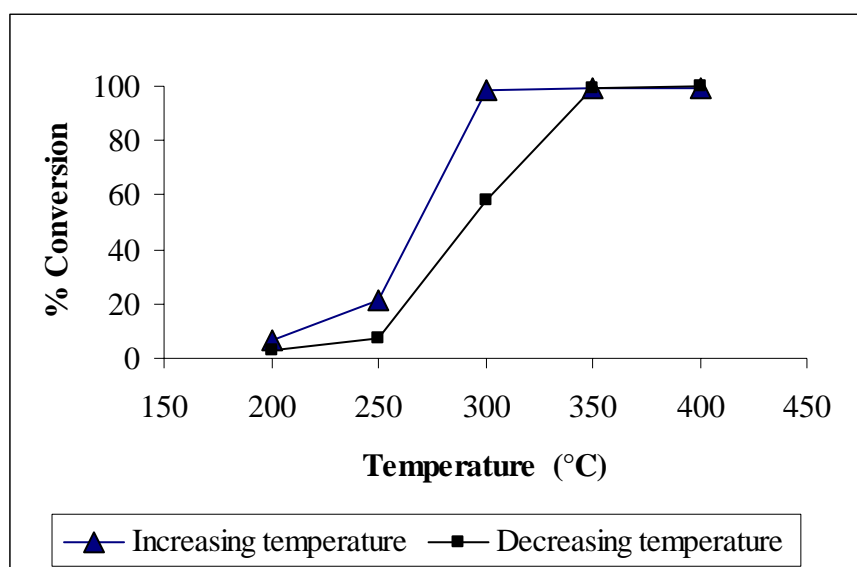


Figure 4.2 Conversion of propane hydrogenolysis over 1Pt/HBEA as the temperature increased (—▲—) and decreased (—■—).

4.1.2 Propane hydrogenolysis over Co/HBEA

The performance of HBEA-supported cobalt catalysts with metal loading of 5, 10 and 15wt% were only evaluated at 300, 350 and 400°C. However, the propane conversion was not observed at 200 and 250°C in all catalysts. Thus, this part only discussed the results from the tests at 300, 350 and 400°C.

The performance of 5Co/HBEA is displayed in Figure 4.3. The conversions of propane increased with temperature, namely 21, 24 and 79% at 300, 350 and 400°C, respectively. For this catalyst, methane was the only observed product. It could be postulated that propane adsorb dissociatively on cobalt to form two methyl species and a carbene. These species could react with surface proton to form methane. Another possibility was that the propane dissociatively adsorb as methyl and ethyl. Then the surface ethyl underwent sequential hydrogenolysis to produce methane.

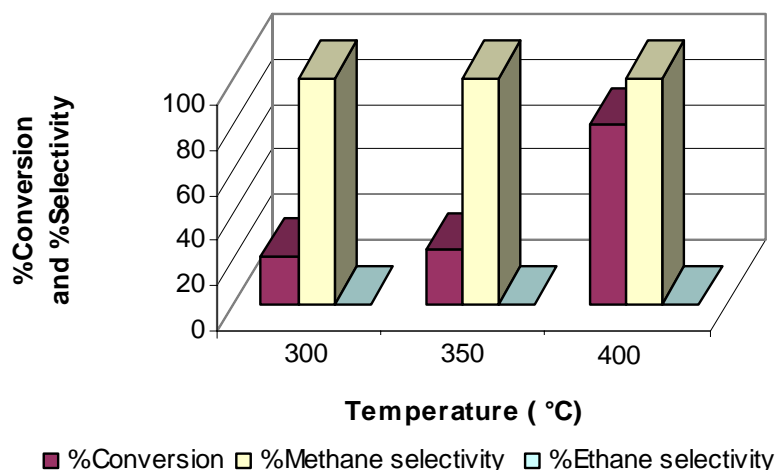


Figure 4.3 Conversion and selectivities of propane hydrogenolysis over 5Co/HBEA.

After testing at 400°C, the catalyst was cooled down and the catalytic performance was repeated with similar conditions. The run-down conversions were compared with the run-up conversions as displayed in Figure 4.4 and the full details are tabulated in Appendix B. The conversions were only slightly decreased (less than 3%) indicating that the catalyst deactivation of the catalyst was not significant at this condition. Because the catalyst color after the reaction was darker than at the beginning of the test, coking also occurred at this condition.

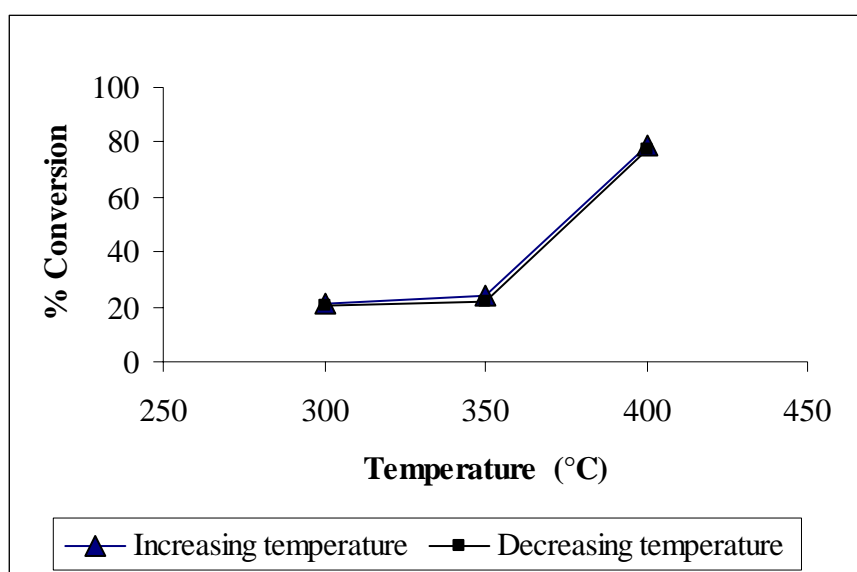


Figure 4.4 Conversion of propane hydrogenolysis over 5Co/HBEA as the temperature increased (—▲—) and decreased (—■—).

The performance of 10Co/HBEA is displayed in Figure 4.5. The conversions of propane also increased with temperature, namely 4, 77 and 93% at 300, 350 and 400°C, respectively. Similar to the 5Co/HBEA, methane was the only observed product. This confirmed that indicating that the sequential ethane dehydrogenation was a preferred reaction over ethane desorption.

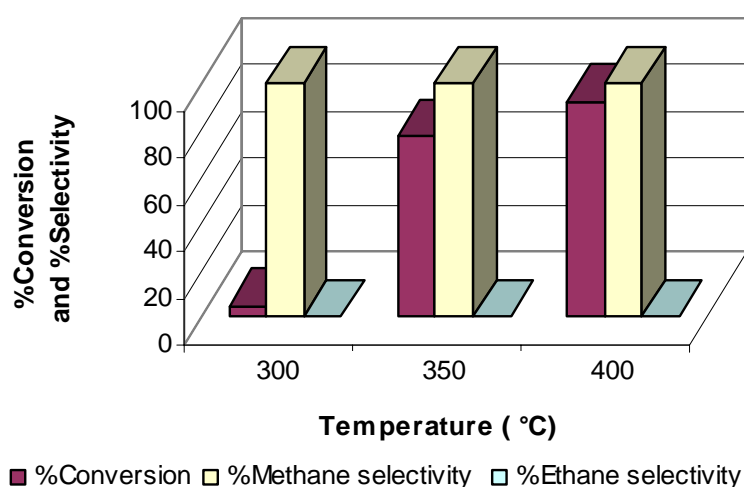


Figure 4.5 Conversion and selectivities of propane hydrogenolysis over 10Co/HBEA.

After decreasing the temperature, the performance was studied again. As shown in Figure 4.6, the decreased of propane conversion was significantly observed at 350°C. This was also caused by coking as confirmed by the catalyst appearance after the reaction.

The performance of 15Co/HBEA is displayed in Figure 4.7. The conversions of propane also increased with temperature, namely 69, 78 and 100% at 300, 350 and 400°C, respectively and methane was the only observed product.

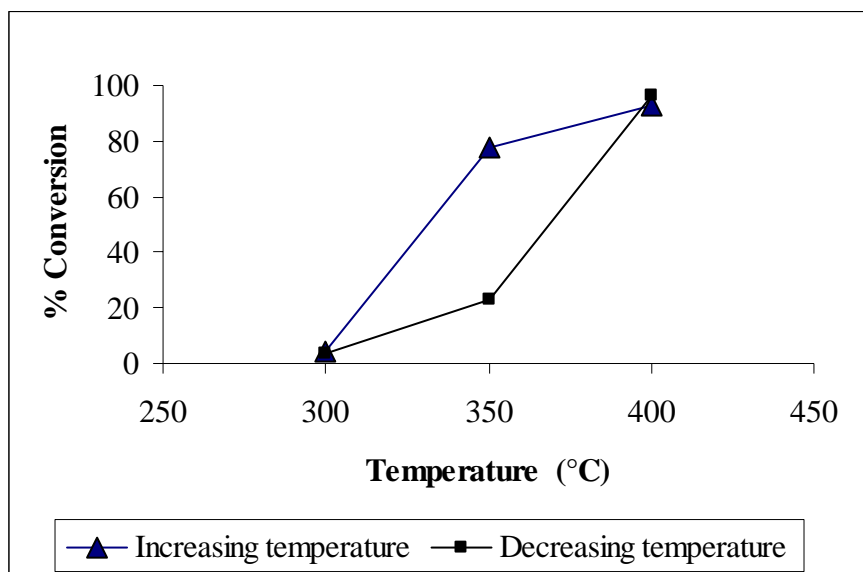


Figure 4.6 Conversion of propane hydrogenolysis over 10Co/HBEA as the temperature increased (\blacktriangle) and decreased (\blacksquare).

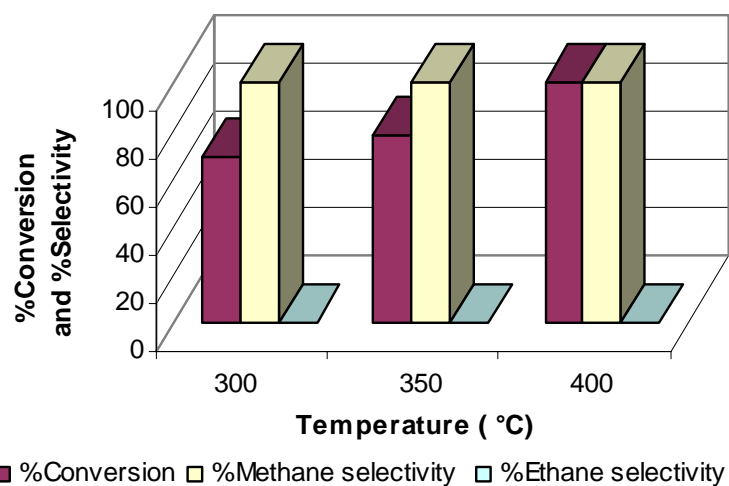


Figure 4.7 Conversion and selectivities of propane hydrogenolysis over 15Co/HBEA.

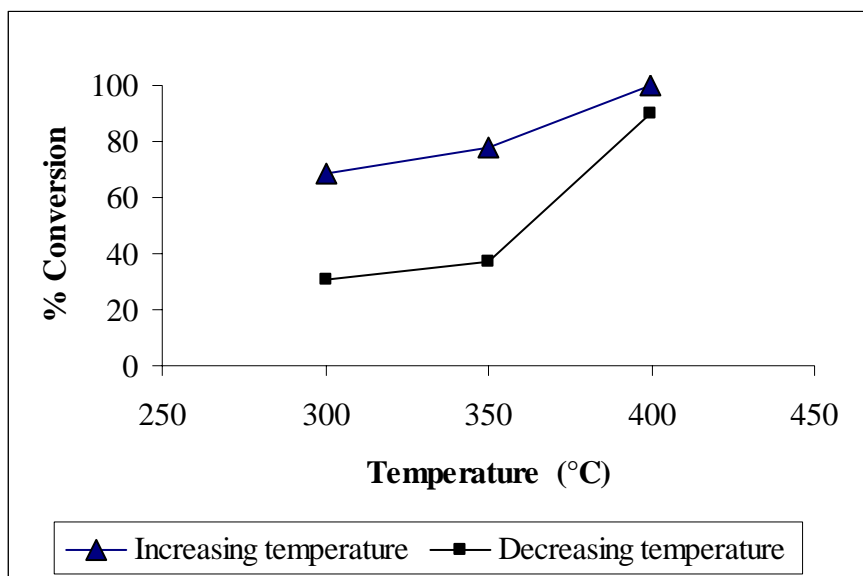


Figure 4.8 Conversion of propane hydrogenolysis over 15Co/HBEA as the temperature increased (—▲—) and decreased (—■—).

After testing at 400°C, the temperature was decreased and the catalytic performance was studied again to observe catalyst deactivation. The propane conversion decreased significantly in the run-down temperature (see Figure 4.8). Thus, coking became more severe with higher Co loading.

4.2 Propane hydrogenolysis over bimetallic CoPt/HBEA

The HBEA-supported bimetallic catalysts in this study were 5Co-1Pt/HBEA, 10Co-1Pt/HBEA, 15Co-1Pt/HBEA. At the beginning, a physically mixed catalyst between 5Co/HBEA with 1Pt/HBEA was also tested to compare with the bimetallic 5Co-1Pt/HBEA to ensure that the preparation of bimetallic catalysts by impregnation improved the catalytic performance. All catalysts were evaluated at 200 - 325°C. The results included propane conversion and product selectivity.

4.2.1 Propane hydrogenolysis over a physically mixed catalyst 1Pt/HBEA and 5Co/HBEA

This study was carried out to ensure that the catalysts prepared by co-impregnation had better performance for propane hydrogenolysis than that obtained by physically mixing of Pt/HBEA and Co/HBEA. The comparison was made only on the catalysts with 1Pt and 5Co loading because the 5Co/HBEA showed the best stability.

The propane conversions and product selectivities over the physically mixed catalyst 1Pt/HBEA and 5Co/HBEA are shown in Figure 4.9. The conversion increased with the temperature; it was less than 3% at 200 and 250°C and approached the maximum conversion of 96% at 400°C. There were two products at all temperature. The major product was methane and the minor product was ethane. The performances of the physically mixed catalyst were more or less similar to the monometallic 1Pt/HBEA and monometallic 5Co/HBEA. When the monometallic 1Pt/HBEA catalyst was tested, ethane was observed as a minor product at all temperature. When the monometallic 5Co/HBEA catalyst was tested, the propane conversion increased with temperature and reached the maximum at 400°C. Because

the two catalysts were only physically mixed, there was no interaction or enhancing effect on each other's catalytic performance.

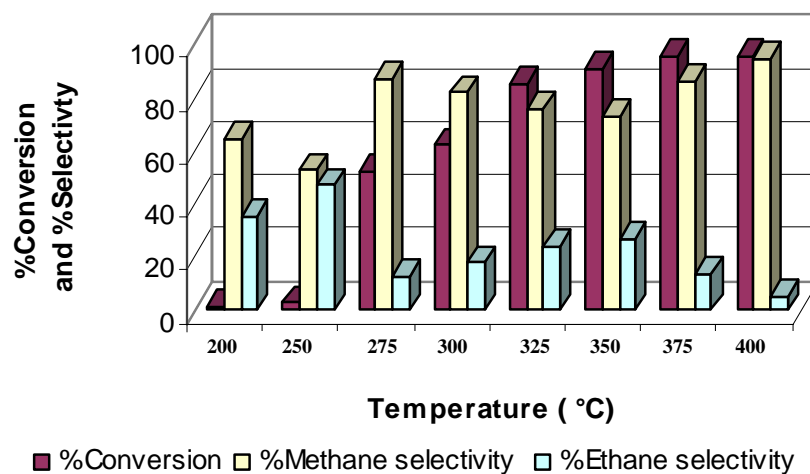


Figure 4.9 Conversion and selectivities of propane hydrogenolysis over a physically mixed catalyst 1Pt/HBEA and 5Co/HBEA.

After the test at 400°C, the catalyst was cooled down and the catalytic performance was determined again to observe catalytic deactivation. The comparison between the conversions with the increased temperature and the decreased temperature is shown in Figure 4.10. The conversion after cooling down was lower than the beginning indicated that catalyst deactivation occurred. From the darker appearance of the catalyst after the test, coking was the major cause of catalyst deactivation.

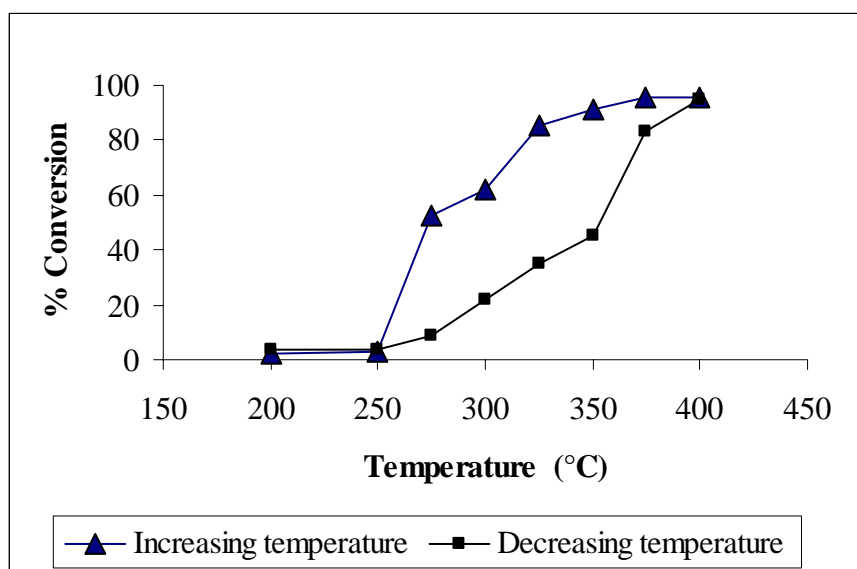


Figure 4.10 Conversion of propane hydrogenolysis over a physically mixed 1Pt/HBEA and 5Co/HBEA as the temperature increased (\blacktriangle) and decreased (\blacksquare).

4.2.2 Propane hydrogenolysis over CoPt/HBEA prepared by co-impregnation

The propane conversion over 5Co-1Pt/HBEA is shown in Figure 4.11. The conversion increased with temperature and reached 99% at 325°C and the only observed product at all tested temperature was methane. To observe deactivation, the run-down conversion was determined. The run-down conversion decreased slightly as shown in Figure 4.12 indicating that the degree of deactivation was low.

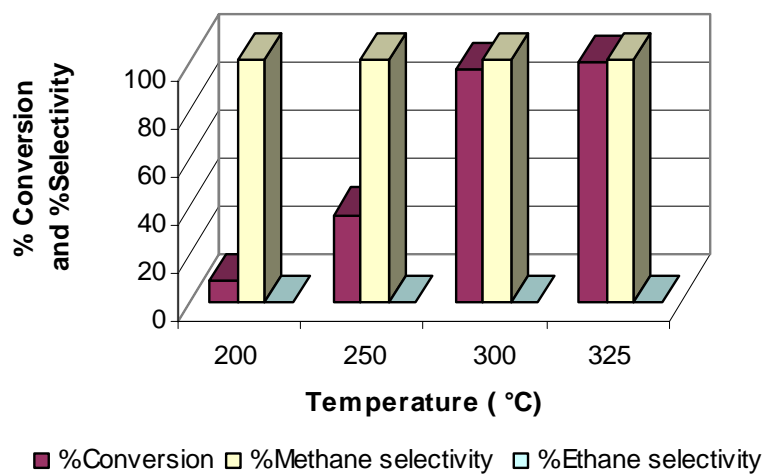


Figure 4.11 Conversion and selectivities of propane hydrogenolysis over 5Co-1Pt/HBEA.

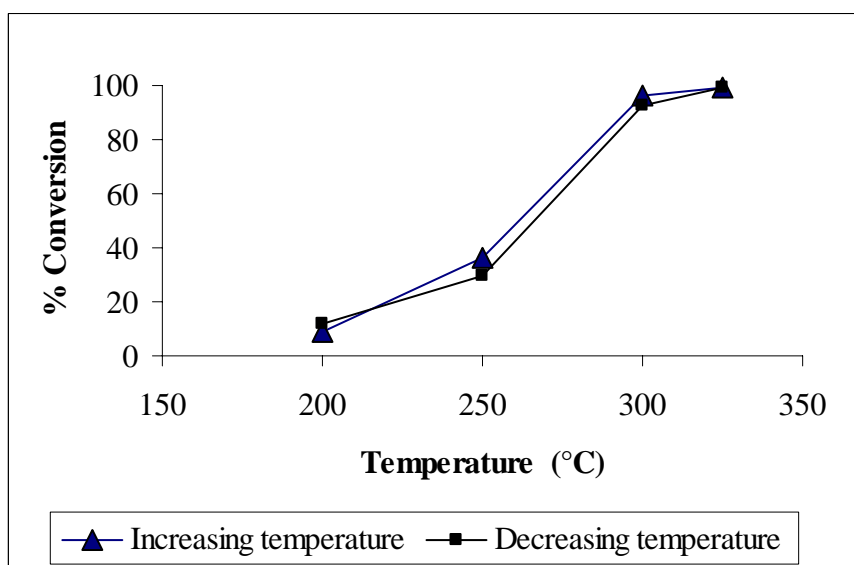


Figure 4.12 Conversion of propane hydrogenolysis over 5Co-1Pt/HBEA as the temperature increased (\blacktriangle) and decreased (\blacksquare).

The conversion of propane over 10Co-1Pt/HBEA is shown in Figure 4.13. The conversion increased with temperature and reached 93% at 350°C and the only observed product at all tested temperature was methane. When the catalyst was cooled down, the propane conversion decreased more than observed on the 5Co-1Pt/HBEA catalyst as shown in Figure 4.14 indicating that the degree of deactivation increased as the loading of Co increased.

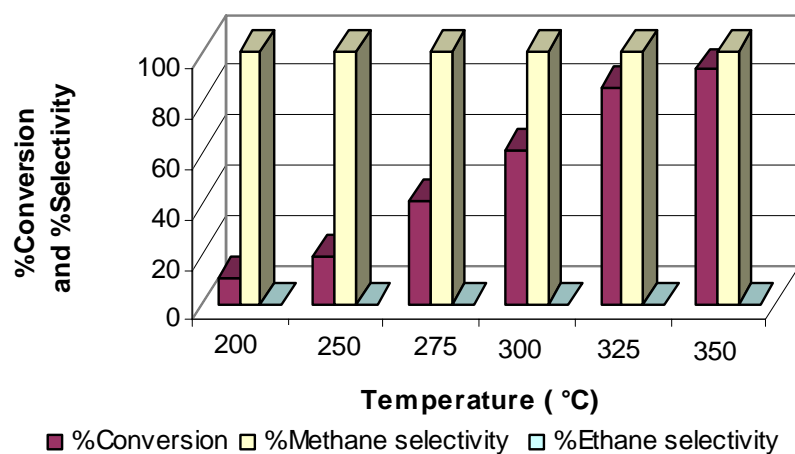


Figure 4.13 Conversion and selectivities of propane hydrogenolysis over 10Co-1Pt/HBEA.

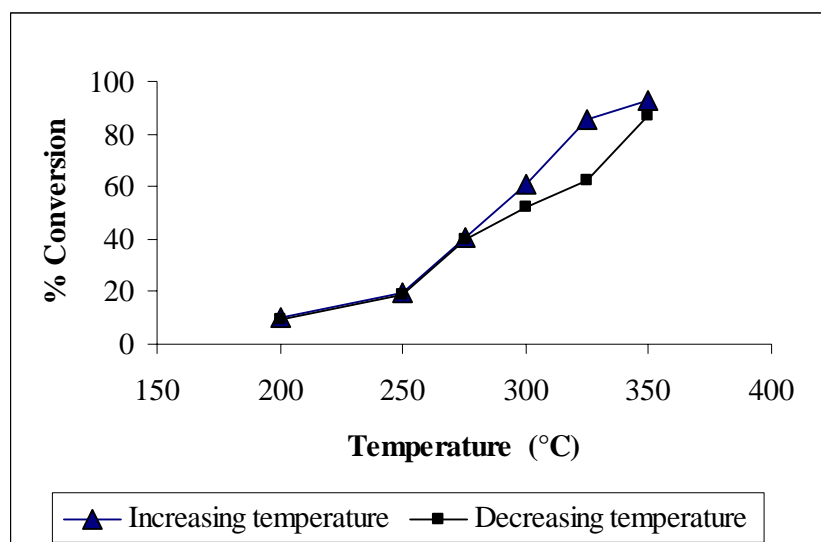


Figure 4.14 Conversion of propane hydrogenolysis over 10Co-1Pt/HBEA as the temperature increased (▲) and decreased (■).

The conversion of propane over 15Co-1Pt/HBEA is shown in Figure 4.15. The conversion increased with temperature and reached 95% at 350°C which was similar to the previous catalyst (5Co-1Pt/HBEA). However, this catalyst was more active than the 10Co-1Pt/HBEA at lower temperature. The only observed product at all tested temperature was also methane. When the catalyst was cooled down, the propane conversion decreased at all tested temperature, more than observed on the catalysts with lower Co loading (see Figure 4.16) confirming that the degree of deactivation increased with Co loading.

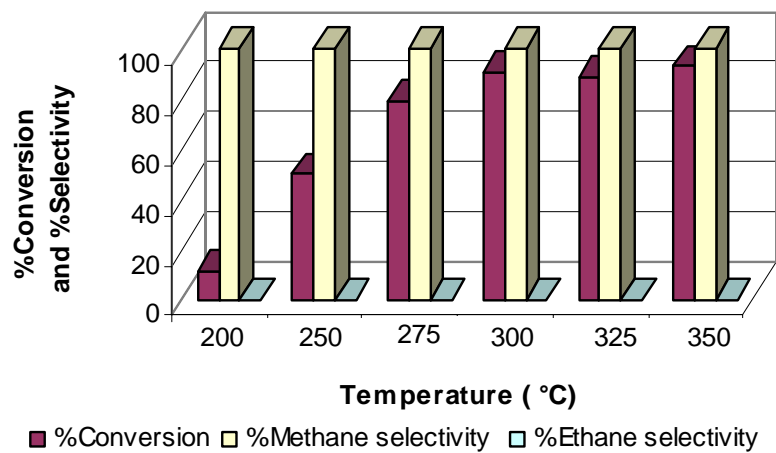


Figure 4.15 Conversion and selectivities of propane hydrogenolysis over 15Co-1Pt/HBEA.

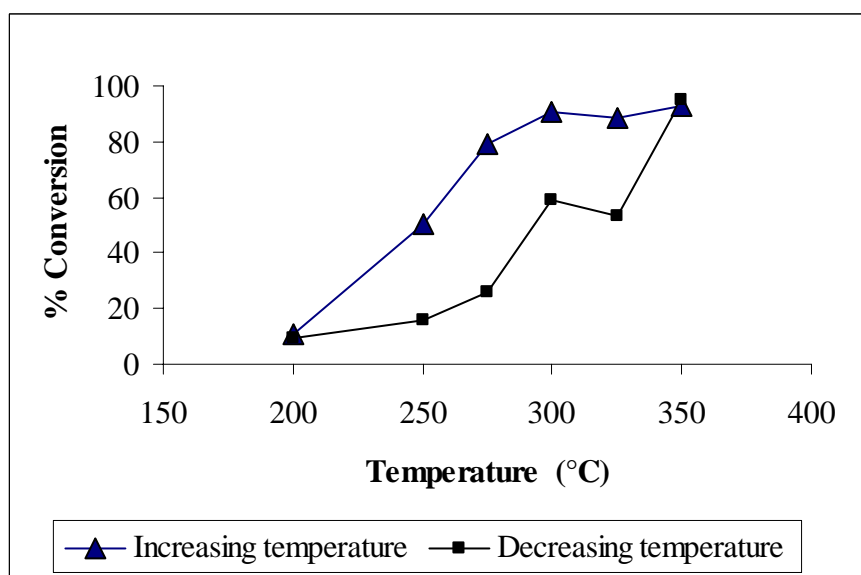


Figure 4.16 Conversion of propane hydrogenolysis over 15Co-1Pt/HBEA as the temperature increased (\blacktriangle) and decreased (\blacksquare).

To compare the catalyst performance with different Co loading, the propane conversion over 5Co-1Pt/HBEA, 10Co-1Pt/HBEA and 15Co-1Pt/HBEA are plotted together in Figure 4.17. At 200°C the conversions over all catalysts were the same (about 10%). Then the conversion increased with temperature. At high temperature the 5Co-1Pt/HBEA was the most active catalyst. It was possible that the catalysts with high Co loading had large metal particles and low surface area, resulting in lower activity.

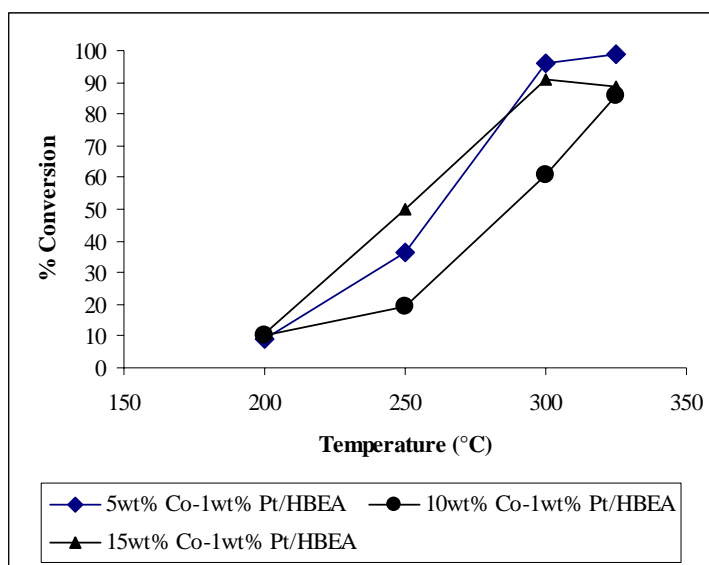


Figure 4.17 Conversion of propane over 5, 10 and 15Co-1Pt/HBEA.

4.2.3 Comparison between performance of 5Co-1Pt/HBEA prepared by co-impregnation and a physically mixed catalyst 1Pt/HBEA and 5Co/HBEA

Figure 4.18 shows comparison of propane conversion over the 5Co-1Pt/HBEA prepared by co-impregnation and physically-mixed between 5Co/HBEA and 1Pt/HBEA. The results indicated that the bimetallic catalyst from co-impregnation had higher propane conversion at all temperature.

When compared with monometallic catalysts, the order of catalyst activity can be ranged in the following order: 1Pt/HBEA \cong 5Co-1Pt/HBEA > physically mixed 5Co/HBEA with 1Pt/HBEA > 5Co/HBEA.

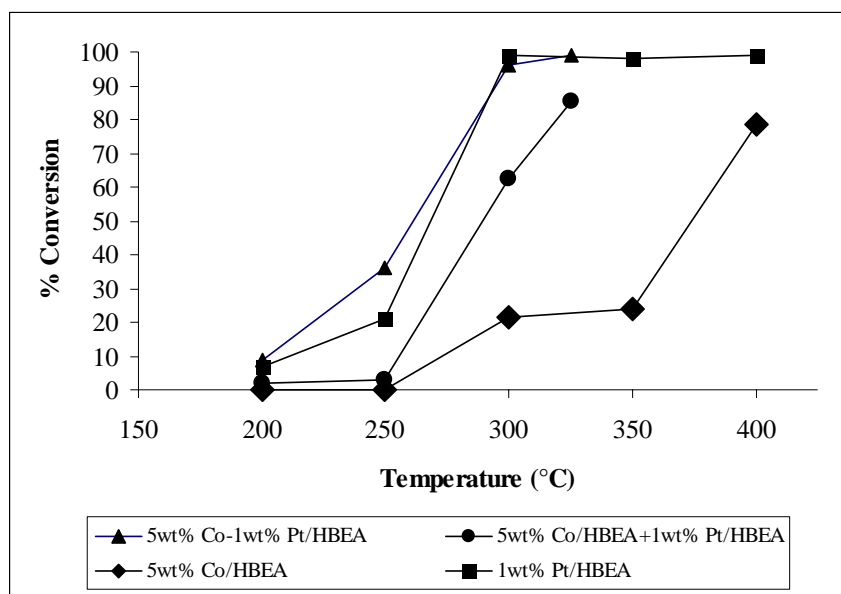


Figure 4.18 Compare conversions of propane over between 5Co-1Pt/HBEA and mix 5Co/HBEA with 1Pt/HBEA.

From Figure 4.19 the products from the 5Co-1Pt/HBEA catalyst prepared by co-impregnation were mainly methane with trace amount of ethane while that from the physically mixed catalysts were both methane and ethane.

Because monometallic platinum was more active than the monometallic cobalt and 5Co/HBEA was the most active cobalt catalyst, therefore 5Co-1Pt/HBEA catalysts were studied to observe the improvement from the monometallic catalysts. The improvement in conversion was observed and the products were only methane. Cobalt catalysts demonstrated much poorer activity than the

platinum. At 300°C the conversion on cobalt catalysts is about four times less than that on platinum catalysts moreover, the PtCo bimetallic catalysts gave higher propane conversion than monometallic catalysts at the same temperature. This suggests that bimetallic catalysts enhanced propane hydrogenolysis.

The physically mixed 5Co/HBEA and 1Pt/HBEA catalysts, gave different propane conversion and selectivity bimetallic catalyst with the same amount of metal. On the bimetallic catalyst, the propane conversion was higher and methane was the only observed product. In addition, the bimetallic catalyst had higher stability.

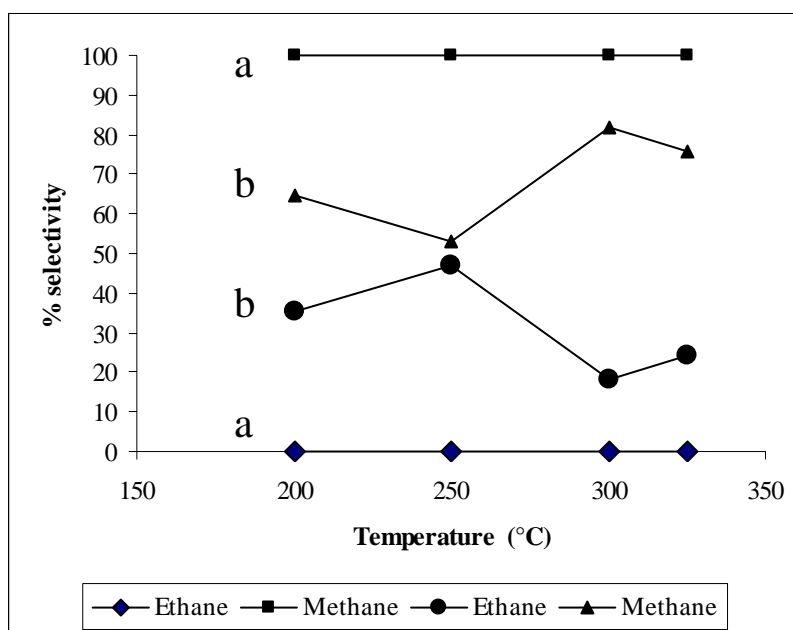


Figure 4.19 Compare product selectivities over between a) 5Co-1Pt/HBEA and b) mix 5Co /HBEA with 1Pt/HBEA.

4.2.4 Stability of 5Co-1Pt/HBEA

According to all the catalytic testing results, the best catalyst was 5Co-1Pt/HBEA because it gave high propane conversion and did not show deactivation in the run-down experiment. Further experiment was performed to observe catalyst deactivation by performing the test for 12 hours. The results are shown in Figure 4.20. This catalyst was not deactivated during the test because the propane conversion remained constant and the only observed product at all tested temperature was methane.

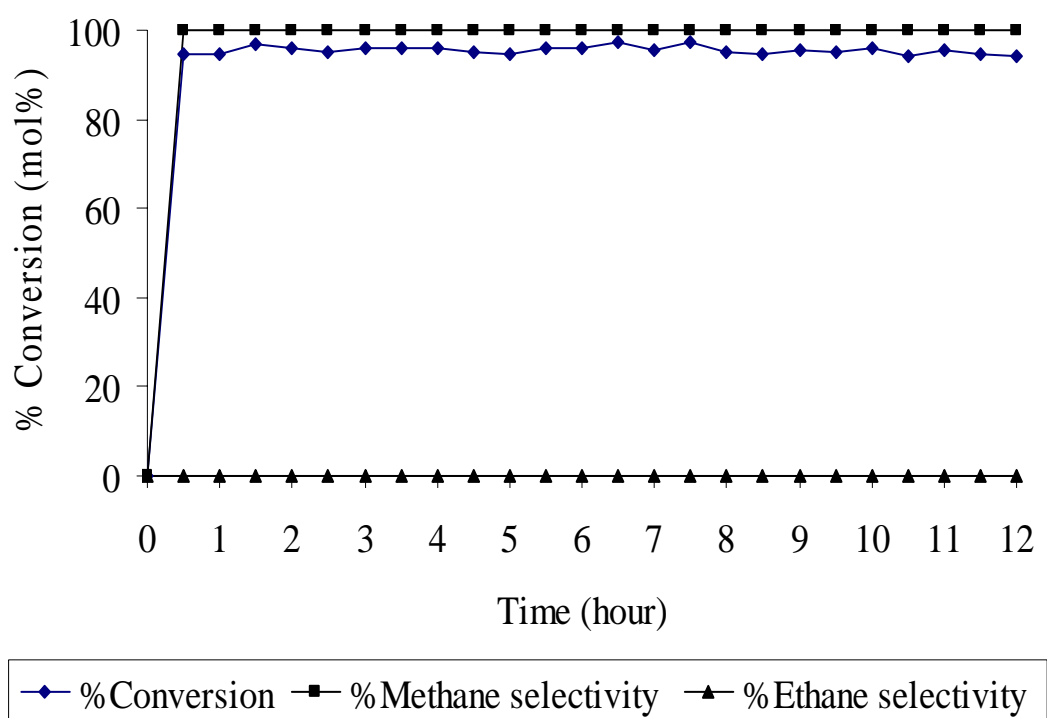
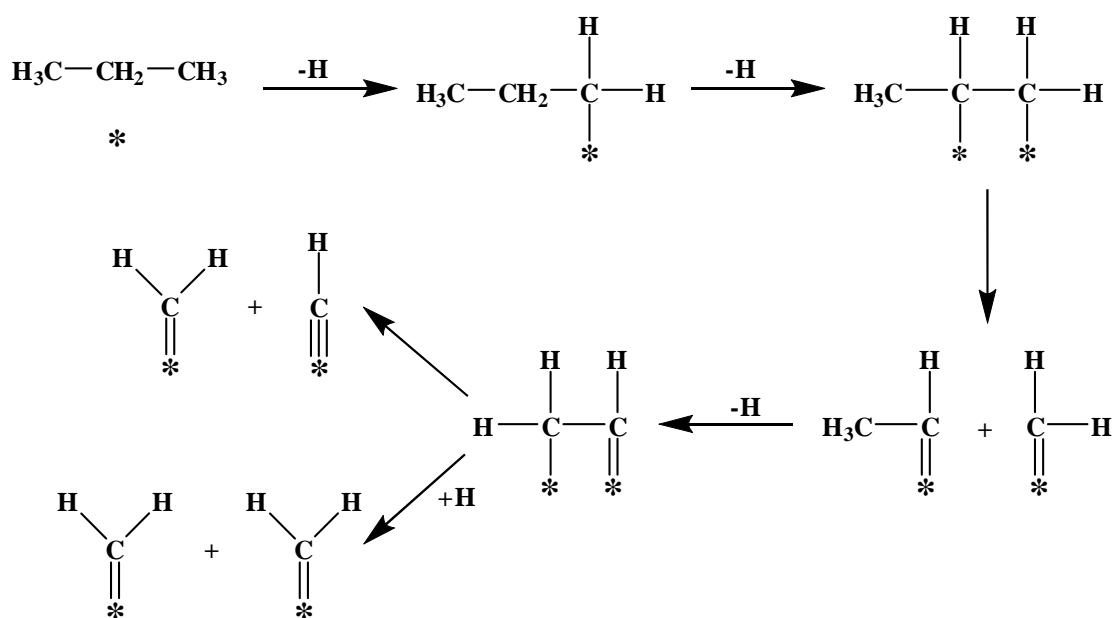


Figure 4.20 Propane conversion and product selectivities over 5Co-1Pt/HBEA at 300°C.

4.3 Surface mechanism of propane hydrogenolysis

Based on the product distributions observed during the catalysts testing in this study and information obtained from other published work, the following mechanistic sequence could be proposed for propane hydrogenation which produced ethane and methane.

(a) Propane dissociative adsorption followed by C–C bond cleavages (Cracking)



(b) Hydrogen dissociative adsorption

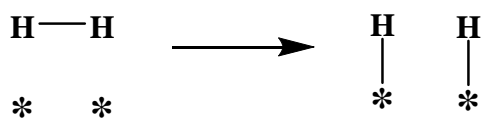


Figure 4.21 (a) A proposed mechanism of propane adsorption and cracking on the surface (b) dissociative adsorption of hydrogen on the surface, * represents catalytic active site.

In the first step, propane dissociatively adsorbs to the surface in the form of surface propyl as shown in Figure 4.21. The adsorbed propyl then undergoes breakage of carbon-carbon bonds to ethyl and methyl species, respectively. Ethyl and methyl formation are desorbed as ethane and methane as shown in Figure 4.22. In addition, hydrogen gas dissociatively adsorbs to form surface hydrogen. Then the surface species from propane react with surface hydrogen to form products.

Figure 4.22 demonstrated the formation of products from surface species derived from propane and surface hydrogen. The dehydrogenation reaction in the presence of platinum or cobalt-based catalysts was significantly higher than that in the absence of catalyst. Thus, these metals help to reduce the activation energy for the above reaction.

Bimetallic catalysts (Co/Pt), suggest that the reaction mechanism on both surfaces was the same. It has been proposed that the precursor for C-C bond breaking is an adsorbed C_3H_6 species bound to the surface via two single carbon-metal bonds, which may involve more than one metal surface atom.

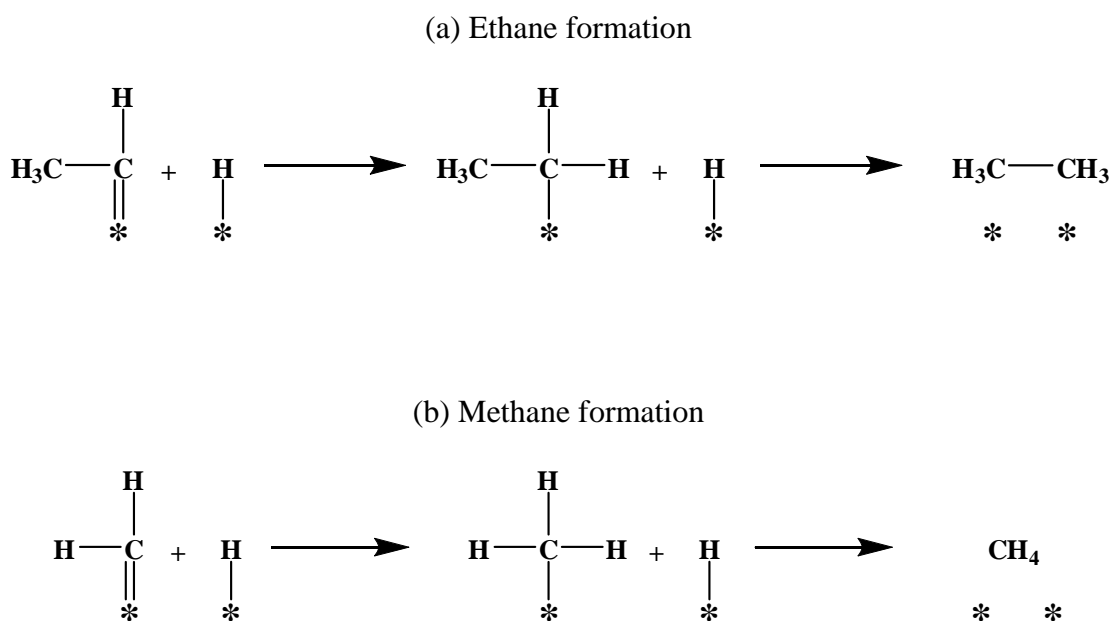


Figure 4.22 A proposed mechanism of (a) ethane and (b) methane formation on surface.

4.4 Causes of catalyst deactivation

The major cause of catalyst deactivation in this work was coking and other possibilities were metal sintering and phase change. Figure 4.23a-c illustrated those three phenomena. Coking could block the active sites on the metal or cause support pore clogging. Sintering could occur from atomic migration or crystallite migration to form larger particle and resulted the loss of catalyst's active surface. The last cause of deactivation is a combination between sintering and solid-solid phase transitions of the washcoat and encapsulation of active metal particles. In this case, the pores of the support collapse and make it impossible for the reactants to diffuse to the active sites. This phenomena also brings the small crystals close to each other and agglomerate to form larger crystals.

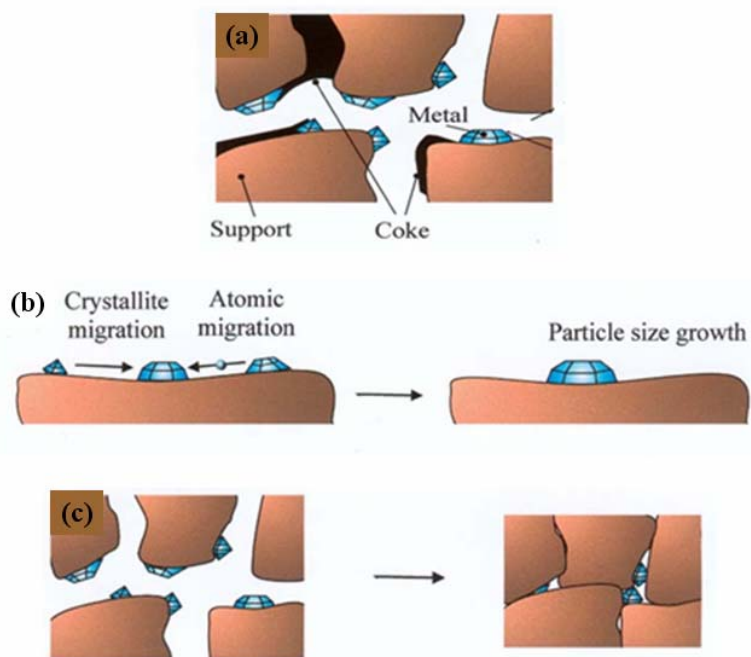


Figure 4.23 Deactivation mechanisms: (a) Coke formation, (b) Sintering of the active metal particles, and (c) Sintering and solid-solid phase transitions of the washcoat and encapsulation of active metal particles.

CHAPTER V

CONCLUSION

Silica from rice husk was used for the synthesis of zeolite beta (BEA) by hydrothermal method. The BEA in proton form (HBEA) was employed as a support for mono- and bimetallic catalysts containing Pt and Co. The Pt metal loading was fixed at 1wt% and that of Co was 5, 10 and 15wt%. The HBEA and HBEA-supported catalysts were characterized by XRD, FTIR, nitrogen adsorption, TEM and X-ray absorption. Results from XRD and FTIR indicated that the structure of HBEA did not change after impregnated with metal. However, with the increase of metal loading the HBEA crystallinity, surface area and pore volume decreased. Platinum nanocrystals (about 20 nm width) were observed in 1Pt/HBEA and in some bimetallic catalysts while cobalt seemed to form amorphous particles. The cobalt in the catalysts was in the form of Co^{2+} and it was surrounded by oxygen.

The HBEA-supported catalysts were active for propane hydrogenolysis. The Pt/HBEA gave low propane conversion (6.97 and 21.14%) at 200 and 250°C and nearly complete conversion (98 - 99%) at 300, 350 and 400°C. The products from the reaction at 200 - 300°C were both methane and ethane while those from the reaction at 350 and 400°C were mainly methane. The propane conversion in Co/HBEA was not observed at 200 and 250°C and then increased with temperature. The maximum conversion was obtained at 400°C over all catalysts and the product was mainly methane. However, faster deactivation was observed with higher Co loading.

To confirm the improvement of bimetallic catalyst preparation, the performance of bimetallic 5Co-1Pt/HBEA catalyst was compared with a physically mixed catalyst between 1Pt/HBEA and 5Co/HBEA. It was satisfactory that the previous catalyst had higher propane conversion and higher tolerance to deactivation. Further investigation over bimetallic catalysts showed that the propane conversion increased with the temperature and the maximum conversion was obtained at 300 and 325°C, lower than that in the monometallic cobalt catalysts. The selectivity did not depend on the amount of cobalt but the deactivation at high temperature increased with the amount of cobalt. The major cause of catalyst deactivation was coking which could be removed by combustion with oxygen.

REFERENCES

REFERENCES

- Absil, R. P., and Hatzikos, G. H. (1998). **U.S. Patent** 5833840.
- Aguilar, J., Corma, A., Melo, F.V., and Sastre, E. (2000). **Catalysis Today** 55: 225-232.
- Atoguchi, T., Kanougi, T., Yamamoto, T., and Yao, S. (2004). **Journal of Molecular Catalysis A: Chemical** 220: 183.
- Bagnasco, G. (1996). **Journal of Catalysis** 159: 249-252.
- Barrer, R. M. (1982). **Hydrothermal Chemistry of Zeolites**. London: Academic Press.
- Bhat, R. N., and Kumar, R. (1990). **Journal Chemistry Biotechnology** 48: 453-466.
- Blomsma, E., Martens, J. A., and Jacobs, P. A. (1997). **Journal of Catalysis** 165: 241-248.
- Bourgeat-Lami, E., Massiani, P., Di Renzo, F., Espiau, P., and Fajula, F. (1991). **Applied Catalysis A** 72: 139-152.
- Calvert, R.B., Chang, C.D., Rubin, M.K., and Valyocsik, E.W. (1987). **US Patent** 4642226.
- Camblor, M. A., and Pérez-Pariente, J. (1991). **Zeolites** 11: 202.
- Casagrande, M., Storaro, I., Lenarda, M., and Ganzerla, R. (2000). **Applied Catalysis A** 201: 263-270.
- Chang, C.D., Rubin, M.K., and Valyocsik, E.W. (1987). **US Patent** 4642226.
- Charles, N. S. (1991). **Heterogeneous Catalysis in Industrial Practise** (2nd ed.), McGraw-Hill Inc.

- Chotisuwan, S. (2004). Preparation, Characterization and Catalytic Performance of Supported Pt-Ru Catalysts Prepared from a Metal Cluster, **Suranaree University of Technology**. Ph.D Thesis.
- Corma, A., Climent, M. J., Garcia, H., and Primo, J. (1989). **Applied Catalysis A** 49: 109-123.
- Costa, C., Dzikh, I. P., Lopes, J. M., Lemos, F., and Ribeiro, F. R. (2000). **Journal of Molecular Catalysis A: Chemical** 154: 193-201.
- Dai, L.X., Hayasaka, R., Iwaki, Y., Koyano, K.A., and Tatsumi, T. (1996). **Chemical Communication** 1071.
- Degnan, T.F. Jr., Smith, C.M., and Venkat, C.R. (2001). **Applied Catalysis A: General** 221: 283-294.
- Eapen, M.J., Reddy, K.S.N., and Shiralkar, V.P. (1994). **Zeolites** 14: 295-302.
- Fierro, J.L.G., (1990), **Spectroscopic Characterization of Heterogeneous Catalysts, Part A: Methods of Surface Analysis**. Amsterdam: Elsevier Science Publishers B.V.
- Flanigen, E.M. (1976). **Zeolite Chemistry and Catalysis**. ACS Monograph, 171: 80-117.
- Gellman, A.J., Farias, M.H., and Somorjai, G.A. (1984). **Journal of Catalysis** 88: 546.
- Jackson, S. D., Kelly, G. J., and Geo, W. (1999). **Physical Chemistry Chemical Physics** 1: 2581-2587.
- Jansen, J. C., Creighton, E. J., Njo, S. L., Koningsveid, H., and Bekkum, H. V. (1997). **Catalysis Today** 38: 205-212.

- Juttu, G. (2001). Modified Microporous Aluminosilicates as Novel Solid Acid Catalysis. **University of Delaware**. Ph.D Thesis.
- Khemtong, P., and Wittayakun, J. (2006). **Proceeding of The Regional Symposium in Chemical Engineering (RSCE)**, 3-5 December 2006, Singapore.
- Kim, D. S., Chang, J.S., Hwang, J.S and Park, S.E. (2004). **Microporous and Mesoporous Materials** 68: 77-82.
- Kiricsi, I., Flego, C., Pazzuconi, G., Parker, J.W. O., Millini, R., Perego, C., and Bellussi, G. (1994). **Journal Physical Chemistry** 98: 4627-4634.
- Kuehl, G. H., and Timken, H. K. C. (2000). **Microporous and Mesoporous Materials** 35: 521-532.
- Loiha, S., Prayoonpokarach, S., Songsiriritthigun, P., and Wittayakun, J. (2007). **Proceeding of The Regional Symposium in Chemical Engineering (RSCE)**, 4-5 December 2007, Jogjakarta, Indonesia.
- Lomot, D., Juszczak, W., Karpinski, Z., and Larsson, R. (2002). **Journal of Molecular Catalysis A: Chemical** 186: 163-172.
- Mies, M.J.M., Rebrov, E.V., Jansen, J.C., and de Croon, M.H.J.M. (2007). **Microporous and Mesoporous Materials** 106: 95-106.
- Nakamoto, K. (1962). **Infrared and Raman Spectra of Inorganic and Coordination Compounds**. A Wiley Interscience Publication- John Wiley & Sons.
- Richard, W. R., and Keptner, D. C. (2004). **Applied Catalysis A: General** 262: 233-239.
- Satterfield, C.N. (1980). **Heterogeneous Catalysis in Practice**. McGraw-Hill, New York.

- Sermon, P. A., Keryou, K. M., and Ahmed, F. (2000). **Physical Chemistry Chemical Physics** 2: 5723-5729.
- Sinfelt, J.E. (1980). **Advances in Catalysis** 23: 91.
- Thongkasam, C. (2006). Dealumination Study of Zeolite Y. **Suranaree University of Technology**. M. sc Thesis.
- Vaudry, F., Renzo, F. D., Espiau, P., Fajula, F., and Schulz, Ph. (1997). **Zeolites** 19(4): 253-258.
- Vrålstad, T., Øye, G., Rønning, M., Glomm, W. R., Stöcker, M., and Sjöblom, J. (2005). **Microporous and Mesoporous Materials** 80:291-300.
- Wadlinger, R. L., Kerr, G. T., and Rosinski, E. J. (1967). **U.S. Patent** 3308069.

APPENDICES

APPENDIX A

ADSORPTION ISOTHERMS OF HBEA AND

HBEA-SUPPORTED CATALYSTS

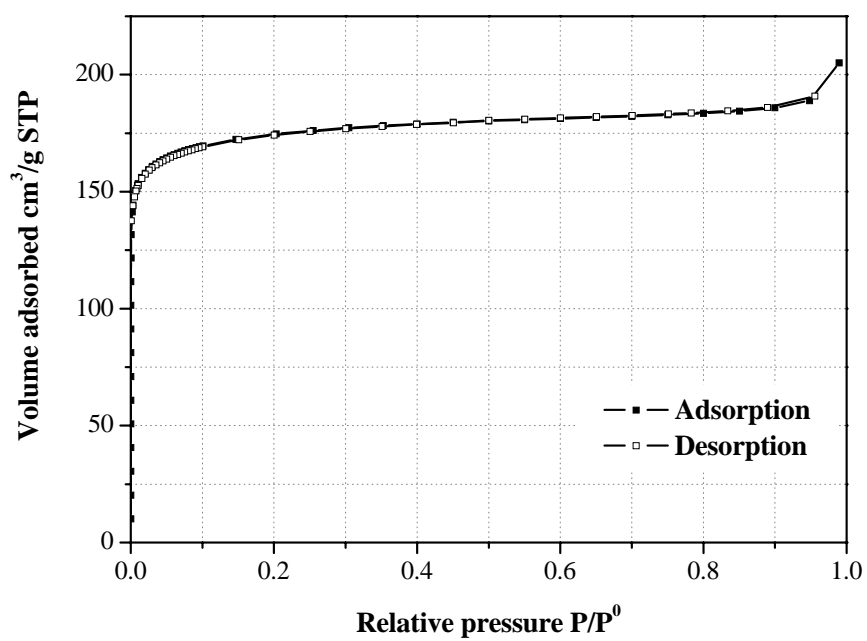


Figure A-1 Nitrogen adsorption-desorption isotherm of HBEA at 77 K.

BET Surface area	625	m ² /g
Micropore volume	0.2515	cm ³ /g
Maximum pore volume	0.2969	cm ³ /g

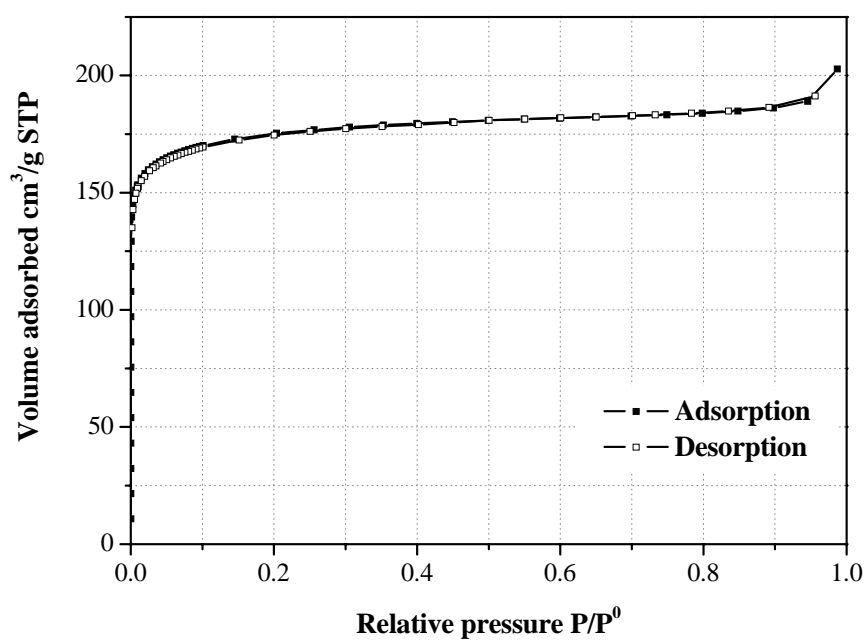


Figure A-2 Nitrogen adsorption-desorption isotherm of 1Pt/HBEA at 77 K.

BET Surface area	579	m ² /g
Micropore volume	0.2221	cm ³ /g
Maximum pore volume	0.2753	cm ³ /g

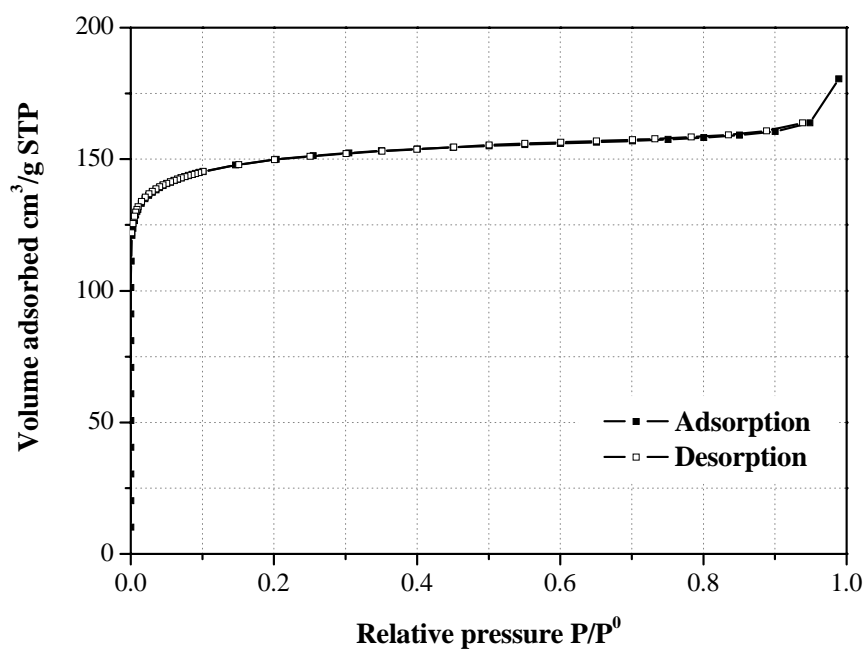


Figure A-3 Nitrogen adsorption-desorption isotherm of 5Co/HBEA at 77 K.

BET Surface area	495	m^2/g
Micropore volume	0.1883	cm^3/g
Maximum pore volume	0.2356	cm^3/g

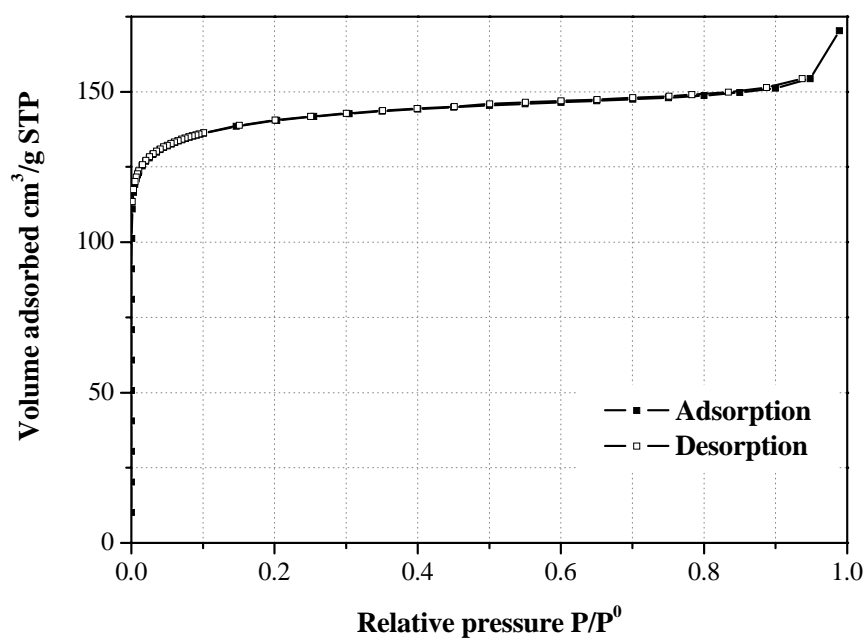


Figure A-4 Nitrogen adsorption-desorption isotherm of 5Co-Pt/HBEA at 77 K.

BET Surface area	464	m^2/g
Micropore volume	0.1772	cm^3/g
Maximum pore volume	0.2208	cm^3/g

APPENDIX B
DETAILS OF CATALYTIC TESTINGS

Table B-1 Propane hydrogenolysis on 1Pt/HBEA at 250°C.**Tested material:** 0.2 g of 1Pt /HBEA and 0.2 g Al₂O₃.**Feed composition:** 0.8 ml/min C₃H₈ + 50.0 ml/min H₂ + 49.2 ml/min He.

Time (min)	Propane (mol/min)	Ethane (mol/min)	Methane (mol/min)	%Conversion
0	0.00	0.00	0.00	0
5	0.00	0.00	0.00	0
20	0.09	0.01	0.01	14
35	0.08	0.01	0.02	22
50	0.08	0.01	0.02	28
65	0.09	0.01	0.01	17

Table B-2 Propane hydrogenolysis on 1Pt/HBEA at 300°C.**Tested material:** 0.2 g of 1Pt /HBEA and 0.2 g Al₂O₃.**Feed composition:** 0.8 ml/min C₃H₈ + 50.0 ml/min H₂ + 49.2 ml/min He.

Time (min)	Propane (mol/min)	Ethane (mol/min)	Methane (mol/min)	%Conversion
0	0.00	0.00	0.00	0
5	0.00	0.00	0.00	0
20	0.00	0.04	0.07	99
35	0.00	0.04	0.07	100
50	0.00	0.03	0.07	99
65	0.00	0.03	0.07	99

Table B-3 Propane hydrogenolysis on 1Pt/HBEA at 350°C.**Tested material:** 0.2 g of 1Pt /HBEA and 0.2 g Al₂O₃.**Feed composition:** 0.8 ml/min C₃H₈ + 50.0 ml/min H₂ + 49.2 ml/min He.

Time (min)	Propane (mol/min)	Ethane (mol/min)	Methane (mol/min)	%Conversion
0	0.00	0.00	0.00	0
5	0.00	0.00	0.00	0
20	0.00	0.00	0.11	99
35	0.00	0.00	0.11	100
50	0.00	0.00	0.11	99
65	0.00	0.00	0.11	99

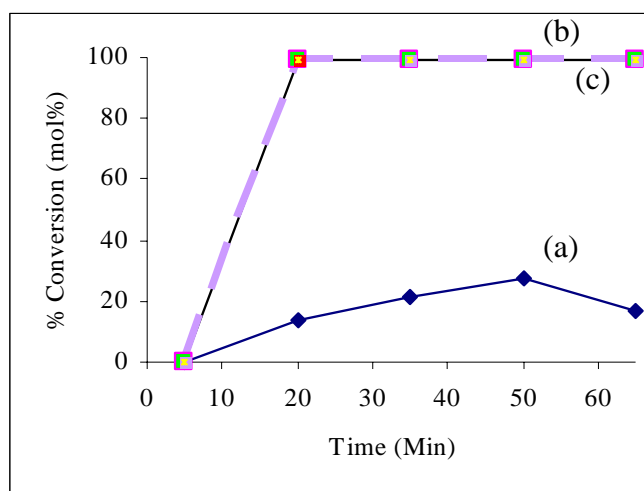
**Figure B-1** The %conversion of Propane over 1Pt/HBEA at (a) 250, (b) 300 and (c) 350°C.

Table B-4 Propane hydrogenolysis on 5Co/HBEA at 300°C.**Tested material:** 0.2 g of 5Co/HBEA and 0.2 g Al₂O₃.**Feed composition:** 0.8 ml/min C₃H₈ + 50.0 ml/min H₂ + 49.2 ml/min He.

Time (min)	Propane (mol/min)	Ethane (mol/min)	Methane (mol/min)	%Conversion
0	0.00	0.00	0.00	0
5	0.00	0.00	0.00	0
20	0.08	0.00	0.03	23
35	0.09	0.00	0.02	18
50	0.08	0.00	0.02	22
65	0.08	0.00	0.02	22

Table B-5 Propane hydrogenolysis on 5Co/HBEA at 350°C.**Tested material:** 0.2 g of 5Co/HBEA and 0.2 g Al₂O₃.**Feed composition:** 0.8 ml/min C₃H₈ + 50.0 ml/min H₂ + 49.2 ml/min He.

Time (min)	Propane (mol/min)	Ethane (mol/min)	Methane (mol/min)	%Conversion
0	0.00	0.00	0.00	0
5	0.00	0.00	0.00	0
20	0.08	0.00	0.03	27
35	0.08	0.00	0.03	24
50	0.08	0.00	0.03	24
65	0.08	0.00	0.03	23

Table B-6 Propane r hydrogenolysis on 5Co/HBEA at 400°C.**Tested material:** 0.2 g of 5Co/HBEA and 0.2 g Al₂O₃.**Feed composition:** 0.8 ml/min C₃H₈ + 50.0 ml/min H₂ + 49.2 ml/min He.

Time (min)	Propane (mol/min)	Ethane (mol/min)	Methane (mol/min)	%Conversion
0	0.00	0.00	0.00	0
5	0.00	0.00	0.00	0
20	0.02	0.00	0.09	80
35	0.02	0.00	0.09	80
50	0.03	0.00	0.08	75
65	0.02	0.00	0.09	81

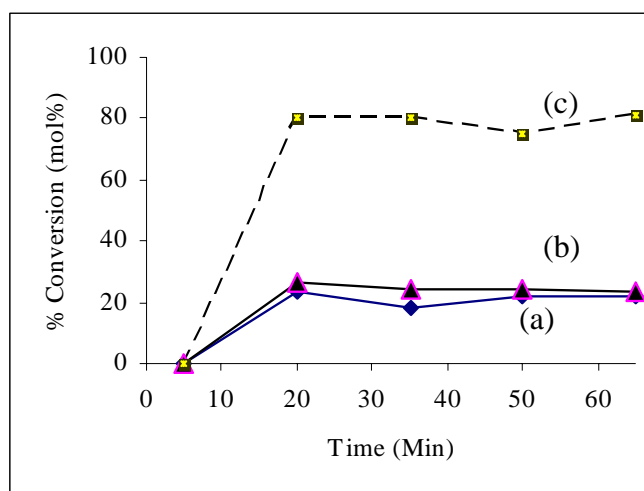
**Figure B-2** The %conversion of Propane over 5Co/HBEA at (a) 300, (b) 350 and (c) 400°C.

Table B-7 Propane hydrogenolysis on 10Co/HBEA at 350°C.**Tested material:** 0.2 g of 10Co/HBEA and 0.2 g Al₂O₃.**Feed composition:** 0.8 ml/min C₃H₈ + 50.0 ml/min H₂ + 49.2 ml/min He.

Time (min)	Propane (mol/min)	Ethane (mol/min)	Methane (mol/min)	%Conversion
0	0.00	0.00	0.00	0
5	0.00	0.00	0.00	0
20	0.08	0.00	0.03	30
35	0.08	0.00	0.03	24
50	0.08	0.00	0.03	24
65	0.08	0.00	0.03	27

Table B-8 Propane hydrogenolysis on 10Co/HBEA at 400°C.**Tested material:** 0.2 g of 10Co/HBEA and 0.2 g Al₂O₃.**Feed composition:** 0.8 ml/min C₃H₈ + 50.0 ml/min H₂ + 49.2 ml/min He.

Time (min)	Propane (mol/min)	Ethane (mol/min)	Methane (mol/min)	%Conversion
0	0.00	0.00	0.00	0
5	0.00	0.00	0.00	0
20	0.00	0.00	0.11	99
35	0.00	0.00	0.10	96
50	0.00	0.00	0.11	99
65	0.00	0.00	0.11	98

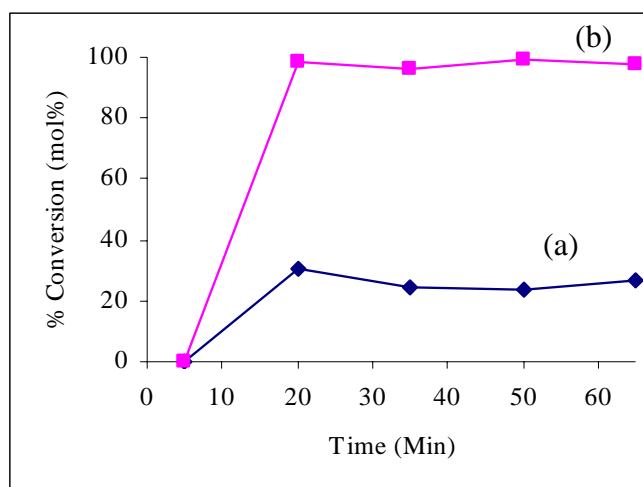


Figure B-3 The %conversion of Propane over 10Co/HBEA at (a) 350 and (b) 400°C.

Table B-9 Propane hydrogenolysis on 15Co/HBEA at 300°C.

Tested material: 0.2 g of 15Co/HBEA and 0.2 g Al₂O₃.

Feed composition: 0.8 ml/min C₃H₈ + 50.0 ml/min H₂ + 49.2 ml/min He.

Time (min)	Propane (mol/min)	Ethane (mol/min)	Methane (mol/min)	%Conversion
0	0.00	0.00	0.00	0.00
5	0.00	0.00	0.00	0.00
20	33.82	0.08	0.00	0.00
35	31.02	0.07	0.00	0.00
50	34.59	0.08	0.00	0.00
65	33.94	0.08	0.00	0.00

Table B-10 Propane hydrogenolysis on 15Co/HBEA at 350°C.**Tested material:** 0.2 g of 15Co/HBEA and 0.2 g Al₂O₃.**Feed composition:** 0.8 ml/min C₃H₈ + 50.0 ml/min H₂ + 49.2 ml/min He.

Time (min)	Propane (mol/min)	Ethane (mol/min)	Methane (mol/min)	%Conversion
0	0.00	0.00	0.00	0.00
5	0.00	0.00	0.00	0.00
20	22.86	0.05	0.00	0.00
35	20.77	0.05	0.00	0.00
50	21.53	0.05	0.00	0.00
65	27.47	0.06	0.00	0.00

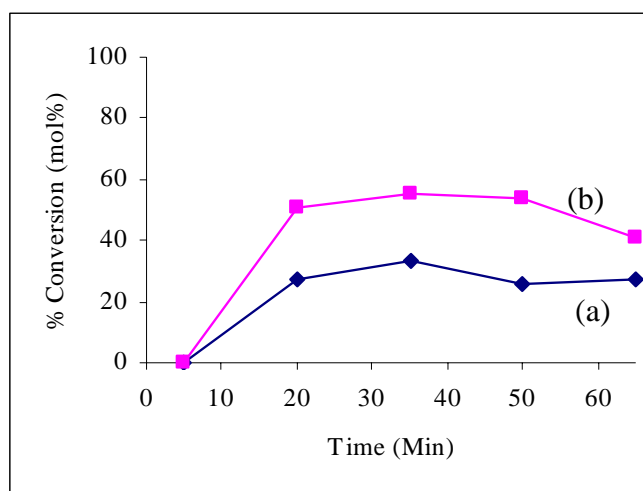
**Figure B-4** The %conversion of Propane over 15Co/HBEA at (a) 300 and (b) 350°C.

Table B-11 Propane hydrogenolysis on 5Co-1Pt/HBEA at 250°C.**Tested material:** 0.2 g of 5Co-1Pt/HBEA and 0.2 g Al₂O₃.**Feed composition:** 0.8 ml/min C₃H₈ + 50.0 ml/min H₂ + 49.2 ml/min He.

Time (min)	Propane (mol/min)	Ethane (mol/min)	Methane (mol/min)	%Conversion
0	0.00	0.00	0.00	0
5	0.00	0.00	0.00	0
20	0.09	0.00	0.02	16
35	0.08	0.00	0.03	26
50	0.08	0.00	0.03	26
65	0.08	0.00	0.03	27

Table B-12 Propane hydrogenolysis on 5Co-1Pt/HBEA at 300°C.**Tested material:** 0.2 g of 5Co-1Pt/HBEA and 0.2 g Al₂O₃.**Feed composition:** 0.8 ml/min C₃H₈ + 50.0 ml/min H₂ + 49.2 ml/min He.

Time (min)	Propane (mol/min)	Ethane (mol/min)	Methane (mol/min)	%Conversion
0	0.00	0.00	0.00	0
5	0.00	0.00	0.00	0
20	0.01	0.00	0.10	94
35	0.00	0.00	0.10	97
50	0.01	0.00	0.10	94
65	0.01	0.00	0.10	95

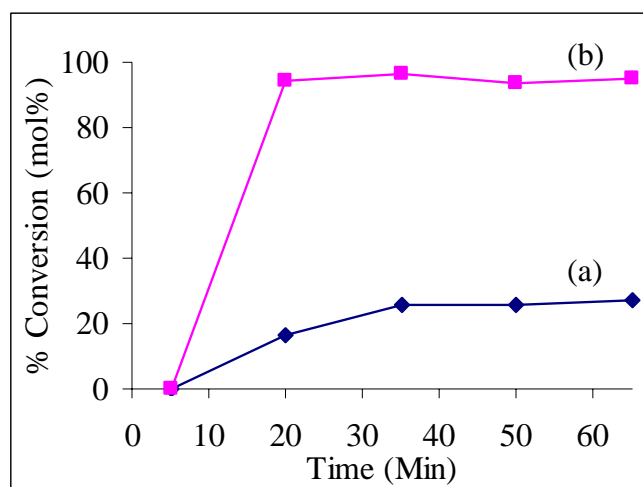


Figure B-5 The %conversion of Propane over 5Co-1Pt/HBEA at (a) 250 and (b) 300°C.

Table B-13 Propane hydrogenolysis on 10Co-1Pt/HBEA at 250°C .

Tested material: 0.2 g of 10Co-1Pt/HBEA and 0.2 g Al₂O₃.

Feed composition: 0.8 ml/min C₃H₈ + 50.0 ml/min H₂ + 49.2 ml/min He.

Time (min)	Propane (mol/min)	Ethane (mol/min)	Methane (mol/min)	%Conversion
0	0.00	0.00	0.00	0
5	0.00	0.00	0.00	0
20	0.07	0.00	0.04	37
35	0.08	0.00	0.03	28
50	0.08	0.00	0.03	26
65	0.08	0.00	0.03	24

Table B-14 Propane hydrogenolysis on 10Co-1Pt/HBEA at 300°C.**Tested material:** 0.2 g of 10Co-1Pt/HBEA and 0.2 g Al₂O₃.**Feed composition:** 0.8 ml/min C₃H₈ + 50.0 ml/min H₂ + 49.2 ml/min He.

Time (min)	Propane (mol/min)	Ethane (mol/min)	Methane (mol/min)	%Conversion
0	0.00	0.00	0.00	0
5	0.00	0.00	0.00	0
20	0.04	0.00	0.07	63
35	0.05	0.00	0.06	54
50	0.04	0.00	0.06	60
65	0.05	0.00	0.06	56

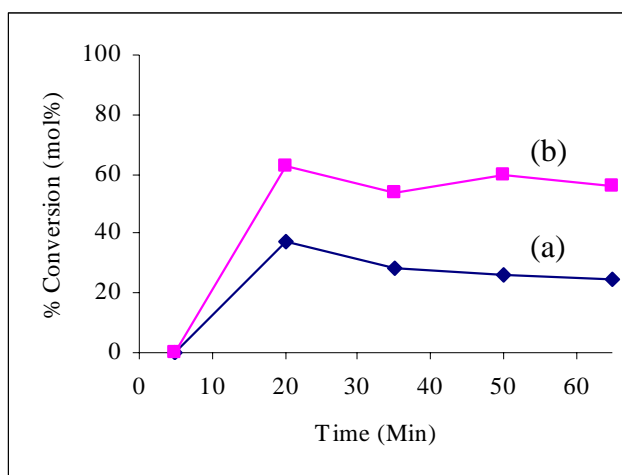
**Figure B-6** The %conversion of Propane over 10Co-1Pt/HBEA at (a) 250 and (b) 300°C.

Table B-15 Propane hydrogenolysis on 15Co-1Pt/HBEA at 250°C.**Tested material:** 0.2 g of 15Co-1Pt/HBEA and 0.2 g Al₂O₃.**Feed composition:** 0.8 ml/min C₃H₈ + 50.0 ml/min H₂ + 49.2 ml/min He.

Time (min)	Propane (mol/min)	Ethane (mol/min)	Methane (mol/min)	%Conversion
0	0.00	0.00	0.00	0
5	0.00	0.00	0.00	0
20	0.09	0.00	0.02	16
35	0.09	0.00	0.01	14
50	0.09	0.00	0.02	16
65	0.08	0.00	0.02	21

Table B-16 Propane hydrogenolysis on 15Co-1Pt/HBEA at 300°C.**Tested material:** 0.2 g of 15Co-1Pt/HBEA and 0.2 g Al₂O₃.**Feed composition:** 0.8 ml/min C₃H₈ + 50.0 ml/min H₂ + 49.2 ml/min He.

Time (min)	Propane (mol/min)	Ethane (mol/min)	Methane (mol/min)	%Conversion
0	0.00	0.00	0.00	0
5	0.00	0.00	0.00	0
20	0.05	0.00	0.06	52
35	0.05	0.00	0.06	56
50	0.05	0.00	0.06	58
65	0.05	0.00	0.06	55

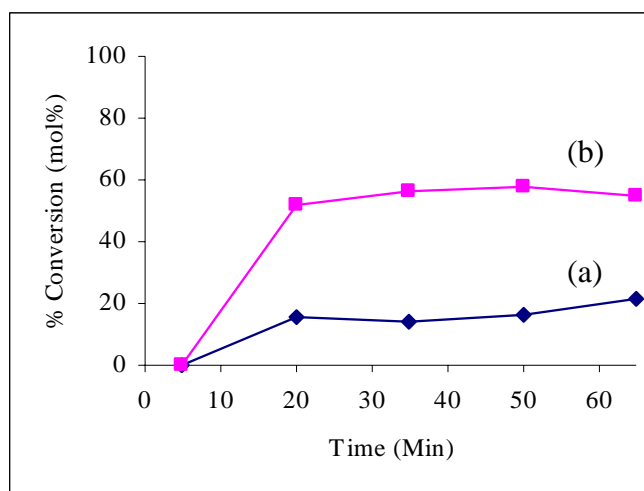


Figure B-7 The %conversion of Propane over 15Co-1Pt/HBEA at (a) 250 and (b) 300°C.

Table B-17 Propane hydrogenolysis on Mix 1Pt/HBEA and 5Co/HBEA at 300°C.

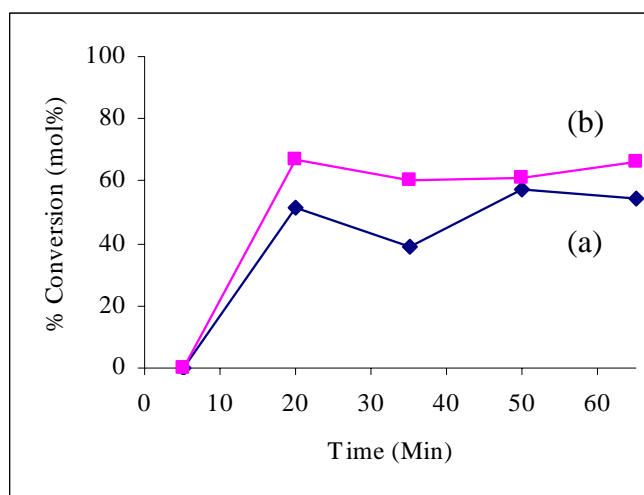
Tested material: 0.2 g of Mix 1Pt/HBEA and 5Co/HBEA and 0.2 g Al₂O₃.

Feed composition: 0.8 ml/min C₃H₈ + 50.0 ml/min H₂ + 49.2 ml/min He.

Time (min)	Propane (mol/min)	Ethane (mol/min)	Methane (mol/min)	%Conversion
0	0.00	0.00	0.00	0
5	0.00	0.00	0.00	0
20	0.05	0.00	0.06	51
35	0.07	0.00	0.04	39
50	0.05	0.00	0.06	58
65	0.05	0.00	0.06	55

Table B-18 Propane hydrogenolysis on Mix 1Pt/HBEA and 5Co/HBEA at 350°C.**Tested material:** 0.2 g of Mix 1Pt/HBEA and 5Co/HBEA and 0.2 g Al₂O₃.**Feed composition:** 0.8 ml/min C₃H₈ + 50.0 ml/min H₂ + 49.2 ml/min He.

Time (min)	Propane (mol/min)	Ethane (mol/min)	Methane (mol/min)	%Conversion
0	0.00	0.00	0.00	0
5	0.00	0.00	0.00	0
20	0.04	0.00	0.07	67
35	0.04	0.00	0.07	60
50	0.04	0.00	0.07	61
65	0.04	0.00	0.07	66

**Figure B-8** The %conversion of Propane over Mix 1Pt/HBEA and 5Co/HBEA at
a) 300 and b) 350°C.

APPENDIX C
THESIS OUTPUT

การสังเคราะห์ซีโอไลต์บีตาโดยใช้ซิลิกาจากแกลบข้าวเพื่อเป็นตัวรองรับแก่แพลทินัม

SYNTHESIS OF ZEOLITE BETA FROM RICE HUSK SILICA AND UTILIZATION AS CATALYTIC SUPPORT FOR PLATINUM

สิทธิชัย กุลวงศ์¹, ศิรินุช ลอยหา¹, จตุพร วิทยาคุณ¹ และ นุรักษ์ กฤษดาณรงค์²

Sittichai Kulawong, Sirinuch Loiha¹, Jatuporn Wittayakun¹, Nurak Grisdanurak²

¹ School of Chemistry, Institute of Science, Suranaree University of Technology, Nakhon Ratchasima, Thailand.

E-mail:sake_ubu@yahoo.com

² Department of Chemical Engineering, Faculty of Engineering, Thammasat university, Pathumthani, Thailand.

บทคัดย่อ: ในงานวิจัยนี้นำซิลิกาจากแกลบข้าวมาใช้เป็นสารตั้งต้นในการสังเคราะห์ซีโอไลต์เบตาโดยใช้วิธีสังเคราะห์แบบไฮโดรเทอร์มัล โดยการบรรจุของผสมในรูปเจลของซิลิกา อลูมินา แคลโตอออน โซเดียม เทตระเอทิลแอมโมเนียม ไฮดรอกไซด์ ซึ่งเป็นสารเทมเพลต และน้ำลงในออโตเคลฟที่มีถ้วยเทฟลอนอยู่ภายใน การตกผลึกของซีโอไลต์ บีตาทำที่ 135 องศาเซลเซียส เวลาที่ใช้ในการตกผลึกของซีโอไลต์ บีตามีค่าระหว่าง 1 ถึง 5 วัน และพบว่าที่เวลาของการตกผลึกที่สมบูรณ์ที่น้อยที่สุดคือ 2 วัน ยืนยันโครงสร้างของซีโอไลต์ บีตาโดยการวิเคราะห์ด้วยการเลี้ยวเบนของรังสีเอกซ์ แล้วใส่แพลทินัมบนผิวซีโอไลต์ บีตาด้วยการทำให้เปียกชื้นโดยใช้สารละลายของแพลทินัมแอสีเตต ในเอซีโตนในปริมาณที่ให้แพลทินัม 1% โดยน้ำหนัก แล้วนำตัวเร่งปฏิกิริยา ซีโอไลต์ บีตาที่ใส่แพลทินัมไปตรวจสอบสมบัติเฉพาะด้วยเทคนิคการเลี้ยวเบนรังสีเอกซ์ พบว่าโครงสร้างของซีโอไลต์ไม่มีการเปลี่ยนแปลงหลังจากเพิ่มโลหะลงไป และเมื่อนำไปทดสอบการเร่งปฏิกิริยาออกซิเดชันของแก๊สคาร์บอนมอนอกไซด์ พบว่าค่าการเปลี่ยนจะเพิ่มขึ้นแบบเอกโปเนนเชียลตามอุณหภูมิที่เพิ่มขึ้น มีค่าการแปลงผันสูงสุดเป็น ร้อยละ 17 ที่อุณหภูมิ 400 องศาเซลเซียส

Abstract: In this research, silica from rice husk was used in the synthesis of zeolite beta by hydrothermal method with the gel containing silica, alumina, sodium cation, tetraethylammonium hydroxide as a template, and water. The gel was transferred to a Teflon-lined autoclave and the crystallization of zeolite beta was done at 135 °C. The crystallization time was varied between 1 to 5 days and it was found that the minimum time to complete crystallization was 2 days. The zeolite beta structure was confirmed by X-ray diffraction analysis. Then platinum was loaded onto the zeolite surface by incipient wetness impregnation with a solution of platinum(II)acetate in acetone with the amount to give 1%Pt by weight. The catalyst was characterized by X-ray diffraction analysis and the zeolite beta was unchanged. The Pt/BEA catalyst was tested for carbon monoxide oxidation. It was found that the conversion was exponentially increased with increasing temperature. The maximum conversion reached 17% at 400 °C.

Introduction:

Rice husk is a byproduct from rice milling and can be considered as solid waste. It is usually disposed of by combustion to give ash which has high silica content. In this work, silica with approximately 98% pure was extracted from rice husk by leaching with hydrochloric acid followed by pyrolysis. It was used as a silica source for the

synthesis of zeolite beta (BEA) which is a useful catalyst in petrochemical application and fine chemical synthesis, including epoxidation, transalkylation, isomerization and alkylation. BEA is large pore zeolite with the formula $\text{Na}_n\{\text{Al}_n\text{Si}_{64-n}\text{O}_{128}\}$, $n < 7$. The Si/Al ratio may vary, start from 8, going to through more siliceous (dealuminated) forms and ending with an aluminium-free homologue. Noble metal-base catalysts have been widely for the oxidation because of their noticeable intrinsic activity and selectivity to CO_x [1-2]. In general, palladium (Pd) is an active catalyst and platinum (Pt) catalysts are more selective to CO_2 [3]. Recently, studies on the applicability of H-type zeolite as potential catalysts for chlorocarbon destruction evidenced the acid sites, mainly Bronsted-type sites, acted as efficient chemisorption sites for chlorinate molecules [4]. In this work Pt was loaded on BEA and tested for the oxidation of carbon monoxide.

Methodology:

Rice husk silica was obtained after leaching the husk in 3M HCl acid under the reflux condition and pyrolysis at 500°C. BEA was synthesized from a procedure described in literature. The reaction mixture was prepared at room temperature. A 29.54 g portion Rice husk was added into the solution of 0.33 g NaOH in 59.4 g water, stirred until dissolved to give solution A. Amounts of TEAOH (40%), 0.53 g NaCl, 1.44 g KCl and 10 g water were mixed and stir until homogenous to give solution B. Solution C was prepared from 1.79 g sodium aluminate and 10 g water and stir until dissolve. Solutions B and C were slowly added into solution A and stirred until homogenous before crystallization in a designed autoclave at condition of 135 °C, pH 12.8 ± 2 and crystallization time varied from 1 to 5 days. The crystalline product of Na-BEA with Si/Al ratio of 13, was confirmed by XRD. Before metal loading, H-BEA was prepared by ion-exchange of Na-BEA with 1M NH_4NO_3 solution and then converted into H-form by calcinations at 550 °C for 5 h.

Platinum salt was loaded on H-form of BEA to give 0.1 wt%Pt by incipient wetness impregnation. In catalyst testing for carbon monoxide oxidation, approximately 0.01 g of Pt/BEA catalyst was loaded on a glass wool-bed in a quartz tube and dried at 120 °C for 12 h,. The catalyst was reduced by 5% H_2 /He with the flow rate of 30 ml/min at 475 °C with the ramp of 5 °C/min for 4 h. After reduction, the catalyst was purged with helium and the temperature was lowered to reaction temperature at 250 °C. Then the catalytic test for CO oxidation were begun. The reactant CO and air was fed into the reactor by mass flow controllers at ratio of CO: air =20.80 ml/min:16.86 ml/min, 10.76 ml/min:16.86 ml/min and 6.13 ml/min:16.86 ml/min and calculated gas space hourly velocity (GSHV)= 1.19×10^5 , 9.4×10^4 and 7.9×10^4 ml/hr.g_{cat} respectively, and 5%hydrogen in helium with flow rate of 20 ml/min/g were passed with reactants and were preheated. The identification of products was done by a gas chromatograph (Shimadzu) with TCD detector.

Results, Discussion and Conclusion:

XRD spectrum of as-synthesized zeolite in Figure 1 indicated that complete Na-BEA was obtained with crystallization time of 2 days with the yield of 90%. After NH_4^+ ion exchange and calcination at 550 °C, 5h, the H-BEA was obtained and the XRD spectrum remained the same. In addition, after impregnation with Pt salt and calcination, the XRD spectrum of Pt/BEA was similar to that of the BEA indicating no change after metal loading. Due to low metal loading, the Pt peak was not observed by XRD.

For catalytic test for carbon monoxide oxidation, the conversion was exponentially increased when temperature was increased (Figure 2 a). The maximum conversion reached 17% at 400 °C. The suitable flow rate was 4.0 cc/min of CO and 1.0 cc/min of O₂. The maximum conversion reached 70% of CO₂ products. Then conversion was plotted versus gas space hourly velocity (GSHV) at 400 °C as shown in Figure 2 b. The conversion of CO decreased as the GSHV increased.

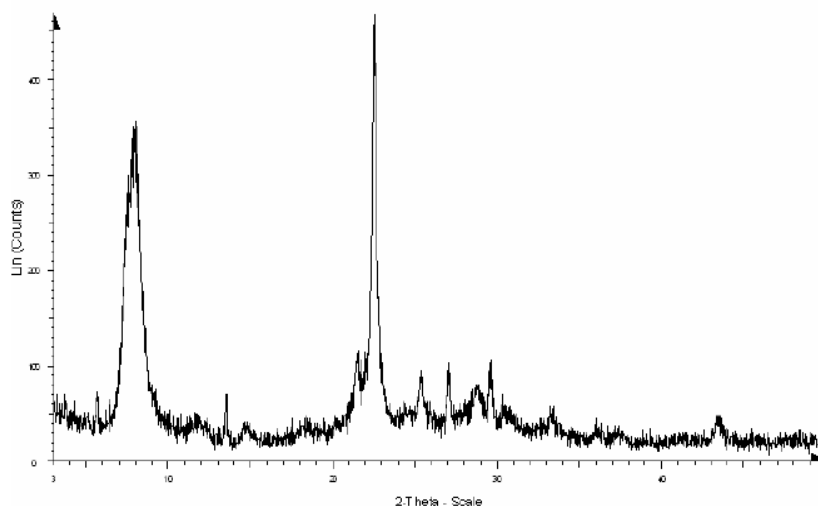


Figure 1. XRD pattern of Na-BEA.

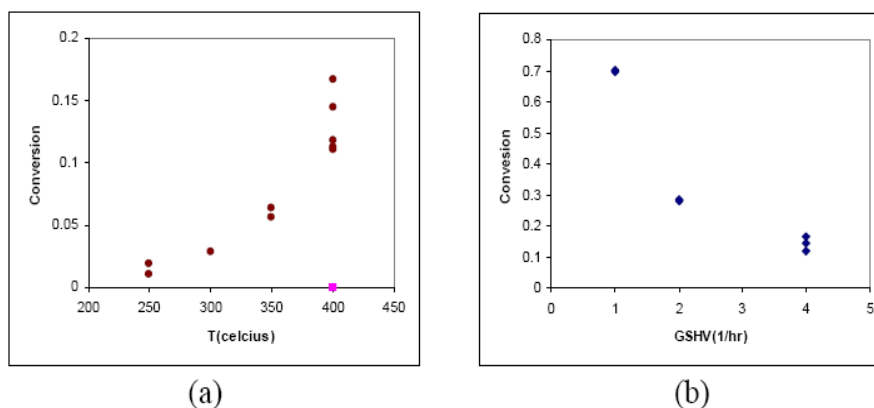


Figure 2. (a) Conversion of CO and O₂ at different temperature (b) conversion of CO and O₂ versus GSHV (1/hr) at 400 °C

Reference:

- [1] M.P. Manning, *Hazard. Waste* 1 (1984) 41.
- [2] H. Windawi, M. Wyatt, *Platinum Met. Rev.* 37 (1993) 186.
- [3] J.R. Gonza'lez-Velasco, A. Aranzabal, J.I. Gutie'rrrez-Ortiz, R. Lo'pez-Fonseca, M.A. Gutie'rrrez-Ortiz, *Appl. Catal. B* 19 (1998) 189.
- [4] R. Lo'pez-Fonseca, A. Aranzabal, P. Steltenpohl, J.I. Gutie'rrrez-Ortiz, J.R. Gonza'lez Velasco, *Catal. Today* 62 (2000) 367.

Keyword: Zeolite beta; platinum; palladium; CO oxidation; catalyst

Acknowledgement

Fundings for this research were from Suranaree University Research Fund and National Synchrotron Research Center Research Fund (Scholarship for Sirinuch Loiha).

Propane hydrogenolysis on bimetallic platinum-cobalt catalysts supported on zeolite beta synthesized with rice husk silica

Sittichai Kulawong^a, Sanchai Prayoonpokarach^a, Nurak Grisdanurak^b and Jatuporn Wittayakun^{a*}

^aSchool of Chemistry, Suranaree University of Technology, Nakhon Ratchasima, 30000 Thailand

^bDepartment of Chemical Engineering, Thammasat University, Pathumthani, 12120, Thailand

*Corresponding author: Tel. +66-44-224-256; Fax. +66-44-224-185 jatuporn@sut.ac.th

Abstract

Mono- and bimetallic catalysts containing Pt and Co supported on HBEA were prepared by impregnation with Pt loading fixed at 1wt% and Co loading of 5, 10 and 15wt%. The HBEA structure did not change after impregnated with metal but the HBEA crystallinity and surface area decreased with the amount of metal loading. All the catalysts were tested for propane hydrogenolysis which is a structure sensitive reaction. For monometallic catalyst, the 1%Pt/HBEA was the most active catalyst with a nearly complete conversion at 300, 350 and 400 °C but deactivated quickly. The activity and deactivation of Co/HBEA increased with metal loading. The major cause of catalyst deactivation was coking which could be removed by combustion with oxygen. Because 1%Pt/HBEA was the most active catalyst and the 5%Co/HBEA showed the least deactivation, the bimetallic 1%Pt-5%Co/HBEA was investigated further and it gave higher propane conversion and had higher tolerance to deactivation than a physically mixture between 1%Pt/HBEA and 5%Co/HBEA. Thus, a small amount of Co improved the coking tolerance of 1%Pt/HBEA catalyst.

Keywords: zeolite beta, rice husk silica, propane hydrogenolysis, platinum, cobalt

1. Introduction

Silica can be extracted from rice husk by leaching the husk with hydrochloric acid and calcined at 550°C to produce rice husk silica (RHS) with 98% purity. This work used the RHS for the synthesis of zeolite beta with Si/Al ratio of 13 in proton form (HBEA). The method was reported by Loiha to give the highest surface area and crystallinity compared to the other ratio. The HBEA was used as a catalytic support for monometallic and bimetallic catalysts containing Pt and/or Co. Both the HBEA and HBEA-supported metal catalysts were characterized by X-ray diffraction (XRD), nitrogen adsorption and transmission electron microscopy. Finally, the HBEA-supported metal catalysts were tested for propane hydrogenolysis in a flow reactor. Parameters including bimetallic ratio and temperature that affect the catalytic performance were studied.

Propane hydrogenolysis is a reaction between propane and hydrogen to produce ethane and methane (Equations 1 and 2). This reaction is simple, structure sensitive, and can be use to determine the change of metal catalyst after modification.



2. Experimental

2.1 Preparation of HBEA support

RHS was prepared by acid leaching of rice husk with a procedure similar to that reported in literature (Khemthong, et al. 2007). NaBEA with the Si/Al ratio of 13 was synthesized with a procedure modified from literature (Cambolor, 1991 and Loiha et al, 2007). The original gel with a molar composition of 1.97Na₂O:1.00K₂O:12.50(TEA)₂O: Al₂O₃:50SiO₂:750H₂O:2.9HCl crystallized in a stainless steel autoclave at 135°C for 3 days. The obtained NaBEA was washed and dried overnight at 77°C and converted to ammonium form NH₄BEA by repeated ion exchange with 1 M NH₄NO₃ for 2 times at 80°C and calcined at 550°C for 5 hours.

2.2 Catalysts preparation and characterization

Both monometallic and bimetallic catalysts were prepared by incipient wetness impregnation with solutions of $\text{H}_2\text{PtCl}_6 \cdot 6\text{H}_2\text{O}$ and/or CoCl_2 onto HBEA. The Pt metal loading was fixed at 1 wt % and that of Co was 5, 10 and 15 wt%. All catalyst samples were dried overnight at 120°C and calcined at 300°C for 3 hours. A physically mixture of 1Pt/HBEA and 5Co/HBEA was prepared by mixing the two monometallic catalysts together. The performance of the physically mixed catalyst would be compared with bimetallic 5Co-1Pt/HBEA to observe the catalytic enhancement by bimetallic catalyst.

The support HBEA and HBEA supported catalysts were characterized by XRD and N_2 adsorption to see the effect of metal loading on crystallinity, surface area and pore volume. In addition, the as-prepared catalysts were analyzed by TEM.

2.3 Catalytic tests

The propane hydrogenolysis was tested in a quartz tube flow reactor operated at atmospheric pressure. Approximately 0.2-0.4 g of catalyst was reduced at to 450°C in a flow of hydrogen for 6 hours to ensure the complete reduction. Then it was cooled in flowing hydrogen to a desired reaction temperature before introducing a gas mixture containing the $\text{He}:\text{H}_2:\text{C}_3\text{H}_8$ with 4 : 4 : 1 ratio. The reaction products were analyzed by a gas chromatography (SRI GC 610C) equipped with a porapak type N column and a thermal conductivity detector. The propane hydrogenolysis was tested by heating from 200 to 400°C (referred to as “run-up”), purged with helium and the reaction was tested again from 400 to 200°C (referred to as “run-down”) in similar conditions to observe deactivation. The performance of each catalyst was reported in term of percent conversion and selectivity.

3. Results and Discussions

3.1 Characterization of HBEA and HBEA-supported catalysts

Before metal loading, the XRD pattern of HBEA was similar to that of BEA reported in literature (Cambor, 1991). After loading with metal, both monometallic and bimetallic catalysts (Figure 1) still showed XRD patterns of HBEA indicating the BEA framework was retained. However, the HBEA crystallinity decreased with the amount of metal. The XRD peak of cobalt oxide at 16 degree was observed in 15%Co and all bimetallic catalysts in which the area of this peak increased with Co loading. This observation indicated that the cobalt particle size increased with the amount of Co loading.

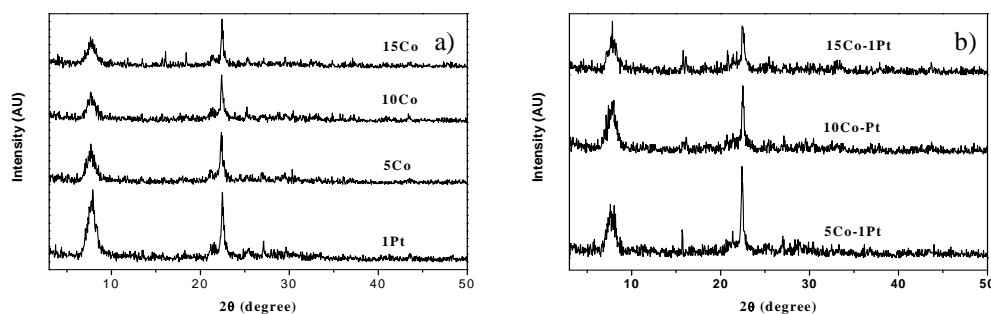


Figure 1 XRD patterns of a) monometallic Pt and Co catalysts and b) bimetallic catalysts on HBEA.

The nitrogen adsorption-desorption isotherms of HBEA and HBEA-supported catalysts were all type I, a characteristic of microporous materials. An example of isotherm is shown in Figure 2 and their surface area and micropore volume are summarized in Table 1. After loading with metal, the BET surface area decreased with the amount of metal. The volume of micropores also in decreased the same order indicating that the metal might reside in the micropores.

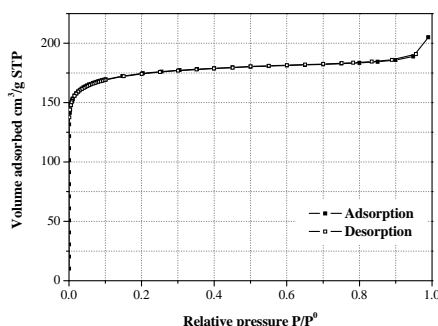


Figure 2 Nitrogen adsorption-desorption isotherm of HBEA.

Table 1 Surface area and pore volume of HBEA and HBEA-supported catalysts.

Samples	BET surface Area (m ² /g)	Micropore Volume (cm ³ /g)	Maximumpore Volume (cm ³ /g)
HBEA	625	0.2515	0.2969
1Pt/HBEA	579	0.2221	0.2753
5Co/HBEA	495	0.1883	0.2356
1Pt5Co/HBEA	464	0.1772	0.2208

3.2 Propane hydrogenolysis over monometallic Pt/HBEA and Co/HBEA

The average conversion of propane over 1Pt/HBEA (Figure 3) increased with temperature and reached a complete conversion at 300, 350 and 400°C. At 200°C the methane selectivity was about 90% and it increased when the temperature was increased to 250 and 300°C. At these temperatures propane and hydrogen adsorbed on the catalysts and reacted, causing a cleavage of C-C bond and produce both methane and ethane. At these temperature, the sequential hydrogenolysis of ethane was slow and ethane desorption was observed. At 350 and 400°C, the methane was the major product (98.7 and 99.8%, respectively indicating that the sequential hydrogenolysis was feasible at high temperature. However, the propane conversion in the run-down experiment was lower indicating that catalyst deactivation occurred. Judging from the catalyst color, coking was the deactivation cause.

The propane conversions over all Co/HBEA catalysts are also displayed in Figure 3. The conversion increased with temperature and the highest conversion was observed at 400°C. Methane was the only observed product indicating that the sequential hydrogenolysis of ethane was more favorable on Co catalysts than the Pt catalysts. From the run-down experiment of cobalt catalysts, the least deactivation was observed on 5%Co/HBEA.

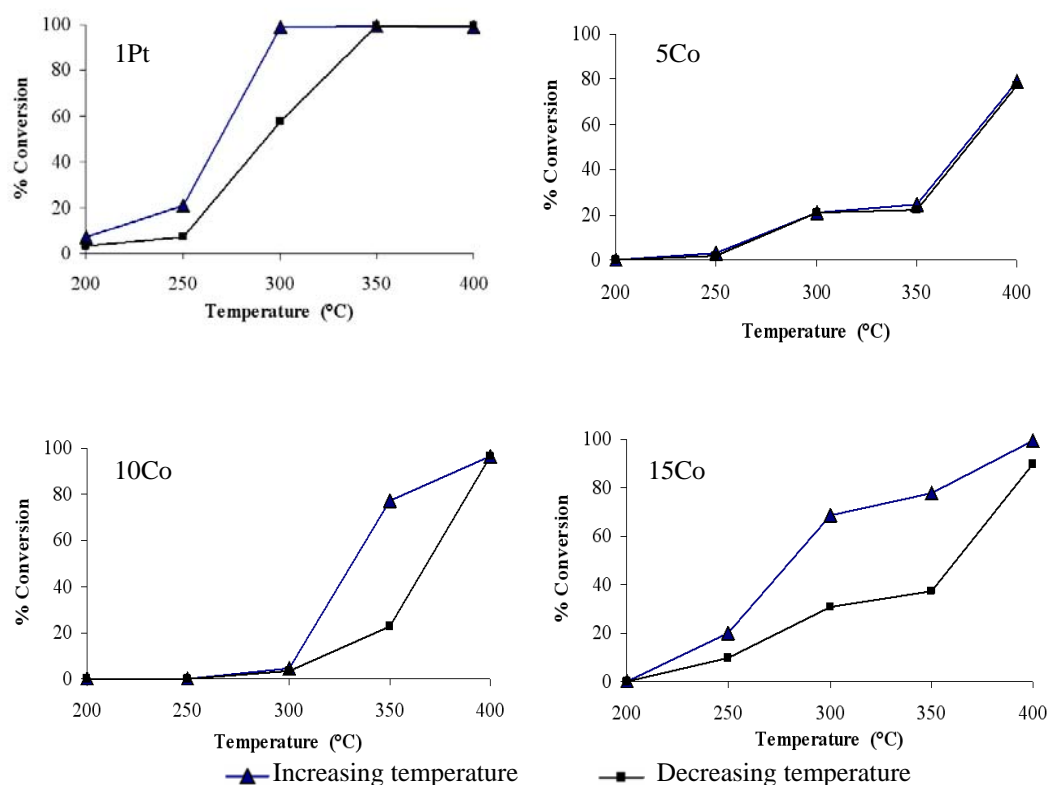


Figure 3 Propane conversion over monometallic catalysts.

3.3 Propane hydrogenolysis over bimetallic CoPt/HBEA

Propane conversions over bimetallic catalysts, shown in Fig. 4, increased with temperature for all catalysts. The run-down experiment of bimetallic catalysts prepared by impregnation revealed that the 1Pt5Co/HBEA had the least difference compared to the other ratios. Thus, this catalyst had the least deactivation and was the most suitable one under the studied conditions. This result indicated that the presence of 5%Co on the same support improve the tolerance for deactivation for 1%Pt/HBEA.

The test over a physically mixed catalyst 1Pt/HBEA and 5Co/HBEA was carried out to ensure that the catalysts prepared by co-impregnation had better performance for propane hydrogenolysis than that obtained by physically mixing of Pt/HBEA and Co/HBEA. The comparison was made only on the catalysts with 1Pt and 5Co loading because the 5Co/HBEA showed the best stability. The run-up conversion of the physically mixed catalyst was lower than that of the 1Pt catalyst but higher than that of the 5Co/HBEA. However, the run-down experiment indicated that the mixture deactivated quickly.

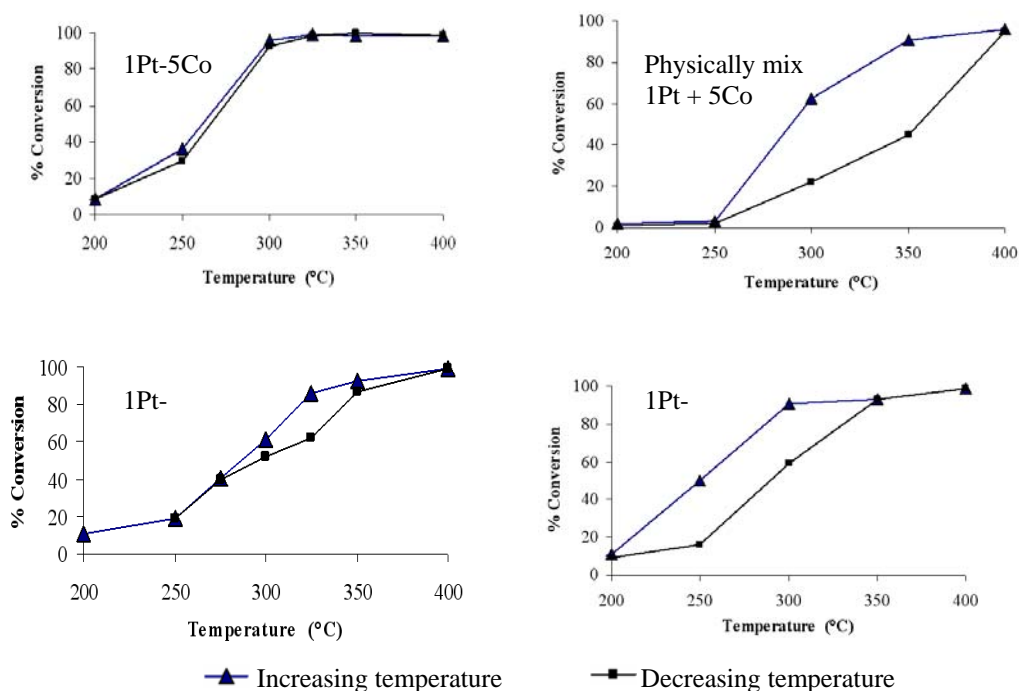


Figure 4 Propane conversion over bimetallic catalysts.

Figure 5 showed the propane conversion and methane selectivity over 5Co-1Pt/HBEA for 12 hours. The conversion remained constant at about 95% throughout the test period and the only observed product was methane.

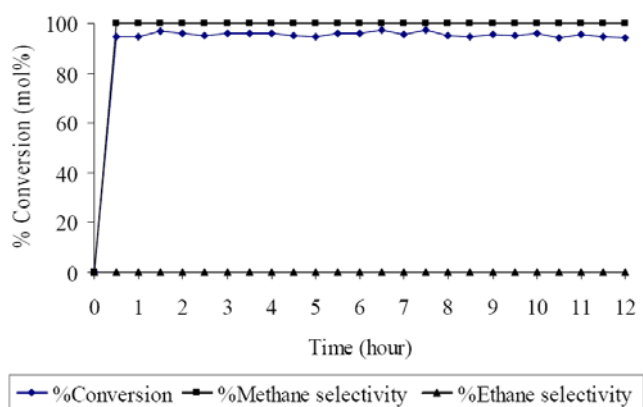


Figure 5 Catalytic performance of 5Co-1Pt/HBEA for 12 hours.

4. Conclusions

Both monometallic and bimetallic catalysts containing Pt and Co were active for propane hydrogenolysis but deactivation was observed in all catalyst. The least deactivation was observed on 1Pt5Co/HBEA. The presence of Co in small amount on the same support helped to stabilize Pt catalysts.

Acknowledgement

Funding for this research was from Suranaree University of Technology.

References

1. Cambor, M. A., and Pérez-Pariente, J. (1991). *Zeolites* 11: 202.
2. Khemtong, P., Prayoonpokarach, S., and Wittayakun, J. (2007). *Suranaree Journal Science Technology* 14(4): 367-379.
3. Loiha, S., Prayoonpokarach, S., Songsirithigun, P., and Wittayakun, J. (2007). *Proceeding of The Regional Symposium in Chemical Engineering (RSCE 2007)*, Indonesia.

CURRICULUM VITAE

MR. SITTICHAJ KULAWONG

Birth Date November 16, 1981

Citizenship Thailand

Education

2000 - 2004 B. Sc. (Chemistry) Ubonratchatane University,
Ubonratchatani, Thailand

2006 - 2008 M. Sc. (Chemistry) Suranaree University of Technology,
Nakhon Ratchasima, Thailand

Presentation

2006 Extended abstract poster presentation “Synthesis of zeolite beta from rice husk silica and utilization as catalytic support for bimetallic transition metals between platinum and nickel”. The 32nd Congress on Science and Technology of Thailand (STT32), October 10-12, 2006.

2008 Abstract accepted for a presentation “Propane hydrogenolysis on bimetallic platinum-cobalt catalysts supported on zeolite beta synthesized with rice husk silica”. The 12th Asian Pacific Confederation of Chemical Engineering Congress (The 12th APCCHE Congress), Dalian World Expo Center, Dalian, China, August 4-6, 2008.